Aerospace Research in Bulgaria

18

Sofia, 2004

C o n t e n t s

С Ъ Д Ъ Р Ж А Н И Е

Bulgarian Academy of Sciences. Space Research Institute.
Aerospace Research in Bulgaria. 18. 2003. Sofia

SPACE TECHNOLOGIES AND THE WAR IN IRAQ

Prof. Petar Getsov

Space Research Institute - Bulgarian Academy of Sciences

Abstract

The paper presents a description of the application of aerospace technologies during the war in Iraq. The specific instrumentation used by the USA and its allies in the field of communication, navigation, and control of weapons and ammunition to schedule war activities is presented. Conclusions are made on the ever growing application of space technologies in modern wars and their impact on the efficiency of decision-making at war times.

State- or private-owned space instrumentation provided coalition troops in Iraq with data of unprecedented scale and quality, required to control military activities at all levels.

This armada of space instrumentation comprises navigation, communication, and meteorological satellites, as well as satellites for remote sensing of the Earth from space (Fig.1) [1].

Navigational provision during the war was supplied by the global navigation system, *Navstar* GPS, owned by the space leadership of the USA Military Air Force. It uses 28 satellites to provide all types of troops with precise data about the objects' location and speed of movement, and time.

The system works steadily, owing to the continuously maintained number of satellites within the group and the continuous replacement of the GPS2A satellites for satellites of the GPS2B and GPS2F type, belonging accordingly to the third and fourth satellite generation, and featuring greater fidelity, precision, and mobility. A typical characteristic of theirs is their nuclear explosion operative identification system, furnished with optical devices and registration sensors for X-ray and electromagnetic emissions.

The major advantages of the *Navstar* GPS, providing for its wide implementation during the Iraqi military operation, are the following: high on-line identification precision of user's 3D coordinates and velocity vector;

global operation zone; independence of GPS precision characteristics on time, weather, or flight height (Fig.2); unlimited system admissibility and user on-board equipment screening during operation; high protection level against jamming and relatively low number of system receivers; multi-purposefulness providing to solve not only navigational, but a large class of other military problems as well.

The *Navstar* signals are captured by the receivers of both mobile and stationary control instrumentation, thus enhancing greatly military decision-taking and implementation processes for various-levelled staff and even for soldiers.

Moreover, the signals obtained by the GPS system are used to control high-precision weapons, including controlled ammunition and rockets (Fig. 1). By comparing the trajectory parameters assigned to them with current on-line parameters, control signals are formed, which jointly with the signals from the correlation system, comparing preset surface and relief images with the area's thermal map, provide to hit the targets with great precision.

The coalition troops used a remarkably great number of images of Iraqi territory and battlefield. To this end, as a rule, private companies (IKONOS, SPOT, QUICKBIRD etc.) are widely used.

Depending on the troops' needs, image taking is scheduled and the ordered images are obtained, which are then processed by dedicated software and submitted for use.

The *Ikonos* satellite flies along a solar-synchronous orbit, providing images featuring resolution of 4 meters for the coloured ones and 1 meter for the black-and-white ones, whereas the *Spot* satellite features a couple of operating spectral ranges, providing spectral-range images, as well as an infrared channel.

These satellites feature a smaller resolution than military space reconnaissance satellites, but provide to form stereo-images. Based on experience from previous wars, this type of satellites is used to plan war activities, inclusive of dealing blows on some particular objects.

Spot's advantage is that it is furnished with standard on-line data transmission equipment, which relieves data access for military users.

Quick Bird provides images featuring resolution of 0.5-1.25 м within the panchromatic range and 2-5 m within the multi-spectral range – 4 ranges within the visible and infrared range. The georeference error of the obtained images following special ground-based processing constitutes no more than 15 m (3σ).

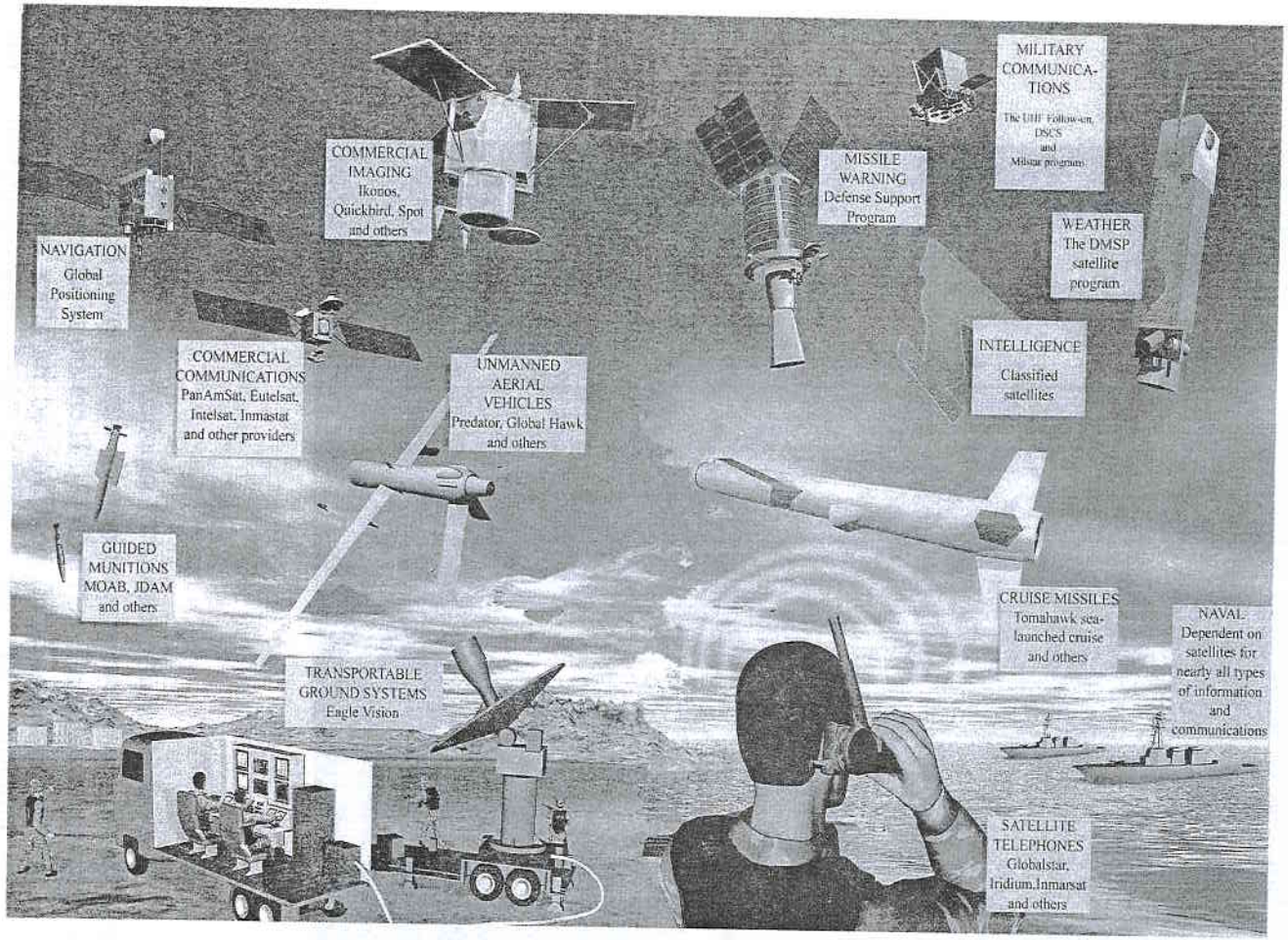
MILITARY COMMUNICA-TIONS
The UHF Follow-on, DSCS and Milstar programs
COMMERCIAL IMAGING
Ikonos, Quickbird, Spot and others
MISSILE WARNING
Defense Support Program
NAVIGATION
Global Positioning System
WEATHER
The DMSP satellite program
COMMERCIAL COMMUNICATIONS
PanAmSat, Eutelsat, Intelsat, Inmastat and other providers
UNMANNED AERIAL VEHICLES
Predator, Global Hawk and others
INTELLIGENCE
Classified satellites
GUIDED MUNITIONS
MOAB, JDAM and others
CRUISE MISSILES
Tomahawk sea-launched cruise and others
NAVAL
Dependent on satellites for nearly all types of information and communications
TRANSPORTABLE GROUND SYSTEMS
Eagle Vision
SATELLITE TELEPHONES
Globalstar, Iridium,Inmarsat and others

Fig. 1

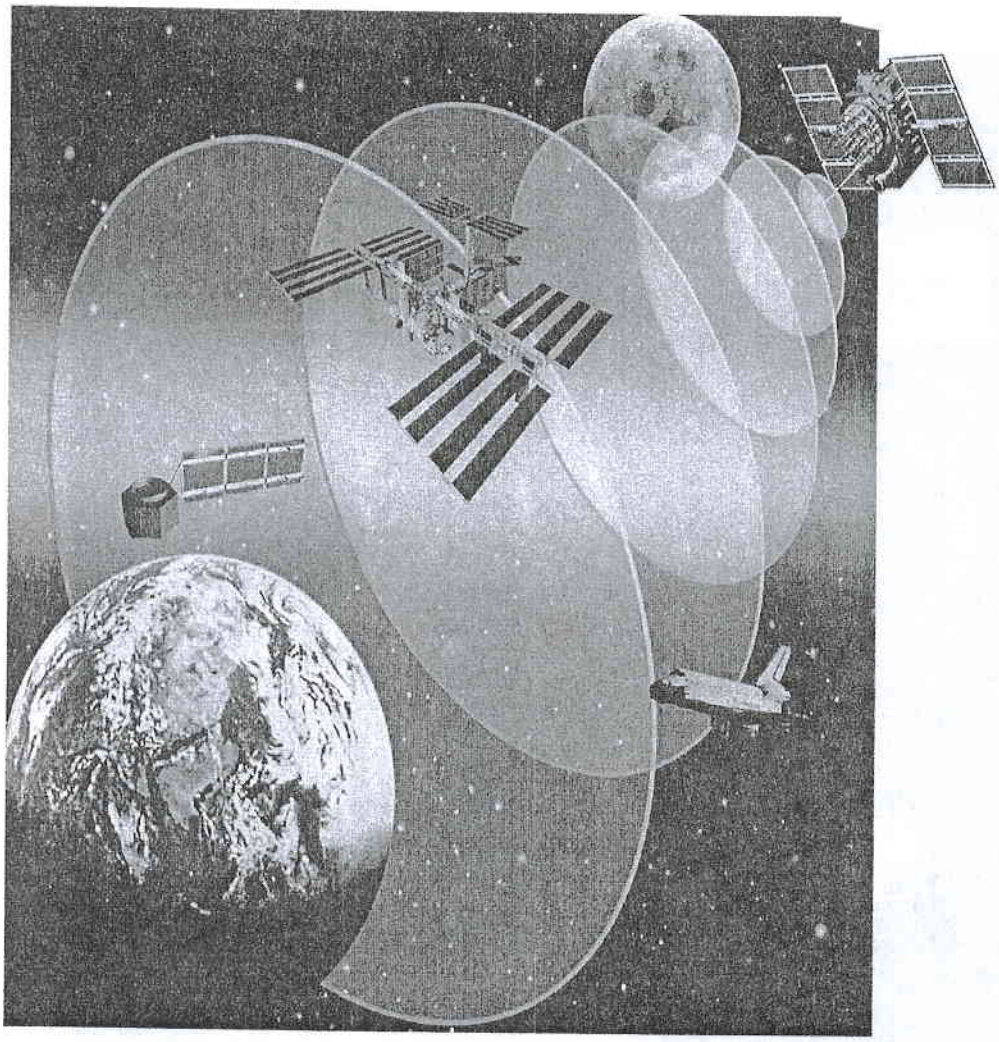

Fig.2

The quantity and intensity of supplied space data (reconnaissance or other) to the appropriate ground-based centers is much greater than it was with all previous war conflicts (Fig.3) [2]. There are several reasons for this:

- the requirement of the USA and its allies for overall space provision of the high-precision instrumentation and ammunition;

- the requirement to provide for harmonization of the actions of the various forces and institutions of the coalition partners, located at great distance from each other.

Since the time the USA and their allies dealt their first blows, major importance has been attributed to the USA military optical-electronic reconnaissance satellites, *KN-11*, and radio-location reconnaissance satellites, *Lacrosse*.

The *KN-11* (***H*=300÷1000 km; *T* = 97,5 min**) satellites perform survey or detailed optical-electronic reconnaissance. Survey optical-electronic reconnaissance is accomplished within **a band of 1250÷2500 km** with resolution of a couple of meters, and detailed optical-electronic reconnaissance is accomplished for some specific regions sized **2,8x2,8 km** at nadir and **8,2x23,3 km** along the band's edges with resolution of up to **15 cm**. This type of satellites provides digital images of the area both within the visible and the infrared range, the latter being successfully used to monitor various objects at night. The obtained images are then transmitted on-line from the on-board equipment via retranslating satellites to ground-based centers where they are processed.

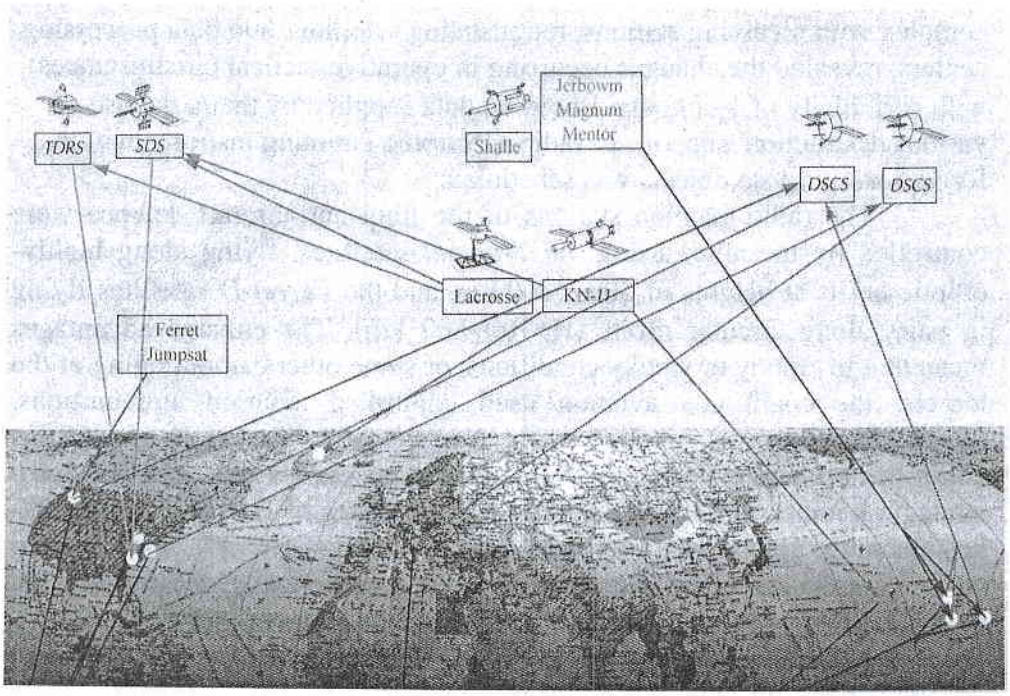

Fig. 3

The *Lacrosse* (***H* = 660÷700 km; *T* = 98 min**) satellite performs radio-location reconnaissance using an on-board **RLS with synthesized aperture**, providing to monitor various objects at night or in cloudy weather with great resolution (**0,6–3 m**), comparable to the resolution of the optical-electronic equipment. With **viewing** band width of **1000 km,** the **range** width is **20-40 km**. Using this satellite makes it possible to identify under various conditions armoured tanks or cars, artillery weapons, parked airplanes, anti-aircraft rocket complexes, and camouflaged, but radio-location-contrast targets, inclusive of targets located under camouflage networks. The obtained images are transmitted nearly on-line via a **TDRS retranslating satellite** to a ground-based centre to identify the targets for the USA airplanes, the **Tomahawk** and **Cruise** flying rockets.

Alongside with optical-electronic and radio-location reconnaissance, the USA are using on a wide scale satellites intended for radio-technical and radio reconnaissance, designed under the **Magnum, Orion, Ferret-D, Trumpet, and Vortex** programs. They are flying along various earth orbits, inclusive of geostationary ones, and account for about 80% of the USA reconnaissance satellites. During the war conflict, these satellites, in complex with receiving stations, retranslating satellites, and data processing centers, revealed the changes occurring in operative-tactical circumstances with periodicity of 1–2 hours. Based on data supplied by them, the use of various destruction weapons or radio-electronic jamming instrumentation for various-purpose objects was scheduled.

The radio-location stations of the Iraqi anti-aircraft defence were controlled by the allies using the *Trumpet* satellites, flying along highly-elliptic orbits at heights of 500–3900 km, and the *Ferret-D* satellites flying in pairs along circular orbits (H=700÷800 km). The enlisted advantages mean that in cloudy or smoky conditions, or some other camouflaging of the targets, the coalition's aviation used controlled aviation ammunitions, whose correction was supplied by the *Navstar* GPS. The major user of this controlled armament during the Iraqi military operations was the *B-2A Spirit* strategic bomber. It delivers successfully 16 pieces of IDAM cassette 907-kg planning aviobombs (versions GBU-29 and GBU-30) with inertial control system and GPS correction. These bombs were also delivered by the B-52N bombers. The target-hitting precision was of the order of 10–15 m.

A similar system complex featuring the same precision was accomplished by the USA deck fighters **F/A-18C Hornet**, using experimental specimen of the controlled aviation bomb cassettes Δ GM-154.

The global *Navstar* GPS provided for flight control of the sea-based **Tomahawk** flying rockets and the **Cruise** rockets delivered by the B-52N strategic bombers, whereas the deviation from the scheduled targets lied also within the range of 10–15 m.

It should be noted that the targeting systems of the strategic bombers **B-1B** and **B-52N** are supplied with built-in GPS-receivers, which makes it possible to deliver effectively 227-kg or 454-kg frec-falling bombs onto area targets.

The strategic-, operative- and tactic-level control of the USA forces and missiles during the Iraqi operation was provided for by communication satellites. The various users obtain data from the **DSCS** system, from retranslating satellites with various destination and functional relations with other satellite systems, as well as from the **Skynet** (Great Britain) and **UFO** (USA) satellites.

The optic-electronic reconnaissance satellites, obtaining images from the visible and the infrared spectrum, have monitored targets with plausible physical characteristics, which were further scheduled to be hit by rocket or aviation equipment.

Using the USA early-warning system satellites, **DSP,** data about the start of the Iraqi **Scud** operative-tactical rockets was collected providing for their destroyal by the **Patriot anti-aircraft rocket complex**.

The changing atmospheric conditions forced into using a substantial number of meteorological satellites during the operation. They (military earth satellites **Block-5D2** of the **DMSP** system, meteorological satellites **"NOAA"** (Fig.4) and **Meteosat)** provided data about the status and change of synoptic circumstances in the region of military activities

with periodicity of 1 hour. Judging the data about cloud cover provided by the *Block-5D2* satellites, it was decided which satellites fit best for optical-electronic reconnaissance (military or civil).

Summarizing the foregoing, it could be concluded:

1. Space systems and reconnaissance, navigation, communication, and meteorological provision instrumentation are essential to providing information superiority in modern military conflicts.

2. The *Navstar* GPS ensures great accuracy of navigation, carrier and destroying instrumentation's launch, if the latter are provided with adequate receiving-indicating equipment.

The system's operation for the needs of aviation and flying rockets does not depend on meteorological conditions, daytime, relief characteristics, or

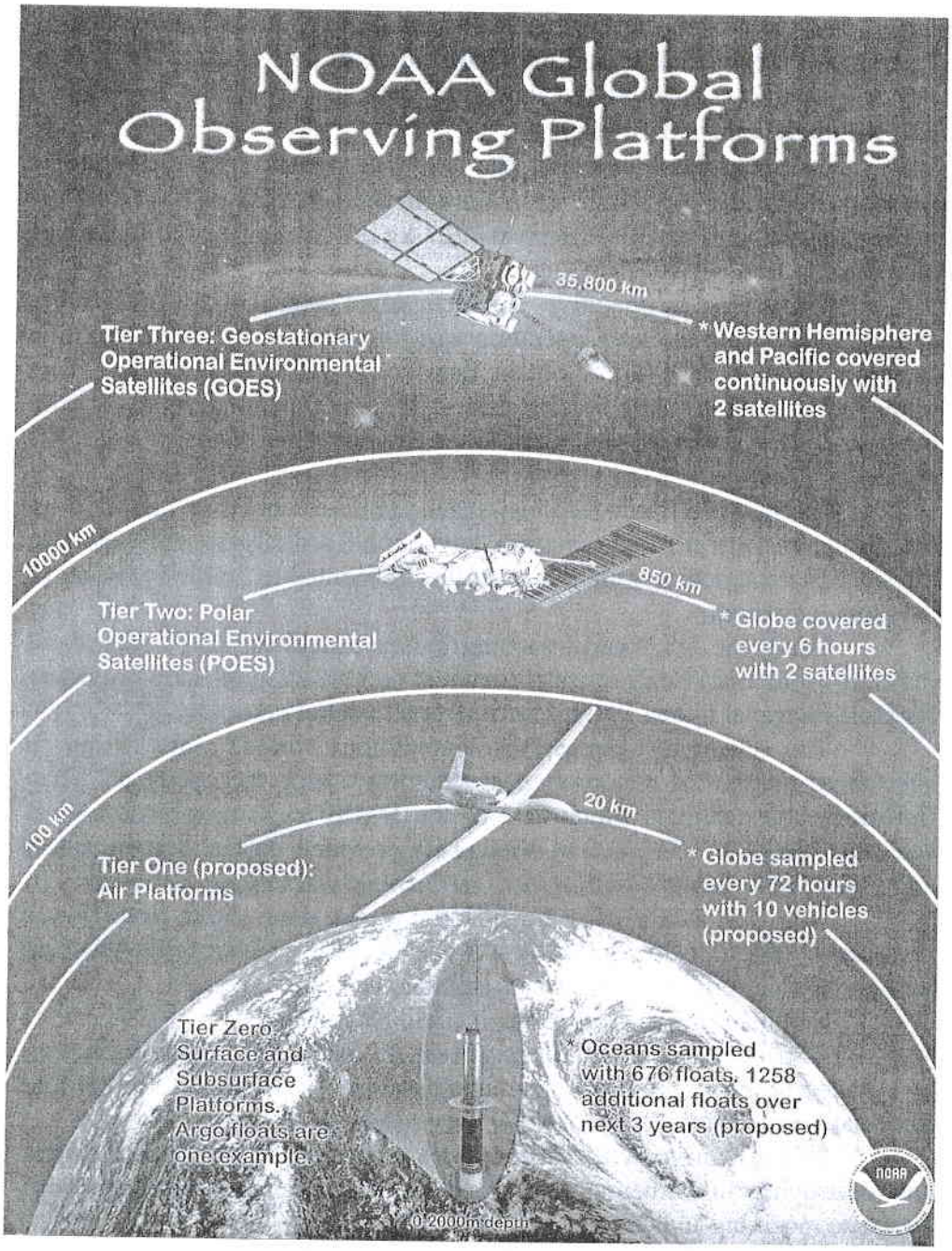
NOAA Global Observing Platforms
35,800 km
Tier Three: Geostationary Operational Environmental Satellites (GOES)
* Western Hemisphere and Pacific covered continuously with 2 satellites
10000 km
850 km
Tier Two: Polar Operational Environmental Satellites (POES)
* Globe covered every 6 hours with 2 satellites
100 km
20 km
Tier One (proposed): Air Platforms
* Globe sampled every 72 hours with 10 vehicles (proposed)
Tier Zero: Surface and Subsurface Platforms. Argo floats are one example
* Oceans sampled with 676 floats. 1258 additional floats over next 3 years (proposed)
0-2000m depth
NOAA

Fig. 4

flight height. It should be noted down, however, that during the last war in Iraq, certain cases of GPS signals' disturbance and substantial deviations of the controlled objects were observed, which calls for design of supplementing protection.

3. The armies of the countries, which do not have their own space systems or instrumentation and do not use these to provide for war activities, are lagging dramatically behind and have no chances with possible military conflicts.

4. The analysis of the space instrumentation used by the NATO and USA troops during the wars in the Persian Gulf, the Republic of Yugoslavia, and Afghanistan evidence of a persisting tendency for introduction of space reconnaissance, intercommunication, navigation and rescue instrumentation to provide for the troops' military actions, reaching as far as the technical level. It reveals the potentials of using strategic reconnaissance instrumentation at the tactical level in the conditions of local conflicts, which complies with the requirements for provision of the national security of each individual country.

References:

1. Space News, April 7, 2003.
2. П.С.Гецов, Космос, екология, сигурност, 211 стр., Нов български университет, 2002.
3. Пенев П.Б., Спътниковата информация и борбата за информационно превъзходство, 12 стр., ОС на ГЩ на БА, 06.10.1998.

АЕРОКОСМИЧЕСКИ ТЕХНОЛОГИИ ВЪВ ВОЙНАТА В ИРАК

Резюме

Петър Гецов

В статията се разглежда приложението на аерокосмическите технологии във войната в Ирак. Показани са конкретните средства, които САЩ и коалицията използват в областта на комуникацията, навигацията и управлението на оръжията и хората при воденето на военните действия. Направени са изводи за все по-широкото приложение на аерокосмическите технологии в съвременните войни и за тяхното влияние върху ефективността при вземането на военните решения.

Bulgarian Academy of Sciences. Space Research Institute.
Aerospace Research in Bulgaria. 18. 2003. Sofia

30 YEARS BULGARIAN EQUIPMENT IN SPACE

Tania Ivanova, Svetlana Sapunova, Ivan Dandolov

Space Research Institute - Bulgarian Academy of Sciences

Abstract

The first Bulgarian space device for ionosphere plasma parameter measurement was launched onboard the satellite Intercosmos-8 on December 1, 1972. Launching successfully its own scientific equipment in outer space Bulgaria became 18th "space country" on the list of the United Nations. Celebrating the 30th anniversary of this historical year, Bulgarian engineers can report large activity and achievements basically in the fields of Space Physics, Remote Sensing and Space Technology.

The history of Bulgarian developments of space scientific equipment dates since 1969 when a Group of Space Physics at Bulgarian Academy of Sciences was established. It continued successfully after this group grew into the Central Laboratory for Space Research in 1975 and the Space Research Institute in 1987. Bulgarian researchers participated successfully in the "Intercosmos" Program, developing equipment and carrying out experiments onboard the satellites "Intercosmos – 8, 12, 14, 19" and the geophysical rockets "Vertical - 3, 4, 6, 7, 10". The scientific programs and equipment for the flight of the first (1979) and the second (1988) Bulgarian cosmonauts were entirely designed by Bulgarian scientists. Two satellites were launched in 1981 with Bulgarian scientific equipment for ionosphere-magnetosphere measurements and remote sensing of the Earth. Bulgarian scientists also participated successfully in international programs such as VENUS-HALLEY (1985), PHOBOS (1988), AKTIVEN (1989), APEX (1990) and INTEBALL (1995-96). Special attention is paid to the recent achievements of Bulgarian scientists in the field of Space Biology and Medicine onboard the MIR Orbital Station and the new International Space Station.

1. Introduction

Bulgarian participation in space research began at the time when the first satellite of the Earth was launched. By the end of 1957 Bulgarian Astronautical Society was established. Under an agreement of 1967, eminent scientists from Eastern Europe, Cuba and Mongolia signed a complex program for international collaboration in space research and peaceful use of outer space, known as the "Intercosmos" Program. According to this program the countries could take part in space research in their favorite field of study with their own scientific instrumentation using free-of-charge the Russian spacecraft (satellites, rockets, etc.) and launching facilities. The main scientific trends within the "Intercosmos" Program

are in the fields of Space Physics, Space Meteorology, Space Communications, Space Biology and Medicine and Remote Sensing of the Earth. Some Bulgarian scientists headed by acad. L. Krustanov and acad. K. Serafimov took part in the establishment of the "Intercosmos" Program and the organization of Bulgarian space activity in it - the National Committee for Space Research was founded in 1968. The **Group of Space Physics** (GSP) at Bulgarian **Academy of Sciences Presidium was created in 1969** with the first scientific team dealing entirely with space research and technology development [1].

2. First Steps and the First Bulgarian Cosmonaut in the 70s

Bulgarian space era started with ionosphere studies in the field of Space Physics. The ionosphere is an atmosphere layer of great importance for the near space because even life on the Earth depends on it. The Earth gets from the Sun the main energy resources necessary to support life. But together with its life-giving energy the Sun emits the life-threatening X-rays, ultraviolet and corpuscular rays. Therefore, one of the problems of great scientific importance is to study how the Sun influences climate, harvest, man and the environment i.e. to determine the concrete forms of the solar-terrestrial connections and interactions.

The first Bulgarian space probe device, named P-1, was launched onboard the satellite "Intercosmos-8" on December 1, 1972. It was designed to carry out direct measurements of space plasma parameters in the satellite's proximity. A cylindrical Langmuir probe (for measurement of electron plasma parameters such as electron density and temperature distribution) and a spherical ion trap (for measurement of ion plasma parameters – ion concentration, temperatures, mass composition and energy distribution) was mounted on long rods projecting out of the protective satellite cover. The hardware was developed by a team of young engineers (S. Chapkunov - at the head, T. Ivanova and M. Petrunova), and technicians (G. Karamishev and S. Lesseva), using mostly Bulgarian electronic components and materials. The equipment was of enough high quality and passed successfully all accepting tests (vibration, impact, temperature and electromagnetic tests, etc.) required for the equipment to be allowed onboard. After an extremely exiting night start, filled with emotions for Bulgarian scientists who had developed the hardware, the "Intercosmos-8" satellite was launched successfully into orbit. **Sending in space its own scientific equipment Bulgaria ranked 18th on the list of the "space countries"**, according to a convention adopted by the United Nations in 1968.

Along with the equipment, our hopes for successful entering of Bulgaria in the space era which involves the brightest prospects of mankind for an all-round development of our civilization flied off in space, too. In the past 30 years these hopes were justified and Bulgarian scientists took active part in many interesting

projects in almost all fields of space research. A second scientific line, "Remote Sensing of the Earth", was created in the GSP in 1974, directed by acad. D. Mishev [2].

The Central Laboratory for Space Research (CLSR), based on the GSP, was established in 1975. Bulgarian scientists gained significant experience through their investigations in the field of Space Physics and their successful participation in the "Intercosmos" Program. A number of other Bulgarian instruments for direct ionosphere measurements were developed. The P-2 and P-3 instruments were launched onboard the satellites "Intercosmos-12, 14" and other modifications of this equipment – onboard the heavy geophysical rockets "Vertical-3, 4, 6, 7, 10". In 1978, along with the P-4 multipurpose probe instruments, the electrophotometer EMO-1 for investigation of the natural optical emissions flied onboard the Automated Universal Orbital Station (AUOS) "Ionozond-Intercosmos-19". AUOS is a heavy spacecraft using solar (not only chemical) batteries. Scientists from some other eastern countries participated in all these starts with their own instruments and the equipment complex was larger and more informative - valuable information was obtained about wide plasma spectrum and optical processes.

In the years that followed, an ever-growing number of Bulgarian scientists and institutes joined in the arrangement and implementation of space experiments. The scientific program and preparation for the flight of **the first Bulgarian cosmonaut Georgi Ivanov** were the most important and exciting event in our space activity to the end of the 70th. Bulgaria became the 6th country in the world with its own cosmonaut. The start took place on **April 10, 1979 onboard the spacecraft "Soyuz-33"** with the participation of the Russian cosmonaut Nikolay Rukavishnikov. The flight was exceptionally complicated and dramatic - the spacecraft couldn't dock with the SOLYUT-6 Space Station due to breakdown in the main engine. Even the return of the cosmonauts to Earth was under question!

The crew showed exceptional heroism, self-control and strength and they proved experimentally, for the first time, that a spacecraft of the "Soyuz" type could come safely back to Earth using a ballistic orbit. This inspired confidence in the success of the future space flights. And the best proof was the recent flight of two "space" tourists - Dennis Tito and Mark Shuttleworth on board of a spacecraft of the same kind. The equipment developed by Bulgarian scientists for this flight ("Spectar-15", "Duga", "Sredets", "Vital") was used by the next crews but Bulgaria had all the rights over the scientific results.

3. Apogee of Bulgarian Space Activity and the Second Cosmonaut in the 80s

One of the most significant Bulgarian scientific achievements in the field of space research was the "Bulgaria-1300" Program carried out in 1981, in honor of the

1300th anniversary of the foundation of Bulgarian State. Two satellites were launched for studying the ionosphere-magnetosphere interaction and for remote investigation of the Earth. **The first satellite "Intercosmos-Bulgaria-1300"** (IC-B-1300) was entirely equipped with Bulgarian scientific instrumentation for research in the field of Space Physics. This satellite was launched into orbit at a height of 900 km. The program also included Remote Sensing of the Earth by Bulgarian scientific instrumentation installed in **the second satellite "Meteor-Priroda"** flying along a lower orbit (600 km). Both scientific complexes had remarkably long life - more than 3 years of perfect work in space.

Bulgarian scientists developed and produced a lot of instruments functioning onboard the "IC-B-1300" such as instruments for measurement of energetic electron and proton flows, the quasi-constant electric field and the low-frequency electromagnetic field, the concentration and drift of plasma ion components, the ion and electron concentration and temperature, the quasi-constant magnetic field, and the flows of energetic ions. The data obtained was processed, analyzed and used by both Bulgarian and foreign specialists. The results concerned the structure and dynamics of the ionosphere-magnetosphere plasma parameters and their interaction with some ground-based phenomena - earthquakes, volcanoes, etc.

Using data from all the "Intercosmos" satellites, the global ionosphere-magnetosphere connections and interactions were explored. The mechanisms determining the concentration and temperature distribution and heterogeneity in the ionosphere and thermosphere were studied.

After the "Bulgaria-1300" Program, Bulgarian scientists directed their efforts to investigation of other planets of the Solar System. In 1984-86, Bulgarian scientists together with Russia and France developed a multi-channel system that worked successfully onboard the **VEGA Space Station** and studied the glow of the Halley comet tail under the VENUS-HALLEY Project.

The video-spectrometric and navigation complex PHREGAT was developed with the leading participation of Bulgarian scientists and mounted onboard the **PHOBOS-1, 2 Space Stations** in 1988. Unique pictures of the MARS planet and its satellite PHOBOS were obtained and after processing they were placed at the disposal of other scientists in the world working in the planetary research area.

In 1987, the CLRS became Space Research Institute (SRI). The accumulated experience and scientific knowledge helped Bulgarian scientists to develop the new scientific **"Shipka" Program for the flight of the second Bulgarian cosmonaut Alexander Alexandrov.** He was launched on board of "Soyuz-TM5" in 1988 in a crew with the experienced Russian cosmonauts Anatoly Solovyov and Victor Savinih. For this historical flight a wide scientific program and corresponding equipment complex for research in the field of space physics, remote sensing, space biology and medicine, space materials and microgravity technology was developed.

Dozens of scientific institutions in BAS and out of it with SRI as a leading institute were involved in this project. Fifteen research devices and complexes, that continued working onboard the MIR Orbital Station (OS) long after Bulgarian flight ("LIULIN" and "SPECTAR-256"), were developed and 49 scientific experiments were conducted. Detailed extensive research directed to study of fundamental problems of the Space and its influence on man were carried out and extremely interesting new data and results were obtained. The main Bulgarian equipment developed on the "Shipka" Program and its objective is shown on Table 1.

Table 1. The main Bulgarian scientific equipment developed for the flight of the second Bulgarian cosmonaut Alexander Alexandrov on the "Shipka" Program in 1988

Equipment	Objective
"ROJEN"	An astronomical complex for identifying of objects in the celestial sphere.
"PARALAX-ZAGORKA"	An image amplifier for recording of pictures of the polar oval small-scale structure.
"TERMA"	A pulse photometer for investigations of the natural optical emissions in the Earth atmosphere.
"SPECTAR-256"	A multi-channel spectrometric system for study of the spectral reflecting characteristics of various natural anthropogenic formations on the Earth surface.
"ZORA"	A computer system for acquisition and storage of information obtained during complex psycho-physiological study of man in long-lasting manned space flights.
"PLEVEN-87"	A computer system for psycho-physiological monitoring of the cosmonauts status.
"SAN-3"	A portable magnetic recorder for 12-hour non-stop record of physiological signals (electro-cardiogram and electro-encephalogram).
"LIULIN"	Space dosimetric complex equipment for investigations of the radiation environment.
"DOZA-B"	An autonomous kit containing integral detectors for evaluation of the distribution of radiation doses.

Another scientific line - "Space Biology and Medicine", developed in the framework of the "Shipka" Program, establishing itself as a priority direction in Bulgarian space research. Many scientific teams and institutions were involved there and the work along this line became a tradition. They were invited to participate in recent international projects in this field of Life Sciences.

For example, very important experiments such as: "Statokinetika" - to study the dynamics of changes arising in the systems for movement control during the critical period of adaptation, "Potential" - to study the state of the muscular fibers driving membranes and "Labirint" - to clear up the phenomena of rise, progress and prophylaxis of the so-called "space disease" in order to raise the operator's working capacity, were carried out using the "ZORA" equipment. The methods used and scientific results obtained were so good that Germany ordered a later "ZORA" modification, called Neurolab-B, used widely onboard the MIR OS in the 90s.

The dynamics of high-energy fluxes and space radiation doses in Earth radiation belts depending on the Solar and magnetic activity level were investigated in the period 1988-1994 using the "LYULIN" dosimeter – radiometer. The data provides to investigate the inner magnetosphere variations. The variations of the Galactic Cosmic Ray fluxes and doses were investigated as well. Long-term global investigations of the MIR OS radiation environment in quiet and solar proton event conditions were used for building up a new experimental model. The model provides to evaluate the risk of cosmic ray exposure in long-term manned space missions and was used for prediction of the expected doses and fluxes on the International Space Station (ISS).

4. Recent Achievements in the 90s of the 20th Century

The main space activity on research projects was centralized at Bulgarian Academy of Sciences - SRI and the Solar-Terrestrial Influences Laboratory (STIL), detached from the SRI in 1990. After closing the "Intercosmos" Program in 1991, the major part of the international scientific activity was organized based on bilateral collaboration with external financial support. Accounting for the interdisciplinary nature of space research and its significance for the national priorities in the field of ecology, agriculture, communication and national security, the Interinstitutional Committee on Space Issues at the Council of Ministers of Bulgaria was established and a National Space Program was elaborated.

The big international space projects with the participation of Bulgarian scientists in the fields of Space Biology and Medicine (SVET Space Greenhouse and Neurolab-B) for MIR OS and Space Physics ("Interball" Project) were successfully carried out till 2000 and they completed with unique results.

The first SVET Space Greenhouse (SG) is an automated system for precise measurement and control of the environmental parameters for higher plant growth under microgravity. Plants could be a major link of the

future Biological Life Support Systems (BLSS), providing the crew with food and oxygen during long-term manned space missions. SVET SG was developed and produced in the SRI (patent is issued), and the development was funded in whole by Bulgarian Government [3].

The SVET SG was launched onboard the Crystal module on a Bulgarian-Russian project and docked to the MIR OS on June 10, 1990. A series of total 680 days of successful plant space experiments was conducted in the SVET SG facility under different scientific programs ("Intercosmos" and MIR-NASA) during the period 1990-2000 [4]. A few months before MIR OS plunged into the Pacific (March 23, 2001), 4 species of different lettuce crops were grown in the SVET SG and tasted for the first time by the last, 28th crew.

Unique and very important results in the field of Fundamental Gravitational Biology were obtained during the plant flight experiments in the SVET SG. It was proven that the lack of gravity is not an obstacle for normal plant development in space. Reiteration of the full life cycle of plant growth was achieved (second generation wheat seeds were produsedl). It became clear that plants could be successfully used in the future BLSS [5].

Another recent project developed by a SRI engineering team in the field of Space Medicine is the **Neurolab-B system** for monitoring the astronaut psycho-physiological status. Neurolab-B was successfully launched from the Baikonur Space Center onboard the "Spectur" module to the MIR OS on April 22, 1996 and was immediately operational. Neurolab-B was developed in cooperation with the German Space Agency and the Russian Space Agency.

The Neurolab-B complex was adapted to work in hospitals and clinics on Earth. A small-sized multi-channel Holter system was designed for recording some physiological parameters: electro-cardiogram, breathing, blood pressure, temperature etc. The system has been successfully tested in English clinics.

Bulgarian scientists have been participating successfully in the "Interball" International Space Program, in the field of solar-terrestrial physics. The program was aimed at direct study of the plasma processes in the Earth magnetosphere. The **"Interball" Project includes two main satellites launched in orbit in 1995 and 1996,** accordingly, each one having a sub-satellite. The first of them is the Magnetosphere Probe launched at a very high orbit, 200 thousands of kilometers in apogee, which was used to study the interaction between the magnetosphere and the solar wind. The second satellite, the so-called Auroral Probe, was launched at the

height of 20 thousands of kilometers above the polar areas and used to study the polar caps and polar ionosphere.

Bulgarian scientists from STIL and SRI developed seven scientific instruments such as AMEI-2 - an ion mass and energy analyzer, IMAP-3 - a magnetic field meter, UVSIPS - a ultra-violet scanning spectrometer and KEM-3 - an electric field meter for supporting a series of space experiments. Both satellites transmitted unique data for the measured parameters till the end of 2000 and this data is at present processed and analyzed by scientists from over 20 countries participating in the project.

As an active participant in the "Interball" project Bulgaria was a host of the International Scientific Symposium, held through COSPAR in February 2002 to mark the 20th anniversary of the project. 120 scientists from all over the world took part in it to discuss on the experimental results.

5. Future prospects for the 21st century

Bulgarian engineers are developing a new generation of equipment for scientific experiments and investigations onboard the ISS during the next 10-15 years of the 21st century. A new Concept for the SVET Space Greenhouse, based on Bulgarian experience and "know-how", is developed in the SRI. Using the physiological parameter measurement data the controller evaluates the plant status and performs adaptive environmental control – "stress-free" plant growth and optimal experimental results under the condition of microgravity [6].

Modifications of the LYULIN device on the "Shipka" Program, developed in the STIL, will be launched on board the ISS for assessment of crew radiation risks [7]. Lyulin-5 is an active dosimetric telescope designed for measurement of the in-depth distribution of space radiation doses in a human platform on the Russian Segment of the ISS (a part of the international project MATROSHKA-R). Another Bulgarian instrument – the Radiation Risks Radiometer - Dosimeter (R3D) will measure the solar radiation and cosmic ionizing radiation in the EXPOSE facility (ESA project) that will be attached to the external platform of the ISS.

Nowadays, Bulgarian scientists, whose achievements are well known and acknowledged, are welcome partners for different international projects. In addition to the development of equipment for bio-medical research onboard the ISS, Bulgarian scientists take part in the space programs relating to other priority scientific directions – Space Physics, Remote Sensing of the Earth, and Space Material Science. The recent SRI activity is mainly in the European level projects, like IMAGE 2000, OSNET, COST-Action 283, including FP5 participation and FP6 proposals. The scientific

research results are published in monographs and hundreds of papers in scientific journals in Bulgaria and abroad.

References

1. Serafimov, K. Space Research in Bulgaria. Sofia, BAS Publ. House, 1979 (in Russian).
2. Mishev, D. Remote Sensing of the Earth. Sofia, BAS Publ. House, 1981(in Bulgarian).
3. Ivanova, T.N. P.T.Kostov, S.M.Sapunova, I.W.Dandolov, et al. Six-Month Space Greenhouse Experiments - a Step to Creation of Future Biological Life Support Systems. *Acta Astronautica*, Vol.42, 1998, 1-8, 11-23.
4. Ivanova, T. V. Stoyanov, Greenhouse over the sky. Sofia, VST Publ. House, 2002 (in Bulgarian).
5. Ivanova, T. Greenhouse Aboard Mir Shows Plants Can Thrive in Space. *21st CENTURY - Science and Technology*, Summer, 2002, 39-47.
6. Kostov, P. T.Ivanova, I.Dandolov, S.Sapunova, I.Ilieva. Adaptive Environmental Control for Optimal Results during Plant Microgravity Experiments. *Acta Astronautica*, Vol.51, 2002, 1-9, 213-220.
7. Semkova, J.V. G.Todorova, R.T.Koleva, et al. Charged Particle Spectrometers for use in Manned Spacecraft, Proc. 8th Confer. *Contemporary problems of solar-terrestrial influences*, Sofia, STIL/BAS Publ. House, 2001,162-165.

Fig.1

Fig.2.

Fig. 1 A team of the Space Physics Group – BAS, which has designed the first Bulgarian probe space unit, P-1, with its Head, Dipl. Eng. Stefan Chapkunov (above, in the middle) and his associates Tanya Ivanova (below), Mariya Petrunova (above, on the left), and Georgi Karamishev. Upon its launch on-board the "Intercosmoc-8" satellite on December 1, 1972, Bulgaria became the 18th space country on the UN's ranking list.

Fig.2. The "Intercosmos-Bulgaria-1300" satellite launched in 1981 on the occasion of the 1300th anniversary of the foundation of the Bulgarian State was furnished entirely with Bulgarian research equipment intended for studies in the field of space physics. Jointly with

the Russian coordinator, G.L.Gdalevich, from SRI-AS USSR, the leading researchers of the probe units, P6-IL and P7-ZL, Katya Georgieva, Tanya Ivanova, and Svetlana Sapunova (from left to tight) from the CLSR-BAS are shown.

30 ГОДИНИ БЪЛГАРСКА АПАРАТУРА В КОСМОСА

Таня Иванова, Светлана Сапунова, Иван Дандолов

Резюме

Първият български космически прибор за измерване на параметрите на йоносферната плазма беше изстрелян на борда на спътника "Интеркосмос-8" на 1 декември 1972 г. Изстрелвайки успешно своя собствена научна апаратура в космическото пространство България стана 18-та "космическа държава" в ранг-листата на ООН. Чествайки 30-та годишнина от тази историческа дата българските инженери отчитат разностранна дейност и постижения, основно в областта на космическата физика, дистанционните изследвания и космическите технологии.

Историята на българските разработки на космическа научна апаратура датира от 1969 г., когато беше основана Група по физика на Космоса към БАН. Тя продължи успешно след като тази група прерасна в Централна лаборатория за космически изследвания през 1975 г. и в Институт за космически изследвания през 1987 г. Българските изследователи участваха успешно в програмата "Интеркосмос", разработвайки апаратура и осъществявайки експерименти на борда на спътниците "Интеркосмос-8, 12,14, 19" и на геофизичните ракети "Вертикал-3,4,6,7,10". Научната програма и апаратурата за полета на първия (1979 г.) и втория (1988 г.) български космонавт бяха изцяло разработени от български учени. Два спътника с българска научна апаратура за йоносферни-магнитосферни измервания и дистанционни изследвания на Земята бяха изстреляни през 1981 г. Българските учени участваха успешно и в международни програми като ВЕНЕРА-ХАЛЕЙ (1985 г.), ФОБОС (1988 г.), АКТИВЕН (1989 г.), АПЕКС (1990 г.) и ИНТЕРБОЛ (1995-96 г.). Специално внимание е обърнато на последните постижения на българските учени в областта космическата биология и медицина на борда на ОС МИР и новата МКС.

Bulgarian Academy of Sciences. Space Research Institute.
Aerospace Research in Bulgaria. 18. 2003. Sofia

THE INFLUENCE OF SOME SPECIFIC TYPES OF INSTABILITY ON STRUCTURE FORMATIONS IN ACCRETION DISCS

D. Andreeva, L. Filipov, M. Dimitrova
Space Research Institute - Bulgarian Academy of Sciences

Abstract

When we investigate the different structures in accretion flows, we reveal the relation between the generation of a certain type of instability and the arising of a structure formation mechanism, when all required conditions are available.Here, we shall consider the effect of some instabilities and the formations generated by them.

Magnetohydrodynamical instabilities

a) Balbus-Hawley instability

There are places in hydrodynamical flows, where the velocity field changes abruptly (the shock fronts). In these places, as a result of the differential rotation of the parts of the flow with great differences in density and velocity, conditions are generated for magnetic shear instability, which is known as Balbus-Hawley instability. In the presence of a magnetic field, destabilization effect of the differentially rotating flows is available, and this instability is the mechanism generating flow turbulence [7].

b) Kelvin - Helmholtz instability

This instability acts on the boundary of two fluid flows, which in our case could be the two parts of an accretion flow. If the boundary is weakly perturbed, velocities increase and at different densities, the following instability condition is derived:

$$(1) \quad \rho_1\rho_2((v_1 - v_2)k)^2 \le (\rho_1 + \rho_2)(\rho_1 - \rho_2)k_\lambda g$$

where v_1 and v_2 are the velocities of two flows

and ρ_1 , ρ_2 are their densities.

The relation between frequency ω and wave vector k_λ is given by the dispersion relation [4]:

(2) $$\frac{\omega}{k} = \frac{\rho_1 v_1 + \rho_2 v_2}{\rho_1 + \rho_2} \pm \left[\frac{g}{k}\left(\frac{\rho_1 - \rho_2}{\rho_1 + \rho_2}\right) - \frac{\rho_1 \rho_2 (v_1 - v_2)^2}{(\rho_1 + \rho_2)^2} \right]^{1/2}$$

The Kelvin - Helmholtz instability is generated when the expression in the square brackets of the above relation is negative and there is a difference in the two flows' velocities. In the presence of this instability, undulations are formed at the boundary; as a result of this, with further progressing of this instability, vortices are formed.

Other instabilities

The generation of structures in accretion discs is caused not only by magnetohydrodynamical instability. In the fluid media of accretion discs, conditions for other types of instabilities are observed.

a) Turing instability

In some systems, the coupling between two transport processes generates instability mechanism. Then the development of this instability is determined by the difference of the diffusion coefficients along the different directions of the transport acting there [1].

The diffusion coefficient participates in the reaction-diffusion equation, which has the following standard form [2]:

(2) $$\frac{\partial C}{\partial t} = F(C) + D\nabla^2 C$$

where the first term in the right-hand side is reaction and the second is diffusion. D is the diffusion coefficient (or matrix of the transport coefficient), C - a concentration of matter.

The reaction-diffusion systems are a manifestation of spatial or temporal patterns if they are far from thermo-dynamical equilibrium [2], which is an important condition for dissipative structures' formation [8]. An key aspect of all application of the reaction-diffusion equation, such as

partial differential equation, is this simple combination of reaction and diffusion in the right-hand side of the equation.

Then, taking into account the condition for Turing instability, the reaction-diffusion equation takes the form:

$$(3) \quad \frac{\partial C}{\partial t} = F(C) + D_x \frac{\partial^2 C}{\partial x^2} + D_y \frac{\partial^2 C}{\partial y^2}$$

This difference between the diffusion coefficients of the two components is the necessary restriction for generation of Turing instability [2].

This assertion can be derived by the following representations and transformations.

The accretion disc is considered as a hydro-dynamical system and is described by hydro-dynamical equations [3].

First, this is the continuity equation, which expresses mass conservation:

$$(4) \quad \frac{\partial \rho}{\partial t} + \nabla.(\rho v) = 0$$

The conservation of momentum for each gas element is represented by Euler equation:

$$(5) \quad \rho \frac{\partial v}{\partial t} + \rho v.\nabla v = -\nabla P + F$$

where for both equations, the quantities ρ, v, P, F are respectively: density, velocity, pressure and a certain force.

Let us present the motion equation for viscous fluid (Navier-Stokes eq.) in cylindrical coordinates. Because averaging takes place along the z-direction, we shall express all derivatives in the terms of the coordinates (r, φ):

$$(6) \quad \frac{\partial V_r}{\partial t} + V_r \frac{\partial V_r}{\partial r} + \frac{V_\varphi}{r} \frac{\partial V_r}{\partial \varphi} - \frac{V_\varphi^{\,2}}{r} = -\frac{1}{\rho} \frac{\partial P}{\partial r} + \frac{1}{\rho} F_r + \nu \left(\frac{\partial^2 V_r}{\partial r^2} + \frac{1}{r^2} \frac{\partial^2 V_r}{\partial \varphi^2} + \frac{1}{r} \frac{\partial V_r}{\partial r} - \frac{2}{r^2} \frac{\partial V_\varphi}{\partial \varphi} - \frac{V_r}{r^2} \right)$$

$$(7)\quad \frac{\partial V_\varphi}{\partial t}+V_r\frac{\partial V_\varphi}{\partial r}+\frac{V_\varphi}{r}\frac{\partial V_\varphi}{\partial \varphi}-\frac{V_r V_\varphi}{r}=-\frac{1}{\rho r}\frac{\partial P}{\partial \varphi}+\frac{1}{\rho}F_\varphi+ \nu\left(\frac{\partial^2 V_\varphi}{\partial r^2}+\frac{1}{r^2}\frac{\partial^2 V_\varphi}{\partial \varphi^2}+\frac{1}{r}\frac{\partial V_\varphi}{\partial r}-\frac{2}{r^2}\frac{\partial V_r}{\partial \varphi}-\frac{V_\varphi}{r^2}\right)$$

Here ν is kinematic viscosity, V_r and V_φ are the two velocity components.

The energy transfer equation can be represented as follows:

$$(9)\quad \frac{\partial}{\partial t}\left(\frac{1}{2}\rho v^2+\rho\varepsilon\right)+\left[\left(\frac{1}{2}\rho v^2+\rho\varepsilon+P\right)v\right]=f.v-\nabla.F_{rad}$$

where $\frac{1}{2}\rho v^2$ - the kinetic energy per unit volume,

$\rho\varepsilon$ - internal or thermal energy per unit volume.

The last term in the square brackets represents the so-called pressure work.

On the right-hand side:

F_{rad} - the radiative flux vector;

$-\nabla.F_{rad}$ - expresses the rate at which radiant energy is being lost by emission, or increased by absorption.

In an accretion disc we consider the transport of "vortical" function or vorticity, which may be denoted by Ψ. This term is provided by vortical equation [5]:

$$(10)\quad \left(\frac{\partial}{\partial t}+\vec{v}.\nabla\right)\frac{\nabla\times\vec{v}}{\rho}=0$$

which is obtained combining the rotation of the momentum equation and the continuity equation. Thus, $\Psi=\nabla\times\vec{v}$ and eq. (10) yields:

$$(11)\quad \left[\frac{\partial\Psi}{\partial t}+\nabla.(\Psi\vec{v})\right]\frac{1}{\rho}=f$$

We express this equation in cylindrical coordinates in terms of the r,φ again:

$$(12)\quad \left[\frac{\partial \Psi_r}{\partial t}+V_r\frac{\partial \Psi_r}{\partial r}+\frac{\Psi_\varphi}{r}\frac{\partial V_r}{\partial \varphi}-\frac{\Psi_\varphi^{\,2}}{r}\right]\frac{1}{\rho}=f$$

$$(13)\quad \left[\frac{\partial \Psi_\varphi}{\partial t}+V_r\frac{\partial \Psi_\varphi}{\partial r}+\frac{\Psi_\varphi}{r}\frac{\partial V_\varphi}{\partial \varphi}-\frac{\Psi_r\Psi_\varphi}{r}\right]\frac{1}{\rho}=f$$

Here, f expresses the transport mechanism of the vortex or this is the diffusion from eq. (3) and in our consideration, f has the form: $D\nabla^2\Psi$.

Taking into account vortical equation (11) and expressions (12) and (13), the reaction-diffusion equation (3) takes the form [8]:

$$(14)\quad \frac{\partial \Psi_r}{\partial t}=h(r,\varphi)+D_r\nabla^2\Psi_r$$

$$(15)\quad \frac{\partial \Psi_\varphi}{\partial t}=g(r,\varphi)+D_\varphi\nabla^2\Psi_\varphi$$

where h and g are the source functions, having the form: $(\Psi.\nabla)v$

Thus we obtain two equations with different diffusion coefficients, expressed for both components.

The evidence that, in accretion discs, the necessary restriction for the ratio between D_r and D_φ to be not equal to unit confirms the possibility for generation of Turing instability in this reaction-diffusion system.

Since these instabilities are the expression of a spatial pattern for the bifurcation area, as a result of them, some structures may be formed in the disc, namely: vortical structures and the so-called Rossby solitons.

The theory of the Turing structures is just one of a variety of such mechanisms of pattern structures formation; here, we showed that this mechanism holds for the hydro-dynamical system of the accretion disk.

But what do actually the Rossby vortices represent and which other instabilities give rise to them.

b) Rossby instability

In studying a non-magnetized Keplerian accretion disc, as a result of non-axisymmetric perturbations, instability arises which generates Rossby

vortices in non-linear limit. The presence of such vortices might be crucial for the hydro-dynamical transport of angular momentum in accretion discs [6]. A wave of non-linear Rossby vortices carries the mass and entropy maximum inward, exciting further vortices, which transport the angular momentum outward.

Here, we shall use again the cylindrical system of coordinate to express the basic equations of a non-barotropic disc. We shall consider surface density $\Sigma(r)=\int_{-h}^{h} dz\rho(r,z)$ and vertically integrated pressure $P(r)=\int_{-h}^{h} dzp(r,z)$. The perturbed quantities of surface density, pressure and velocity are expressed as follows:

$$\begin{aligned} \tilde{\Sigma} &= \Sigma + \delta\Sigma(r,\phi,t) \\ \tilde{P} &= P + \delta P(r,\phi.t) \\ \tilde{v} &= v + \delta v(r,\phi,t) \end{aligned} \tag{16}$$

Thus, we obtain the equations for the perturbed disc:

$$\begin{aligned} &\frac{D\tilde{\Sigma}}{Dt} + \tilde{\Sigma}\nabla.\tilde{v} = 0 \\ &\frac{D\tilde{v}}{Dt} = -\frac{1}{\tilde{\Sigma}}\nabla\tilde{P} - \nabla\Phi \\ &\frac{D}{Dt}\left(\frac{\tilde{P}}{\tilde{\Sigma}^{\Gamma}}\right) = 0 \end{aligned} \tag{17}$$

where $D/Dt = \partial/\partial t + v.\nabla$ and $S = P/\Sigma^{\Gamma}$ is the entropy of the disc matter. Here, the last eq. ( ) shows the isentropic behavior of the disc matter.

Since this instability is related to the entropy behaviour, ultimately, the so-called key function $\Re(r)=\Lambda(r)S^{2/\Gamma}(r)$ is derived, which has a maximum or minimum. Then, instability is possible only provided $\ln\left(\Lambda S^{2/\Gamma}\right)$ disappears at some r.

Here, in the way described above, we obtain again the vortical equation in the form:

$$\frac{D}{Dt}\left(\frac{\Psi_z}{\Sigma}\right)=\frac{\nabla\Sigma\times\nabla P}{\Sigma^3}, \text{ where } \Psi_z = \hat{z}.\nabla\times v \text{ is the vorticity.}$$

For a barotropic flow the right-hand side of the equation is zero and each fluid element conserves its specific vorticity.

In the opposite case, the term $\nabla\Sigma\times\nabla P \propto \nabla T\times\nabla S$ destroys this conservation, providing the pressure force to generate vortices in the flow.

Comments

Here we have not mentioned all types of instabilities, which act in accretion flow in general. Our aim was to show their reference to structures formation in accretion discs. This was proven by analytical computation, based on the major accretion disc equations and the relevant instability expressions.

References

1. Borckmans P., Dewel G., Wit A. De., Walgraef D., Turing bifurcations and Pattern selection, 2001, submitted in Chemical Waves and Patterns
2. Engelhardt R., Modeling Pattern Formation in Reaction-Diffusion Systems, 1994, Univ. of Copenhagen
3. Frank J., King A. R., Raive D. J., Accretion Power in Astrophysics, 1991, Cambridge University press
4. Graham J.R., Astrophysical Gas Dynamics, 2000, http://astron.berkely.edu
5. Nauta M. D., 2000, Two-Dimensional Vortices and Accretion Disks, Utrecht University
6. Lovelace R.V.E., Li H., Colgate S.A., Nelson A.F., 1999, Ap.J.,513, 805-810
7. Primavera L., Rudiger G., Elstner D., 1997, Acta Astron. et Geophys. Univ. Comenianae XIX, 155-161
8. Andreeva D. V., Filipov L. G., Dimitrova M. M., Turing Formations in Accretion Disc - as a Reaction-Diffusion System, 2002, 3-rd Bulgarian-Serbian Astronomical Meeting, Gyulechitsa

ВЛИЯНИЕТО НА ОПРЕДЕЛЕН ВИД НЕУСТОЙЧИВОСТИ ПРИ СТРУКТУРООБРАЗУВАНЕТО В АКРЕЦИОНЕН ДИСК

Д.В. Андреева, Л.Г. Филипов, М. М. Димитрова
Институт за космически изследвания, БАН

Резюме

От важно значение при изследването на акреционните течения е откриването на връзката между появата на вид неустойчивост и възникването на механизъм за структурообразуване, като са налице всички изисквани условия за този процес. Тук ще разгледаме проявата само на някои видове неустойчивости и зараждащите се вследствие на тях формирования.

Bulgarian Academy of Sciences. Space Research Institute.
Aerospace Research in Bulgaria. 18. 2003. Sofia

ANALYSIS OF THE PRECISION OF GEORECTIFICATION OF SATELLITE IMAGERY USING DISTRIBUTORY DATA VS. GROUND-BASED GPS MEASUREMENTS

Nicola Georgiev, Svetlin Fotev, Avram Stoyanov

Space Research Institute - Bulgarian Academy of Sciences

Abstract

The present work makes a comparative analysis of the precision of geometric rectification (georectification) of satellite imagery using in parallel distributor data - coordinates of the central and corner pixels and high precision ground-based GPS measurements.

This work is further step in the research of rectification problems that has been made so far on satellite imagery by defining ground control points of (GCP) with GPS measurements [2, 3, 4, 7].

1. Introduction and purpose of the research

Satellite data occupy an important place in various spheres of theory, practice, and military activities. The modern state of satellite imagery provides real possibility for large-scale mapping, upgrading of available maps, monitoring of the earth cover and other practical and research objectives where it is necessary to determine with high precision the mutual location among different discrete points or contours in a given region [1,2,3,4,5,6,7].

To accomplish these objectives it is necessary to perform coordinate rectification of the images of the identified ground control points (GCP) on satellite imagery using GPS measurements. The distributor of the American-Israeli Group IAI/Core of the "EROS" satellite shares the same opinion. At the conference organized by the Ministry of Defense in October 2001, when discussing these issues he confirmed that defining the coordinates of the GP using GPS measurements improves precision 3 to 4 times which in reality corresponds to the resolution of the space imagery.

Various companies and corporations provide program support for solving this problem. Here, it is of crucial importance to know the geometric characteristics of

the different types of space imagery (scenes). Users have to bear in mind these facts when choosing program packages for processing different types of scenes.
These issues are addressed in greater detail in [2,5,6,7], and on the basis of the performed research and analysis the following conclusion has been reached: many users know that the bigger part of the available program products for imagery processing are not able to handle geometric configurations.
Most often the worked out and classified satellite imagery is not a final product. Raster aero and satellite imagery must be combined with other information sources, either spatial (topographic and soil maps, vegetation, roads, numeric models of the relief and others) or non-spatial (temperature, moisture of air and soil) information or database. In a number of applications, the numeric analysis of satellite raster imagery is accomplished using supplementing information taken from the vector data, on which GIS are based.
Aero and satellite imagery play an important role in monitoring the changes of the land cover as a result of human activities or biophysical processes. In this case, the time analysis requires using imageries received from different sources at different periods of time.
From the above stated it can be concluded that a combination of different imagery and maps from different sources and periods of time requires precise geometric rectification and this is a process that has to be performed prior to integrating data for mutual processing.
The present work makes a comparative analysis of the precision of geometric rectification (georectification) of satellite imagery using in parallel distributor data – coordinates of the central and corner pixels and high precision ground-based GPS measurements.
This work is further step in the research of rectification problems that has been made so far on satellite imagery by defining ground control points of (GCP) with GPS measurements [2, 3, 4, 7].

2. Selection of analysis area and data

The area where the measurements were conducted lies in the north-east of Plovdiv; it is presented on map list **К-9-47-Б** (RAKOVSKI), scale **1:50 000,** 3d edition, 1993, covering territory **20 x 20 км.** I was chosen because the satellite picture was analyzed as a scene from **SPOT 2** with the following parameters given by the distributor – **SPOT-IMAGE**, Toulouse, 22/03/1994. The GCP coordinates were measured by a differential GPS, supplied by section "Laboratory for Communication and Navigation Instrumentation". The equipment precision, using basic transmitter ad accumulation time of 10 min for every measurement is (0.5±0.2) m. This precision was completely sufficient for our purposes having in mind:

- The resolution of scanner HVR 2 in the spectral channels – pixel 20 x 20 m
- The scale of the used map list – 1:50 000

3. Methodology

3.1. Coordinate rectification of satellite imagery using distributor data

The georectification of the above-presented SPOT scene was made using the program product ENVI, version 3.5, from October 2001. Three different rectification methods: RST, Polynomial and Triangular were applied. The standard parameters from the rectification of these points are presented on Table 1. The comparison of the results from the three methods did not reveal any deviation in the coordinates of the chosen control points (Fig. 1).

Table 1. Rectification of the analyzed scene by distributor data

	Map X	Map Y	Image X	Image Y	Predict X	Predict Y	Error X	Error Y	RMS
#1	326984	4676608	1577.50	1502.50	1577.4466	1501.8068	-0.0534	-0.6931	0.6852
#2	306436	4712489	155.50	1.50	155.5141	1.6828	0.0141	0.1828	0.1834
#3	364902	4698272	3163.50	1.50	3163.5126	1.6640	0.0126	0.1640	0.1645
#4	289259	4654854	1.50	3003.50	1.5127	3003.6650	0.0127	0.1650	0.1655
#5	347727	4640642	3010.00	3004.00	3010.0140	3004.1814	0.0140	0.1814	0.1819

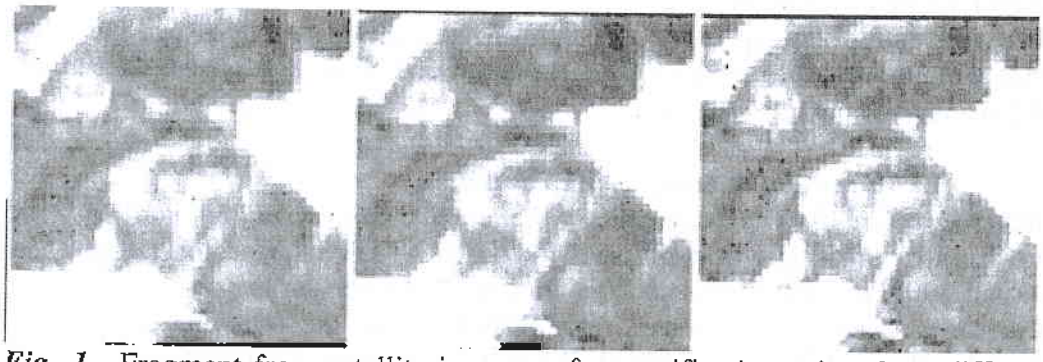

Fig 1. Fragment from satellite imagery after rectification using three different methods - RST, Polynomial and Triangular.

3.2. Coordinate rectification of satellite imagery using ground-based GPS measurements

Having in mind the similar results obtained when applying each of the geometric correction methods, the polynomial method was selected for rectification. Five of a total of ten measured GCPs were used (Fig. 2).

Fig. 2. Selection of GPS measured GP

On Table 2, the standard parameters from the rectification of the measured ground control points are presented.

Table 2. Rectification on the analyzed scene based on GCPs from GPS measurement

	Map X	Map Y	Image X	Image Y	Predict X	Predict Y	Error X	Error Y	RMS
#1	319550	4676716	1218.00	1580.89	1217.0451	1580.7490	-0.9549	-0.1410	0.9652
#2	318651	4674863	1195.89	1691.56	1195.9719	1681.5721	0.0819	0.0121	0.0828
#3	334736	4676472	1955.75	1416.50	1955.6258	1416.4817	-0.1242	-0.0183	0.1255
#4	321852	4673171	1370.25	1725.00	1370.6529	1725.0595	0.4029	0.0595	0.4073
#5	321287	4679324	1269.57	1434.57	1270.1642	1434.6577	0.5942	0.0877	0.6007

3.3. Results assessment

To control the obtained results, a digitalized map list with scale 1:50000 was used. The digitalizing of the map list was done on scanner A4. Before mosaicing of the four images, geometric correction of the knots of the coordinate net was performed. This was done to avoid paper deformations or deformations that might appear during the scanning process.

The raster imagery of the digitalized map was mosaiced to the coordinates of the measured GCPs in the geographic projection of the rectified satellite image.

- The coincidence of the GCPs of the two imageries was controlled. The difference in the positions of the GCPs from the two imageries was less than 2 pixels.
- The coincidence of the selected triangulatory points from the map with the respective satellite images was analyzed. The results are graphically presented below.

3.3.1. Deviation of the GCP vs. their real coordinates on the rectified satellite imagery by distributor data (geographical projection: UTM, WGS-84, Zone 35, Pixel 10 m)

Table 3. GCP measurement and deviation from the real situation following rectification by distributor data.

GCP	Географска ширина	Географска дължина	Грешка в поз., m
The bridge after Shishmanci	42.2229515N	24.9975207E	90
Manolsko konare	42.2121323N	24.9510037E	110
Trangular point «Bokludga»	42.2495707N	24.9559323E	120
Dink	42.3194826N	24.7993665E	95
Skutare	42.1904148N	24.8425216E	100
Rakovski	42.2990631N	24.9735579E	105
Voevodino	42.2049088N	24.8032604E	95
Trangular point «Domuztepe»	42.2785440N	24.8751930E	120
The bridge after Kalekovetc	42.2456617N	24.8337894E	115
Kalekovetc (173.7/52г.)	42.2217887N	24.8137240E	110

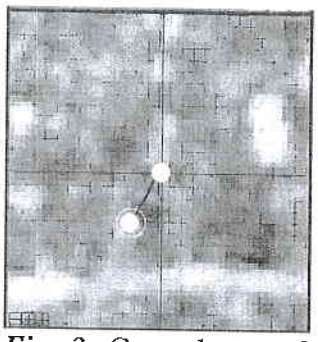
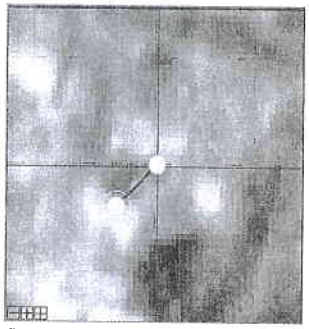

Fig. 3. Ground control points: Skutare village and Kalekovetc village (level 173.7 / 2yrs.), accordingly. The circles identify the points with coordinates equal to the coordinates of the GCPs. The beginning of the coordinate system points to the real location of these points on the imagery following rectification by distributor data.

3.3.2. The deviation of the GCPs location defined using GPS vs. their real location on the rectified satellite imagery is less than 1 pixel (Fig. 4, a, b, c, d). The imagery is in projection: UTM, WGS-84, Zone 35, Pixel 10 m.

a) GCP "Pereseto", 176.0
West of Stryama Village

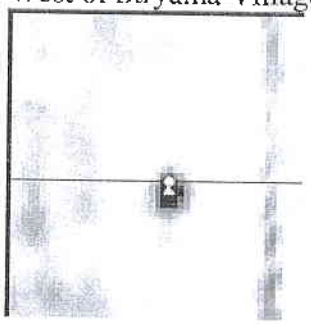

b) TT "Mozartepe"
North of Izgrev quarter

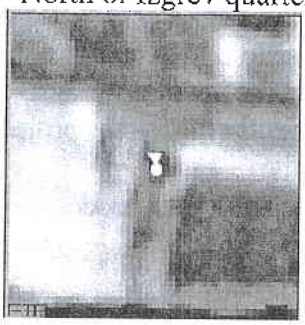

c) TT "Ploska Mogila"
East of Gen. Nikolaevo Village

d) TT 154.0
East of Sadovo village

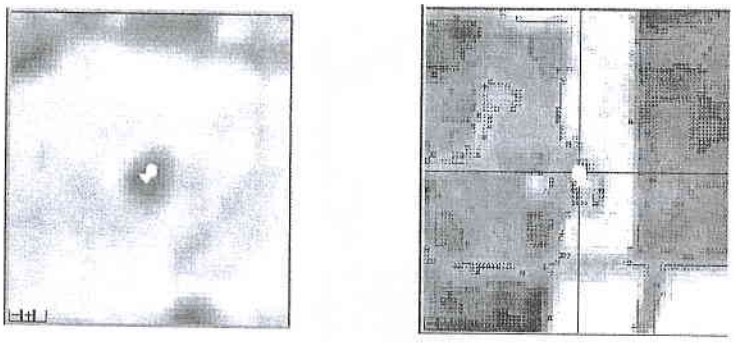

Fig. 4. Rectification of satellite imagery by 5 GCP, GPS measured on the ground. The circle (0) marks the location of the selected triangulatory point on GPS measurement and the triangle (Δ) marks the location of the triangulatory point on the ground.

4. Conclusion

We would like to mention here that due the fact that satellite imagery with resolution of 1 m (from the type "IKONOS", "EROS - A and B" "Quick Bird") was not available, we were forced to experiment with scene from SPOT -2.
In spite of this the results of the GPS measured GCPs feature 4 times higher precision compared with the results submitted by the distributor.

Apart from these requirements, in our opinion, it is necessary to take into consideration the following:

- The changes in the scale coefficient and the relief in the various directions of the scene when rectifying the imagery;
- Using the earth (referent) ellipsoid as projection plane;
- The ellipsoid's heights;
- Applying strict methods for data processing and of result assessment.

References

1. Георгиев, Н., Р. Недков. Ректификация на геометрическите деформации при космическите сканерни изображения чрез апроксимиращи функции, "Аерокосмически изследвания в България", София, 15, 1998.
2. Георгиев, Н., Р. Недков, А. Христов. Високоточен метод за привързване и ректификация на космическите фотографски изображения, сб. "30 год. организирани космически изследвания в България", ИКИ – БАН, 2000, 124-131.
3. Георгиев Н., Р.Недков, Д. Неделчева, Използване на метод и GPS измервания на опорни точки от терена при координатното привързване на космически фотографски изображения . сб.докл. "Международна научна сесия 50 години ГИ - БАН, 2000, с. 179-189.
4. Георгиев, Н.И., Спиридонов, Х.П, Методи за координатно привързване, ректификация и интерпретация на космически изображения . сбор. от доклади на Юбилейна научна сесия "40 години от първия полет на човек в Космоса" Д. Митрополия, 2001, ст. 150-161.
5. Prof. Gordon Petrie. Mapping Awareness, Nov.1999, Depart. of Topographic Science, University of Glasgow.
6. N. Georgiev, R. Nedkov, D. Nedelcheva . Using an Orbital Method and GPS Measurements of the Ground Control Point in Georeference of Space Images, Aerospace Research in Bulgaria, 16, pp. 70-80, Sofia.
7. N. Georgiev, Sv. Fotev, Mathematical Model for coordinate attachment and rectification of space images with high resolution, Aerospace Research in Bulgaria, 17, pp. 35-45, Sofia.

АНАЛИЗ НА ТОЧНОСТТА НА ГЕОМЕТРИЧНОТО ПРИВЪРЗВАНЕ НА КОСМИЧЕСКИТЕ ИЗОБРАЖЕНИЯ ПО ДАННИ ОТ ДОСТАВЧИКА СПРЯМО GPS ИЗМЕРВАНИЯ

Никола Георгиев, Светлин Фотев, Аврам Стоянов
Институт за Космически Изследвания – БАН

Резюме

Сегашното състояние на космическите изображения дава реална възможност за едромащабно картографиране, обновление на съществуващи карти, мониторинг на земното покритие и други практически и изследователски цели, при които е необходимо да се постигат високи точности при определяне взаимното разположение между отделни дискретни точки или контури в определен регион[1,2,3,4,5,6,7].

Целта на настоящата работа бе да сравни точността на геометричното привързване (георектификацията) на сателитните изображения с използваните, от една страна на данни от дист-рибутора, а от друга, на високоточни GPS измервания върху терена.

Независимо от това, че бяхме принудени експериментите да проведем със сцена от SPOT — 2, получените резултати, след като се извършиха GPS измервания на идентифицираните ОТ от терена, са с 3 - 4 пъти по-големи точност, в сравнение с предоставените резултати от доставчика.

Bulgarian Academy of Sciences. Space Research Institute.
Aerospace Research in Bulgaria. 18. 2003. Sofia

PHOTOELECTRIC CURRENT FROM THE SURFACE OF THE "INTERKOSMOS BULGARIA 1300" SATELLITE

Stefan Chapkunov, Nikolai Bankov, Ventzislav Markov

Space Research Institute - Bulgarian Academy of Sciences

Abstract

Based on the information obtained from measurement of electron and ion density onboard the satellite, cases of evidently increasing electron density during the transition from shadow to sunlight are observed. Compared to the almost identical electron and ion density in the other parts of the satellites orbit this increase of electron current is interpreted as a photo current.

1. Introduction

An investigation carried out during the first scientific rocket experiments [1, 2] shows that the photoemission-generated photo current amounts approximately to 10^{-8}-10^{-9} A/cm^2. Similar values are obtained from theoretical calculations [3], producing an approximate photo current of $2{,}5.10^{-9}$ A/cm^2 with surface potential near 0 V.

The study is based on the probe measurements made onboard the "Interkosmos Bulgaria 1300" satellite.

2. Equipment description

This study is based on data for electron temperature and density from the device P7, and ion density from the device P6, as well as the probe-satellite potential difference measured by the device IESP. The value of the probe-satellite potential difference is calculated based on data obtained from the Langmuir probe (device P7) in the way described in [5].

Ion density is estimated based of the data from the three-electrode spherical ion trap (device P6), whose external grid is under "floating potential".

One of the sensors of the device IESP that measured electrical field is used as a base: the potential difference between the probe and the satellite body is measured continuously.

Below are shown the results from the measurements of a couple of selected satellite orbits.

3. Measurement results:

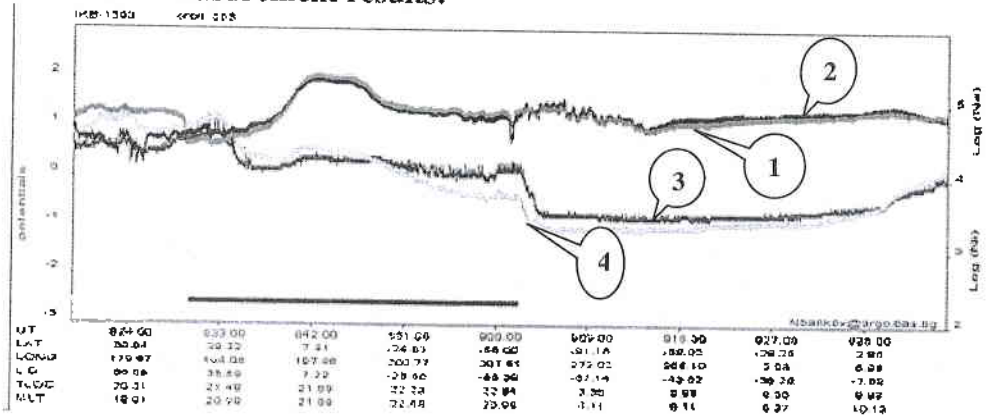

Fig.1

In Fig.1 are presented the results from the measurement of the following parameters along orbit No.583:

1- Ion density; 2-electron density; 3- potential difference between the probe and the satellite body, calculated from the volt-ampere characteristics (device P7); 4- potential difference between the probe and the satellite body, measured directly (device IESP).

The dark line in the lower part of Fig.1 corresponds to "shadow" i.e. the orbit is partially in shadow. The shapes of the two densities are identical except for the points of transition from "sun" to "shadow" and vice versa. This is true almost whenever the condition of electro neutrality of satellite-surrounding plasma is fulfilled.

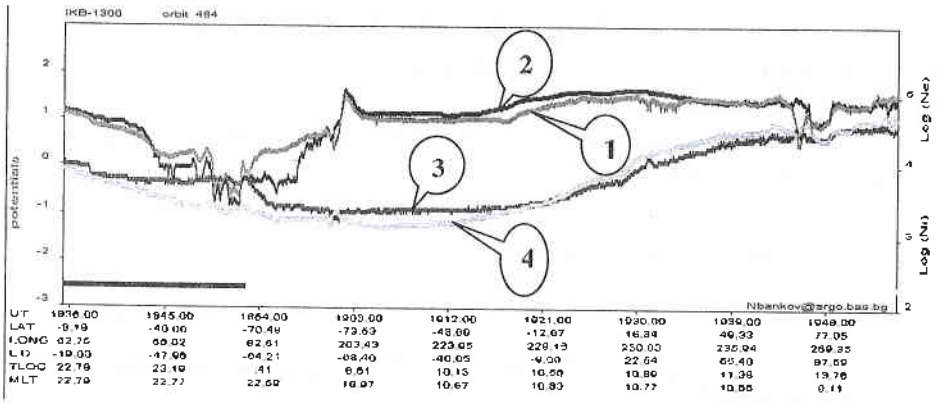

Fig.2

In Fig.2 are shown the same parameters. The difference is that (No.484) in this case, the satellite is completely in the "sun". It may be seen that, in this case, the curves of both concentrations match. With transition from "shadow" to "sun" significant increase in electron density is observed.

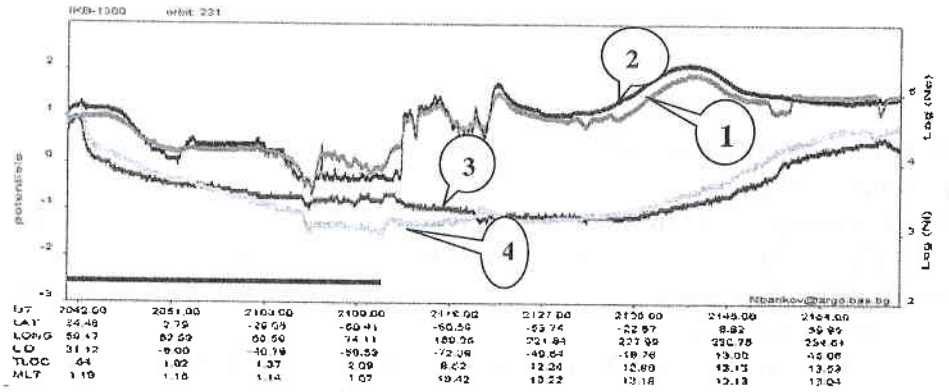

Fig.3

On Fig.3 is sown case of transition of the satellite from dark to sun part of the orbit No.231. It is visible that at a transition between two areas, electron density visible accrues in comparison with ion density, and in the rest part of the orbit both densities are with the same order.

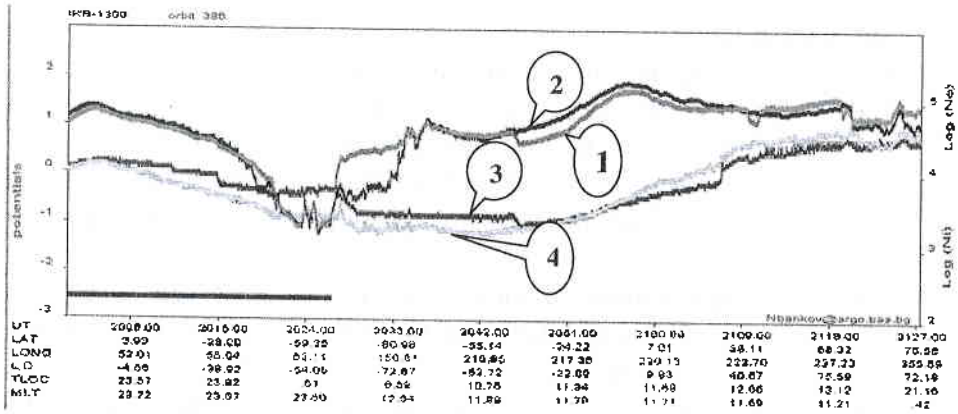

Fig.4

In Fig.4 are shown the same parameters for orbit No.386. In this case the transition from "shadow" to "sun" results in a jump in electron density compared to ion currents. The value of these parameters for (Fig.1 and Fig.2) is about $0,5.10^3$ cm $^{-3}$ for both cases.

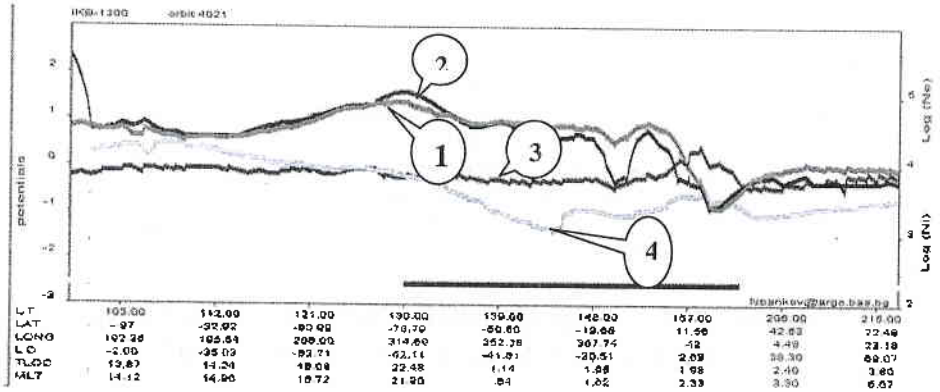

Fig.5

In Fig.5 are shown the values of these parameters for orbit No.4021.

Electron and ion density have almost the same value independently from the two transitions from shadow to sun and vice versa.

In contrast to the cases from Fig.3 and Fig.4, the curves indicating the behavior of the potential difference between the satellite body and the sensor, have value about 0 volts.

4. Conclusions

The analysis of the presented observations shows that:

- It is observed increasing (with jump) of the electron density in the order of $0{,}5.10^3$ cm^{-3} when the potential difference sensor-body is positive through the satellite's transition from dark to sun along the orbit. This phenomenon is attributed to photocurrent.
- The phenomenon "photocurrent is not observed when the potential difference between the sensor and the body of the satellite is negative.
- The equalization of the electron and ion density after the "jump" defined as a photocurrent is probably caused by the next rise in ion density. As was explained above, the outer grid of the three - electrode ion trap (device P6) is isolate from the body and did not influence on the photoelectrons.

References

1. Bourdeau, R. E., J. L. Donely., G. P Serbu., E. C. Whipple, Journ. Astron. Sci., 8, 65,1961
2. Netherlands., 2002 Hinteregger, H. E., K.R. Damon., L.A., Hall, Journ. Geophys. Res., 64, 961, 1959
3. Курт, В.Г., В. И. Морз, Потенциал металлического шара в межпланетном пространстве. Искусственные спутники Земли., вып.7., 1961.
4. Laakso, H. Monitoring of the Spacecraft Potential in the Magnetosphere with a Double Probe Instrument, ESA Space Science Department, Noordwijk.
5. Банков, Н. Г., Ст. К., Чапкънов., Л. Я., Тодориева., Потенциал на корпуса на спътника "ИКБ - 1300", УДК 629.78, 2002 (in print).

ФОТОТОК ОТ ПОВЪРХНОСТТА НА СПЪТНИК "ИНТЕРКОСМОС БЪЛГАРИЯ – 1300"

Ст. К. Чапкънов, Н. Г. Банков, В. Г. Марков

Резюме

На базата на информация от измерители на електронната и йонна концентрация, работили на борда на спътника са установени случаи на видимо повишаване на електронната концентрация при прехода на обекта от неосветената към осветена част на орбитата. На фона на почти съвпадащи си йонна и електронна концентрации в останалата част на посочените орбити това повишаване на електронния ток е интерпретирано като фототок.

Bulgarian Academy of Sciences. Space Research Institute.
Aerospace Research in Bulgaria. 18. 2003. Sofia

TIME OF FLIGHT (TOF) MODE OF OPERATION IN IONOSPHERIC ION DRIFT MEASUREMENTS

Bankov L.G., Vassileva A.K.

Space Research Institute – Bulgarian Academy of Sciences

Abstract

During the past 30 years, ion drift measurements were a very powerful way to study the Earth's ionosphere dynamics in the context of the Sun-Earth relation processes. Here, we propose a combined use of Time-Of-Flight reflectron as a part of the modified Ion Drift Meter (IDM) sensor to obtain valuable mass-spectra and ram ion speed in parallel to the IDM transverse ion drift velocity measurements. This in fact could reduce the measuring technique to a single-sensor IDM/TOF mass-spectrometer.

INTRODUCTION

In situ ion drift measurements in the Earth's ionosphere by means of ion probes onboard the satellites, proceed under the basic assumption that ion thermal speed is small enough in comparison to the satellite velocity, which is almost well satisfied within the entire F-region. S.P. Korolev was the first to propose ion sensors as a part of the ballistic missile angular orientation system in earlier 60's [1]. This measuring technique appeared to be sensitive to the ionospheric ion drift motion, which causes a spurious output signal to the orientation system. Ion drift measurements were proposed as an input current balance method of a double planar ion probe mounted away from the satellite velocity vector on the COSMOS-184 satellite [2]. An improved techniques by means of a Retarding Potential Analyzer (**RPA**) and IDM for ram and transverse ion drift measurements was used on the Atmosphere Explorer C,D,E satellites [3]. It was shown by the authors that ram drift component could be calculated after a fitting procedure of the current-to-voltage curve from the RPA sensor if additional mass-spectrometer information about the present ion species is available. Also, the current ratio offset from the opposite collector pairs of the IDM sensor is proportional to the value of the transverse yaw (horizontal) and

pitch (vertical) ion drift velocity components. Later, this method was successfully used on the Dynamics Explorer-B, San Marco, DMSP, ROCSAT etc. satellites. On the Intercosmos "Bulgaria-1300" (**ICB-1300**) satellite IDM/RPA sensors for ion drift velocity measurements were similarly used at heights of 800km to 1000km [4]. At these heights, the ICB-1300 satellite passed almost beneath, through or higher than O^+/H^+ transition level. In result, the evaluation of the ram velocity from the RPA current-to-voltage curve becomes difficult in the presence of only two major species (predominant O^+ ions at daylight and H^+/He^+ ions at night) without relevant mass-spectrometric data. For the same reason, the IDM output was affected by the presence of light ions at around midnight local times [5]. During an active experiment mission on the Intercosmos 24-"ACTIVE" satellite, a modified IDM sensor with five collector segments as RPA (central collector) and IDM (two side collector pairs) for simultaneous measurement of both components were used [6]. Fast wide dynamic range measurements of ion drift by Digital Ion Drift Meter (**DIDM**) on the CHAMP satellite were made [7]. The DIDM consists of a pin hole camera type of sensors with 2D view of input ion flow projection on position-sensitive micro-channel plate (**MCP**) detector for determination of X/Y shift of count rate maximum due to the presence of ionospheric ion drift component. The sensitivity and accuracy of the method depend on the exact determination of the main count rate maximum position observed on the 2D camera view. At present, it is commonly accepted to use RPA for ram drift component and the IDM for transverse velocity components because of their high accuracy and sufficient sensitivity. One of the important uncertainties of this measuring technique is addressed to the time/space discrepancy between the time resolution of RPA and IDM, accordingly. Yaw and pitch ion drift velocities could be measured with relatively high temporal resolution with IDM instrument limited only by the level of the input current flow. Ram ion drift velocity could be calculated from RPA current-to-voltage curves taken only a few times per second because of the limitation of narrow bandwidth and accuracy at low input current levels when high retarding voltage is applied. Here, we propose a combination of an IDM sensor used on the IC-24 satellite [6] with a TOF mass-reflectron as a mass-spectra/ion drift sensor with relatively high time/space resolution for both ram and transverse ion drift velocity components. The central collector of the IDM [6] could be also used as a duct sensor for ion density irregularities observation and in-flight calibration with the same time resolution. The expected advantages of the proposed method could be summarized as follows:

- Fast mass-spectrometry of the ionospheric ions with high mass resolution
- Direct estimation of ram ion drift velocity and satellite skin potential
- Fast ion drift measurement of both ram and transverse velocity components
- High resolution measurements of ion density irregularities for different ion species

TOF mass-reflectron is a well-known instrument for laboratory laser mass-spectrometry applications with impulsive ion source. Its simple construction and relatively good mass resolution make it quite convenient for satellite application [8,9].

BASIC PRINCIPLES OF THE METHOD

In the Earth's ionosphere, at the height above the bottom side F-region, where ion-neutral collision frequency becomes small enough compared to ion gyro frequency, ions and electrons drift together perpendicularly to the external electric field **E** and the Earth's magnetic field **B** with drift velocity: $\mathbf{V_d}=\mathbf{ExB}/B^2$

Following [3], in a frame of reference moving with the satellite's velocity $\mathbf{V_{sat}}$, the main task to measure $\mathbf{V_d}$ could be divided in two stages, measuring separately the perpendicular ($\mathbf{V_{d\perp}}$) and ram ($\mathbf{V_{d\parallel}}$) components in respect to $\mathbf{V_{sat}}$. While the measuring technique of $\mathbf{V_{d\perp}}$ is fully described in [3], here we will present a more detailed view on the proposed time-of-flight method of ram ion drift $\mathbf{V_{d\parallel}}$ measurements. If we assume satellite skin potential U_{sat}=0v, in a satellite frame of reference ionospheric ions have a ram kinetic energy $\mathbf{E_i}=m_i(\mathbf{V_{sat}}+\mathbf{V_{d\parallel}})^2/2$ where m_i is the ion mass of the different ion species. We assume ram drift velocity equal for different ion species which means pure electrodynamics drift motion. Let us consider the main steps from RPA toward TOF measurement of the $\mathbf{V_{d\parallel}}$. Fig.1(a) shows an example of the expected current-to-voltage curve of a classic RPA sensor for H^+,He^+,O^+ and NO^+ ions (other ion species are omitted for simplicity). The C-V curve is an integral characteristic of the different ion energy distribution functions in the satellite frame of reference. The positive ram velocity $\mathbf{V_{d\parallel}}$ augments the energy of every ion species to the higher energies and vice versa, the negative $\mathbf{V_{d\parallel}}$ reduces ion energy of every ion species in a proportional to m_i way. The satellite skin potential U_{sat} shifts the entire C-V

curve in the energy frame of reference, not changing the relative distance between mass peaks. The corresponding plasma parameters could be found by means of the least square technique used to fit the C-V curve of RPA for ion density N_i, ion mass m_i, ion temperature T_i, ram ion drift $\mathbf{V}_{d\|}$ and satellite potential U_{sat}. An accurate solution of this task could be obtained with the support of mass-spectrometer data for the density of the present ion species [3]. On panel (b) of Fig.1, we show a sketch of ion energy distribution functions already shown on panel (a) in corresponding gray scale amplitudes against the relative thermal velocity distribution function for each ion species around $\mathbf{V}_i = (\mathbf{V}_{sat} + \mathbf{V}_{d\|})$ under the assumption $U_{sat} = 0v$ (Y- axis on the right-hand side of the panel). At a given ion temperature T_i ion thermal velocity V_{th} is larger for light ions, decreasing by a factor of $1/\sqrt{m_i}$ to the higher mass numbers, as illustrated on the right-hand side of the panel for equal density H^+, He^+, O^+ and NO^+ ions. Obviously, in this case TOF mass separation could not be used when different ions enter the sensor with equal ram velocity V_i. In the same format, panel (c) of Fig.1 shows the changes in velocity distribution for different ion species in case of negative ($U_{sat} < 0v$) satellite skin potential and an acceleration with short negative impulse U_{ac} is used. The relative energy shift of the peak in thermal velocity distribution functions is proportional to the ion mass number as $\sqrt{(2e(U_{ac}+U_{sat})/m_i)}$ where e-units charge. Ion speed decreases with ion mass as $1/\sqrt{m_i}$ for a given $U=U_{sat}+U_{ac}$. The TOF mass spectrum after impulse acceleration is shown on the right-hand side of the panel for the expected mass resolution limited by the thermal spread of the different ion species. Better results could be obtained with higher negative amplitude of U, but this will decrease significantly flight time for the ions at fixed distance. The accurate estimation of the U_{ac} amplitude and optimal flight distance gives provides an opportunity for mass separation with moderate mass resolution. Mass resolution at low-mass numbers is very sensitive to the value of accelerating potential U. At least two ion species presented in the mass-spectrum should be available to calculate U and V_i. The main problem is to evaluate the exact position of the mass peak for low ion mass numbers because of the large thermal velocity spread occurring in this part of the spectrum. The shape of the peaks depends on the flight time spread around the central value t_j, which corresponds to the ion velocity thermal spread ($_j$ = 1,n number of observed mass peaks). Considerably better mass resolution could be achieved by time and/or space focusing of the ions. As it was mentioned above, we suggest linear TOF mass reflectron to be used as mass-spectrometer section with relatively good mass-resolution for accurate mass peak position observation. Fig. 1(d) represents the expected changes in

mass resolution when the TOF mass-reflectron is used for flight time focusing of the different ions accelerated with the negative U_{ac} impulse at

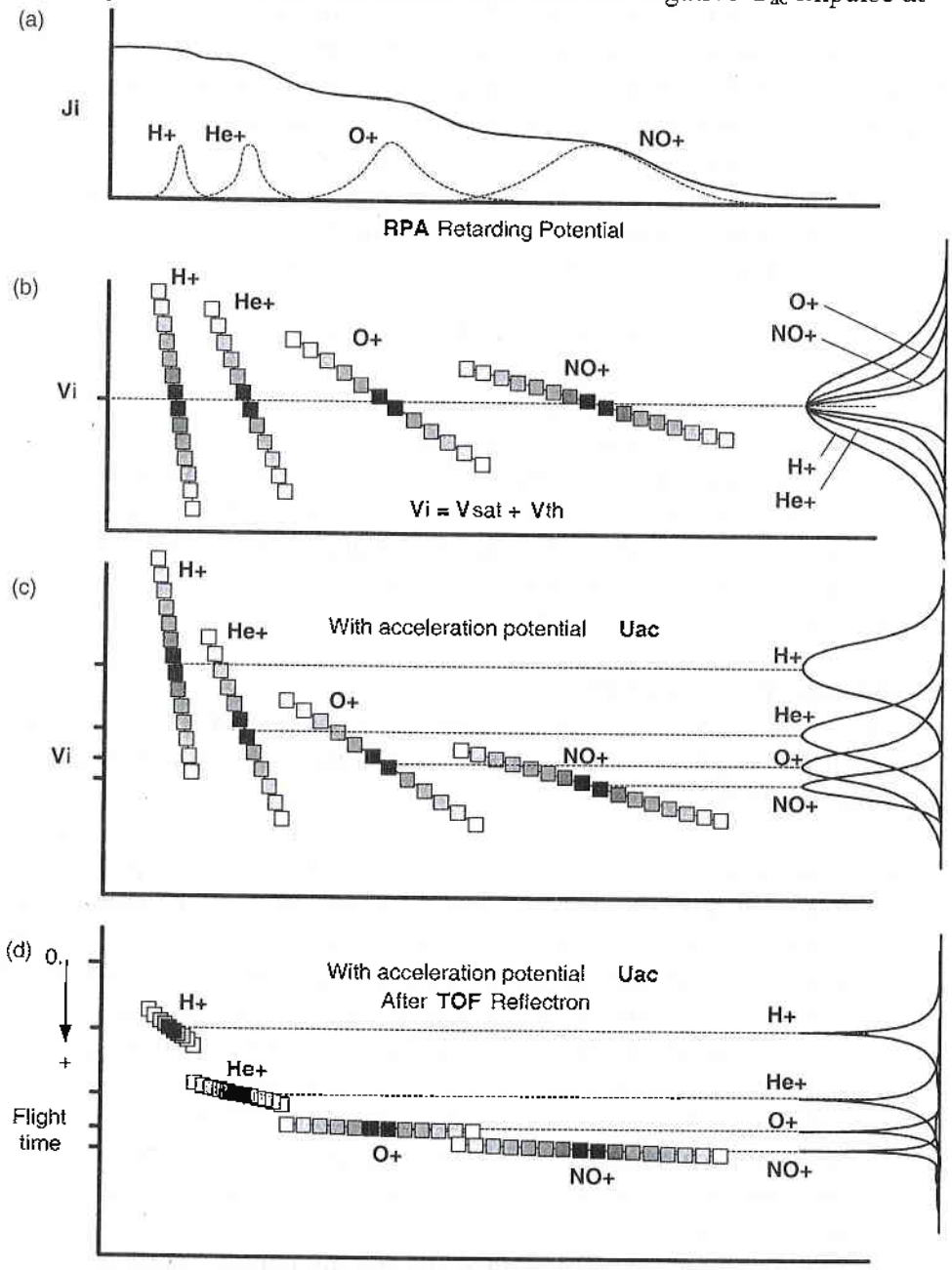

Fig.1

the moment t_o. The left-hand side Y-axis of the panel shows the relative flight time for different ions after t_o. Mass peaks become narrow, because of the used time compensation for different ions inside the reflectron flight space (faster ions with equal mass fly at longer distances than slower ones) [8]. Ram ion drift $\mathbf{V}_{d\parallel}$ shifts mass peaks toward shorter ($\mathbf{V}_{d\parallel}>0$) or larger ($\mathbf{V}_{d\parallel}<0$) flight times. The changes in satellite skin potential ($U_{sat}<0$) affect the relative distance between the peaks while added ion speed becomes proportional to $\sqrt{(2e(U_{ac}+U_{sat})/m_i)}$. To obtain V_i and U, let us consider that two ion species are observed in the mass spectrum. If we assume L to be the ions flight distance we can write for the two observed ion species:

$$(1) \qquad (L/t_1)^2 = V_i^2 + 2cU/m_{i1} \qquad (L/t_2)^2 = V_i^2 + 2eU/m_{i2}$$

These equations (1) could be solved together for $V_i=(V_{sat}+V_{d\parallel})$ and $U=(U_{sat}+U_{ac})$. With accurate attitude information for V_{sat} and amplitude of U_{ac} a correct value for $V_{d\parallel}$ and U_{sat} could be found. More than two registered ion mass peaks will increase the accuracy of measurement. In conclusion, if we neglect T_i measurements, TOF reflectron mass-spectrometry could be an effective method for ram drift velocity measurements.

INSTRUMENTATION

The space application of the measuring technique of TOF/IDM mass reflectron proposed here could be achieved as flight instrument limited by the following factors:

- Input ion flow $N_i.V_{sat}$ at ionospheric heights varies approximately from 10^8-10^{12} (particles.s^{-1} .cm^{-2}) for 10^2-10^6 cm^{-3} of ambient ion density. Input modulation of this flow reduces it from 10^1 to 10^5 possible counts during mass spectrum registration. In addition, the transparency of the whole system and the effectiveness of the MCP registration could reduce this count rate by a factor of about 10-50.
- A maximum count rate for the MCP registration module of up to 10^8counts/s becomes the absolute upper limit of about 5.10^3 counts per mass-spectrum, if the mechanical and electrical parameters of the TOF section refer to a 50μs maximum flight time. It is more realistic to assume $1\text{-}2.10^3$.
- The direct solar UV irradiance and the high-energy particles impact cause background noise in the MCP module. High quality optical trap for UV and shielded MCP module have to be used.

The combined influence of these factors decreases the threshold level sensitivity for single mass-spectrum registration. To expand the dynamical characteristics of the instrument, an accumulation of the counts for repetitive mass-spectra registration and/or a parallel current mode for MCP could be used.

A sketch of the possible solution for mechanical design of the sensor is shown in Fig.2. As it can be seen from the side view of the instrument, the X-axis is aligned along the satellite velocity vector V_{sat}. On the upper part of level **A-A,** the schematic configuration of the IDM sensor with five collector segments is shown. A square input aperture is used to collimate input ion flow before reaching the collector's surface. Grounded grids G_1 and G_2 provide field-free drift space inside the IDM sensor. The input ion flow enters drift space with an angular offset from the X-axis due to the transverse ion drift component. In result, measured current ratio from opposite collector pairs C_1/C_3 is a proportional production of the arrival angle of input ion flow in the X-Y plane (C_2 and C_4 are not seen). Grid G_3 could be grounded or slightly positive to prevent the light ions from reaching the collectors in the special IDM mode [5]. Suppresser grid G_4 has constant negative potential to minimize the photoemission current from the collector surface. A central collector C_5 with adjacent segments could be used for fast total ion current measurements and absolute in-flight calibration of the TOF mass-spectrometer [6]. In the middle of the C_5, along the X-axis, an axial input hole for the TOF section is made. Now let us consider the TOF section operation. A small part of the input ion flow enters the TOF section through input modulator G_5. The TOF section consists of two major stages: free field (G_6, G_7) drift space with length **L** and reflectron section with length **d.** G_8 grid is under positive potential U_r. Chevron type dual micro channel plates with a central hole are used for incident ion detection. The TOF section is continuously connected to a negative potential U_m where $U_m << U_{ac}$ (fig.3), while modulator G_5 is continuously under U_{ac} potential. If we assume U_{ac}=-10v the single mass spectrum duration is about 50μs if L+d is about 0.25m.

At moment t_o, the ions enter G5 volume, accelerated with energy of 10eV in addition to their ram energy in the satellite frame of reference [fig.3]. After some time t_{mod} to the end of mass registration, we close switch SW1 of G5 modulator to U_m and the rest of incoming ions will be accelerated to energy of about eU_m. During this time, a portion of ions from the internal volume of the modulator will enter the TOF section, accelerated only to the energy of 10eV. Within the next 50μs the TOF ion mass

spectrum of this portion is registered on MCP. If we accept having 100 registered points on the spectrum, a 500ns count window for MCP has to be used. To minimize time spread of input ion impulse within the registration period of 50μs, the TOF section potential is settled to $U_m << U_{ac}$. During ion mass spectra registration of the input ion pulse with E_i=10ev, ions entering the TOF section will be accelerated to energy $E_{im}=cU_m$. These particles fly through the TOF section with energy sufficient enough to overcome the positive potential U_r applied to G_8 ($E_{im} >> eU_r$). This type of modulation permits us to have in less than 100ns, ion pulses available for TOF mass-spectrometry. In parallel, registration of mass spectra in current mode of operation for an MCP with fast ADC registration boosts the actual output dynamics and sensitivity of the method. Similar modulation technique has been used for the energy-mass analyser KSANI on the IC-24 satellite [6]. To prevent the influence of incident solar ultraviolet radiation, UV light traps have to be used to minimize scattered UV before reaching the MCP module. Suppresser grid G_9 with small negative potential prevents the photoemission electrons emitted from the light trap section to reach the MCP sensor. Single ion mass TOF spectra registration could be repeated an appropriate number of times to optimize threshold sensitivity level. An adaptive algorithm to input ion flow parameters could be used to provide for flexible characteristics of the instrument and onboard data processing.

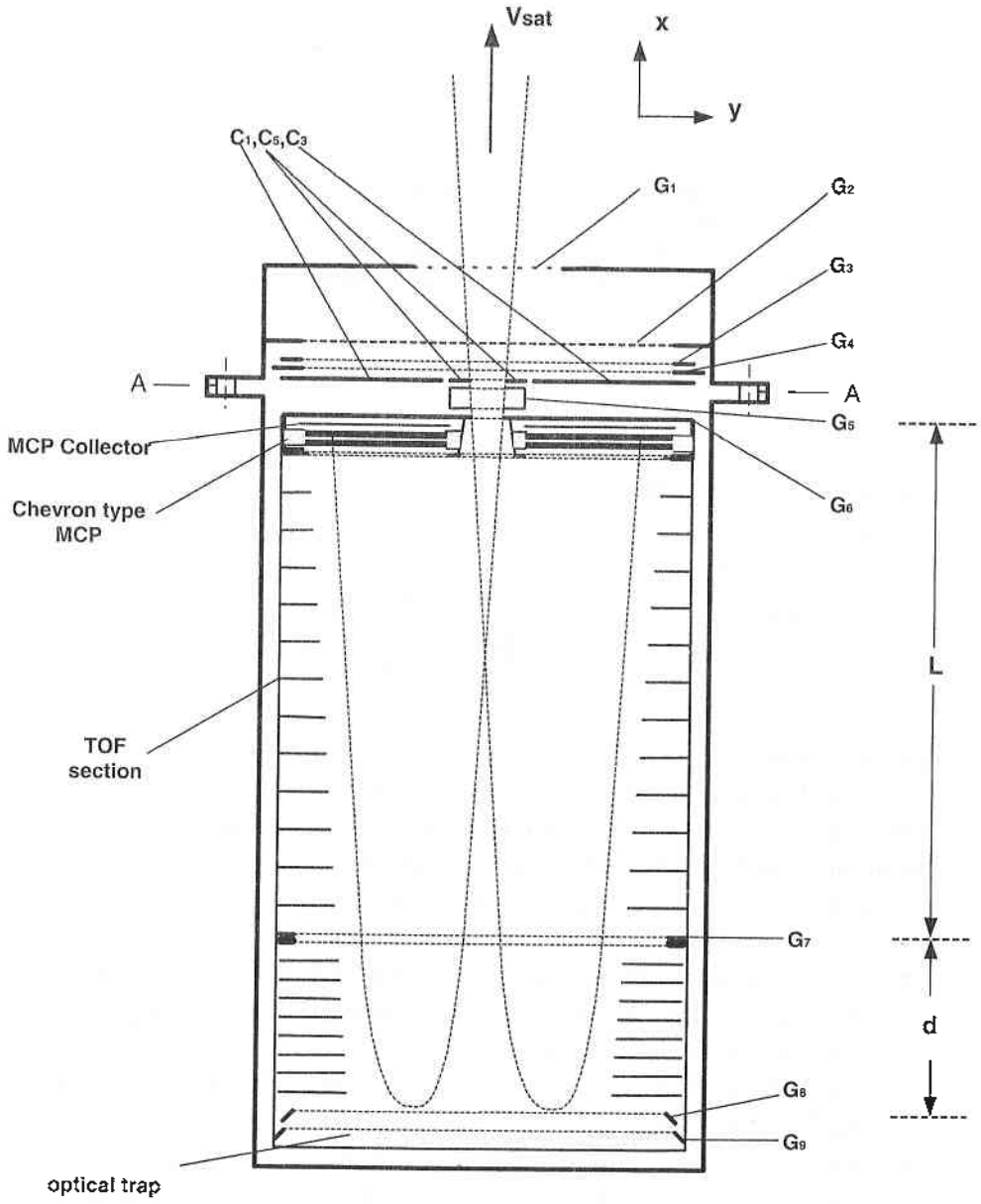
Vsat
x
y
C1,C5,C3
G1
G2
G3
G4
A
A
G5
MCP Collector
Chevron type
MCP
G6
L
TOF
section
G7
d
G8
G9
optical trap

Fig.2

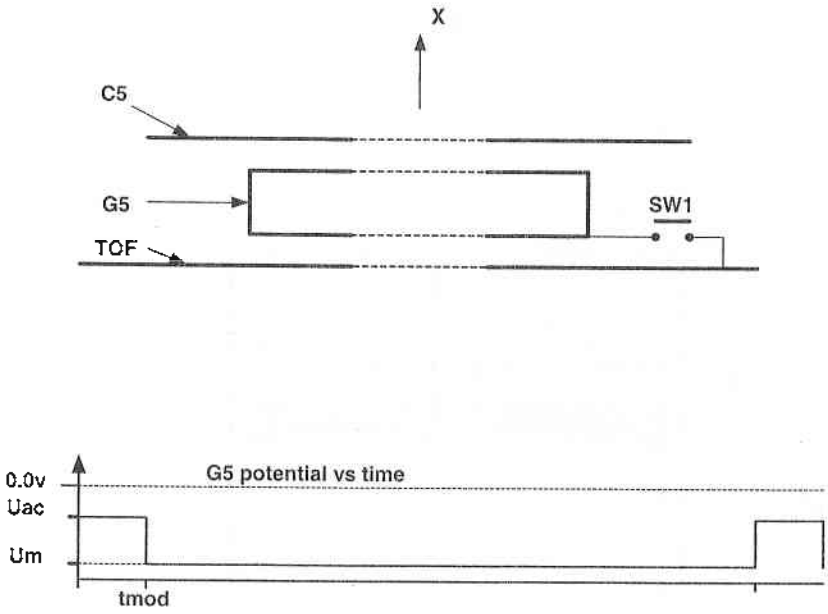

Fig.3

CONCLUSION

The most important reason to evaluate the IDM/TOF measuring technique proposed here is to combine high-speed IDM transverse ion drift measurement with the high-speed performance of Time-of-Flight mass-spectrometry. The main objectives could be as follows:

- With an appropriate operation mode for TOF section it is possible to provide 1÷10ms (20÷200 shots) measuring time for a single mass-spectrum same as IDM opportunities
- The simplicity of equations (1) suppose onboard processing of the m_i, $Vd_{\parallel}$ and Usat
- The MCP sensor with centered hole combined with mass-reflectron section provides a good opportunity to prevent incident ions or UV radiation from reaching the registration module
- Continuous measurements of ion density irregularities by IDM could be successfully used for in-flight calibration of the mass-spectrometer

References

1. S.P. Korolev activity in documents, Moskow, Nauka, 1980
2. Y.I.Galperin et al., Direct measurements of ion drift velocity in the upper atmosphere during a magnetic storm, Kossm.Issl., 11, 273, 1973.
3. W.B.Hanson and R.A.Heelis, Technics for measuring bulk gas moution from satellites, Space Sci. Instrum., 1, 493, 1975.
4. L.G.Bankov et al., An instrument for total ion drift velocity measurements aboard the Intercosmos Bulgaria-1300 satellite, Adv. Space Res., 2, 71, 1983.
5. L.G. Bankov et al., A study of the retarding potential influence on transverse ion drift velocity measurements by means of ion drift meter onboard ICB-1300 satellite,
6. L.G.Bankov et al., Critical ionization velocity CIV experiment XANI onboard the Intercosmos 24-ACTIVE satellite, Adv.Space Res., 13, 10, 193, 1996.
7. D.L.Cookel and C.J.Roth, The digital ion drift meter on CHAMP, status, calibration and data, 3M41C, 2002 AGU Spring meeting.
8. B.A.Mamirin and D.V.Shmik, Linear mass-reflectron, JETPhys., 5, 76, 1500, 1979.
9. Managadze N.G. et al., Quantitative analysis of metal alloys, ceramics, minerals without standard saples with help of compact laser TOF mass-spectrometer, 45 Conference of ASMS, Palm Springs, USA, 1997.

ИЗМЕРВАНЕ НА ЙОННИЯ ДРЕЙФ В ЙОНОСФЕРАТА С ИЗПОЛЗВАНЕ НА РЕЖИМ ВРЕМЕ ЗА ПРЕЛИТАНЕ

Л.Банков и А.Василева

Резюме

През последните 30 години измерванията на йонния дрейф бяха много мощен начин за изучаване на динамиката на земната йоносфера в контекста на процесите на слънчево-земните взаимодействия. В настоящата работа ние предлагаме комбинирано използване на електростатичен рефлектрон с време за прелитане (Time Of Flight– **TOF**), като част от модифициран йонен дрейфметър (Ion Drift Meter - **IDM**) за едновременно определяне както на паралелната така и на напречната скорост на йонния дрейф. Това на практика би могло да сведе измервателната методика до използването на един общ датчик **TOF/IDM**.

Bulgarian Academy of Sciences. Space Research Institute.
Acrospace Research in Bulgaria. 18. 2003. Sofia

ON SOME PROBLEMS OF THE IMPLEMENTATION OF MOVING TARGET INDICATION SYSTEMS IN SMOOTH SCANNING RADARS [+)]

V. Damgov, A. Karamishev

Space Research Institute – Bulgarian Academy of Sciences

Abstract

The paper is dedicated to the problem for selection of passive noise correlation function form and the influence of antenna scanning on the improvement factor assessments of moving target indication systems in smoothly scanning radars.

Analysis

The design methodology of modern scanning radars is mainly directed to the problem of moving targets' effective detection. A number of fundamental monographs (see [1], [2], [3], [4]) and a persistently increasing number of papers are devoted to the theory and design of moving target indication (MTI) systems. Lately, permanent scientific interest in the problem is being witnessed.

An MTI system consists of (cf. Fig.1): phase detector (FD) with a noise phase correction device (NPCD), rejection filter (RF) and integrator (accumulator) with a threshold device.

The system's main unit is RF that plays a central role in interperiod processing. RF increases the signal-to-noise ratio and decorrelates noise in the compensation process.

The improvement factor v is to be regarded as a universal quality index for the MTI systems [3]. The improvement factor v also characterizes the quality of RF. The improvement factor v is defined as a ratio of the

[+)] Research supported by the "Scientific Research" National Council at the Bulgarian Ministry of Education and Sciences under Contract No.H3-1106/01

ratios of the signal's average powers and noise in the RF's output and input, accordingly:

$$v = \frac{\left(\overline{P}_s / P_N\right)_{out}}{\left(\overline{P}_s / P_N\right)_{in}}, \tag{1}$$

where $\left(\overline{P}_s / P_N\right)_{out}$ and $\left(\overline{P}_s / P_N\right)_{in}$ are the output and input power ratios averaged by all target velocities.

We discuss problems affecting the value of the RF factor v of the MTI systems in smoothly scanning radars, which are insufficiently highlighted in literature, namely: the selection of the interperiod correlation function form of passive noise and the influence of antenna beam scanning. Different authors are unanimous on the possibility for the form of the fluctuation interperiod correlation function to be approximately presented by an exponent (cf. [2], [6]):

$$r^s_{k,l} = \exp\left(-|k-l|\frac{T_p}{\tau_s}\right), \tag{2}$$

where T_p is the period of the radar pulse sequence and τ_s is the correlation time of the reflected signal fluctuations. However, an uncertainty exists on the problem for the form of the passive noise interperiod correlation function. Some authors are advocates of the exponential approximation (cf. [2], [6], [8]), i.e.

$$r^N_{k,l} = \exp\left(-|k-l|\frac{T_p}{\tau_N}\right), \tag{3}$$

where τ_N is the correlation time of the passive noise fluctuations. While other authors (cf. [1], [3], [7], [8]) recommend an approximation by a Gaussian curve:

$$r^N_{k,l} = \exp-\left(|k-l|\frac{T_p}{\tau_N}\right)^2. \tag{4}$$

When the form of the correlation function is taken to be of form (3), the optimal RF consists of a device carrying out a one-time overperiod subtraction (OTOPS) with attenuation in the holding channel that corresponds to the coefficient of the noise interperiod correlation (cf. [2], [4]).

When using Gaussian correlation function, the RF structure that provides an optimal compensation is known only in a particular case $r_N \to 1$ and is coming to a OTOPS with maximal frequency rate $m = L - 1$, where L is the number of pulses in the package (see [2], [4]).

In coherent-pulse radars with frequency repetition (F_r) of the order of hundreds of Hz to units of kHz, OTOPS implementation devices with different frequency rates m are widely applied as RFs. At that, the value of v in the output is:

$$v = \frac{\sum_{k=1}^{m+1}\sum_{l=1}^{m+1} C_m^{k-1} C_m^{l-1} (-1)^{k+l} e^{-i(k-l)(\Delta\nu - \Delta\varphi)} r_{k,l}^{s}}{\sum_{k=1}^{m+1}\sum_{l=1}^{m+1} C_m^{k-1} C_m^{l-1} (-1)^{k+l} e^{-i(k-l)(\Delta\psi - \Delta\varphi)} r_{k,l}^{N}}, \tag{5}$$

where C_m^{k-1} and C_m^{l-1} are binomial coefficients, $(\Delta\nu - \Delta\varphi)$ and $(\Delta\psi - \Delta\varphi)$ are Doppler phase accumulation for the signal and the noise during the radar's time T_p. Making a correlation of the noise phase Doppler shift $\Delta\varphi = \Delta\psi = \Omega_{DN} T_p$, the denominator in (5) takes real value components.

Comparative assessment of v for two utmost forms is to be made under one and the same noise correlation time, i.e.

$$\int_0^\infty e^{-\tau} d\tau = \int_0^\infty e^{-\beta^2 r^2} d\tau . \tag{6}$$

The condition is fulfilled at $\beta = \frac{\sqrt{\pi}}{2}$. We obtain:

$$r_{k,l}^{e} = e^{-\frac{|k-l|T_p}{\tau_N}} \quad \text{and} \quad r_{k,l}^{G} = e^{-\left(\frac{\sqrt{\pi}}{2}\right)^2 \left(\frac{|k-l|T_p}{\tau_N}\right)^2}. \tag{7}$$

A diagram of the RF factor v at m = 1, 2, and 3 for the exponential and Gaussian approximation is given in Fig.2 (see v_{exp} and v_G). When increasing the RF elements number, the obtained computed v value for the Gaussian form is larger by 20 to 50 dB in comparison with the exponential one, all other conditions being equal. This fact could be attributed to the singularity of the Gaussian random processes.

Considering from the physical point of view the real form of the interperiod correlation function should be a compromise between two utmost forms. The experimental study (cf. [9], [10]) has shown that the correlation function is decreasing according to the dependence ~ $\frac{1}{\omega^4}$. An exponentially-parabolic function of the following type corresponds to the conditions mentioned:

$$r(\tau) = (1 + b\tau)e^{-b\tau} = \left(1 + b|k - l|\frac{T_p}{\tau_N}\right)e^{-b|k-l|\frac{T_p}{\tau_N}}. \quad (8)$$

The condition for spectrum identification for the exponential and Gaussian functions is fulfilled for the value $b = 2$.

The curves corresponding the to RF factor v dependences for exponentially-parabolic form are also shown in Fig.2 at OTOPS frequency rate m = 1, 2, and 3 (cf. v_{ep}). In this case, computed v values take intermediate position being closer to those for Gaussian approximation and have to be considered as the most likely ones.

One of the basic factors determining the value of the passive noise interperiod correlation coefficient is the antenna motion while scanning (cf. [2], [3], [7]). While scanning, a renovation of the elementary reflectors composition takes place, so that their total number remains one and the same at times t and $t + \tau$. The bigger the τ, the lower the succession.

When the antenna beam diagram is approximated by a Gaussian curve, the corresponding correlation function can be presented as follows:

$$r_a(T_P) = e^{-1{,}57\left(\frac{6\eta T_p}{\theta_{0.5}}\right)^2}, \quad (9)$$

where η reflects the radar antenna revolutions per minute.

Taking into account the reflectors' chaotic shift and the renovation because of diagram scanning, as well as the independency of those two physical processes, the background correlation function can be presented as:

$$r_{back}(\tau) = r_N(\tau).r_a(\tau). \quad (10)$$

Further on, an exponentially-parabolic approximation expression like (8) will be used when analyzing the influence of antenna beam diagram scanning. Fig.3 shows the dependence of the v factor for two-star RF (m =

2), that has been calculated using the expression (5) for strong ($\tau_N = 10ms$) and weak ($\tau_N = 25ms$) correlated noise at resolution velocities of $\eta = 3$ and $6\,\text{min}^{-1}$. For the sake of comparison, the maximal attainable factor v values with motionless antenna are shown as well ($v_{\max reach}$).

It is seen from the diagram in Fig.3 that antenna motion results in decreasing of the v factor values. In this particular case, the decrease is 4 dB at $\eta = 3\,\text{min}^{-1}$ and 10 dB at $\eta = 6\,\text{min}^{-1}$.

An averaged v factor is most often used in practice that is calculated on the basis of expression (5). According to [3], the numerator in (5) is changing by a constant coefficient, as follows: 1 for $m = 1$; 3 for $m = 2$ and 10 for $m = 3$. Fig. 4 shows the dependence of the averaged v factor of a two-star RF on passive noise correlation time for the cases of motionless and moving antenna with $\eta = 6\,\text{min}^{-1}$.

The exponentially-parabolic form determines again an intermediate position. When noise correlation time increases, scanning influence increases as well. The latter can be explained by decorrelation and widening of the noise spectrum.

Conclusion

The basic conclusion is that the advisable form of the passive noise interperiod correlation function is the exponential-parabolic form.

The computed values for the improvement factor v of the order of 40-50 dB are in good coincidence with the data published for smoothly scanning radars.

References

1. М. Сколник, Справочник по радиолокации – том 1, Превод с английского, Москва <<Сов. радио>> 1976.
2. Орхименко А. Е., Основы радиолокации и радиоэлектронная борба, В. И. МОССЕР, Москва, 1983.
3. П. А. Бакулев, В. М. Степин, Методы и устрийства селекции движущихся целей, М., <<Радио и связь>>,1986.
4. Кузьмин С. З., Основы проектирования систем цифровой обработки радиолокационной информации, М., Радио и связ, 1986.
5. А.Е.Охрименко, И.Т.Тосев, Анализ характеристик обнаружения систем междупериодной обработки, М., Радиотехника и Електроника, Т.16.,N 1, 1971.
6. Современная радиолокация. Перевод с англ. Под ред. Ю. Б. Кобзарева, М., <<Сов. радио>>, 1969.

7. Винокурова В.И., Морская радиолокация, Лснинград, <<Судосро-ение>>, 1986.
8. Handle Eberhard, Modelle für Radarstörechs (clutter) und Verglelcmit Mebergabnissen. "AEÜ", 1972; 26, №4.
9. Адрианов В. А., Арманд И. А., Кабардина И. Н., Рассеяние радиоволн подстилающей поверхностью с растительным покровом, Радиотсхника и электроника, АН СССР, №9, 1976.
10. Кулемин Г.П., В.Б.Разказовский,Рассеяние милиметроьіх радиоволн поверхности земли под малым углами, Киев, Наукова дума, 1987.

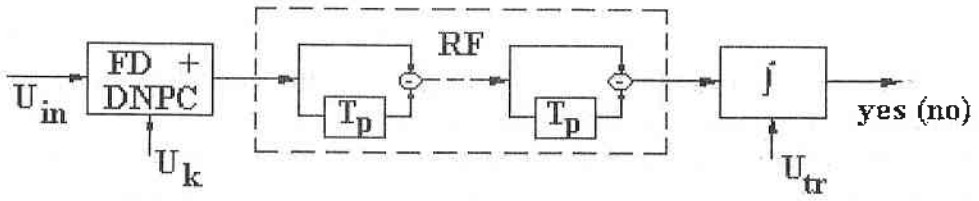

Fig.1

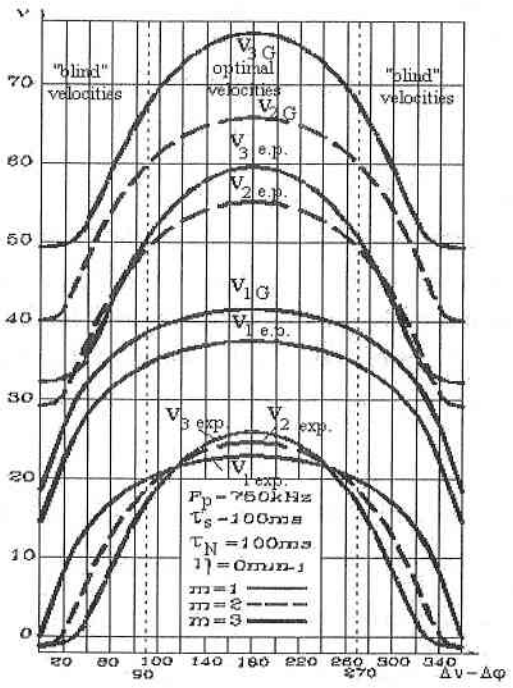

Fig.2

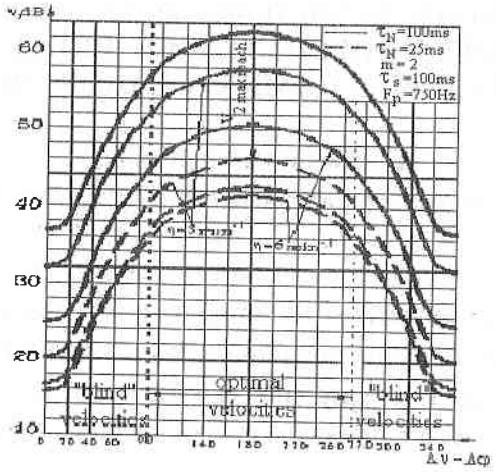
τ_N=100ms
τ_N=25ms
m = 2
τ_g=100ms
F_p=750Hz
60
50
40
30
20
10
"blind" velocities
optimal velocities
"blind" velocities
Δv – Δφ

Fig.3

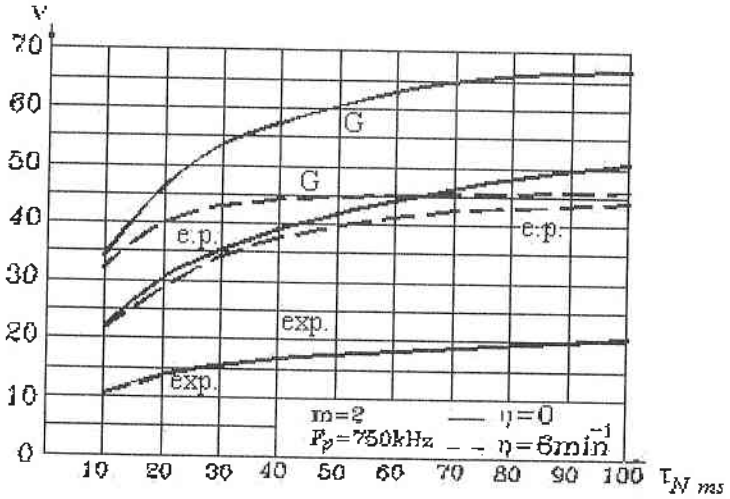
V
70
60
50
40
30
20
10
0
G
G
e.p.
e.p.
exp.
exp.
m=2
F_p=750kHz
η=0
η=6min^{-1}
10 20 30 40 50 60 70 80 90 100
τ_N ms

Fig.4

ВЪРХУ НЯКОИ ПРОБЛЕМИ НА РЕАЛИЗАЦИЯТА НА ИНДИКАЦИОННИ СИСТЕМИ С ДВИЖЕЩА СЕ ЦЕЛ В РАДАРИ С ГЛАДКО СКАНИРАНЕ [+)]

В. Дамгов, А.Карамишев
Институт за космически изследвания - БАН

Резюме

Статията е посветена на проблема за избор на формата на корелационната функция на пасивния шум и влиянието на сканирането на антената върху оценката на фактора на усъвършенстване на индикационни системи с движеща се цел в радари с гладко сканиране.

[+)] Research supported by the "Scientific Research" National Council at the Bulgarian Ministry of Education and Sciences under Contract No.H3-1106/01

Bulgarian Academy of Sciences. Space Research Institute.
Aerospace Research in Bulgaria. 18. 2003. Sofia

THE IONOSPHERE PLASMA STRUCTURAL PARAMETERS INVESTIGATION BY A LANGMUIR CYLINDRICAL PROBE ELIMINATING THE SPACECRAFT FLOATING POTENTIAL INFLUENCE

Mariana Gousheva[1], Plamen Angelov[1], Plamen Hristov[1]
Boyan Kirov[2], Katya Georgieva[2]

[1] *Space Research Institute - Bulgarian Academy of Sciences*
[2] *Solar-Terrestrial Influences Laboratory - Bulgarian Academy of Sciences*

Abstract

The paper presents an analysis of some problems due to the influence of the spacecraft floating potential as well as the analyzing voltage at the ionosphere plasma structural parameters investigation by cylindrical Langmuir probe. A computer simulation using a new high-precision method for periodical measurement of the Langmuir cylindrical probe floating potential when measuring the probe collector current is presented. The advantages of the presented method, which is suitable for measurement of all parts of the V-A probe curve, are discussed.

1. Introduction

The spacecraft as a body submersed in plasma is electrostatically charged under the influences of various kinds of currents. In the static state, the spacecraft is charged to some balanced potential φ_s where the summary current of the body is $\sum I \approx 0$ [1]. φ_s can vary within a wide range taking positive or negative values because the body's surface is under the direct impact of the charged particles streams and electromagnetic radiation. The changes of φ_s are a considerable source of errors as they distort the measurements and sometimes make them impossible because the analyzing control voltage U to the Langmuir cylindrical probe (CLP) electrodes is passed in respect to φ_s. For this reason, three cases are possible:

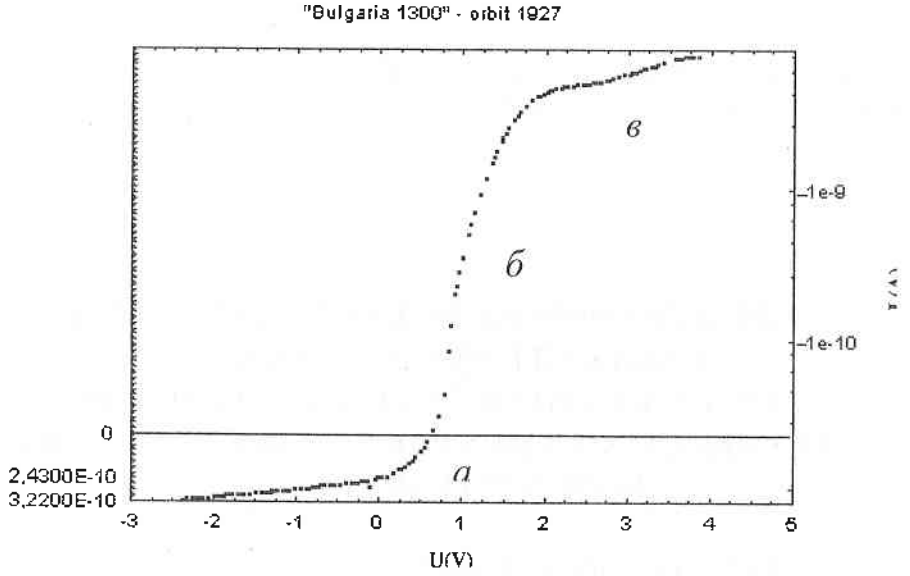

Fig. 1

1 – the measured current is positive: this means that $\varphi_в$ is strongly negative and U continues to be all the time negative compared to the plasma.

2 – the measured current is negative: this means that $\varphi_в$ is strongly positive and U continues to be all the time positive compared to the plasma.

In both cases there is no other possibility but to measure the fluctuations of ion and electron density. In such cases we do not use linear voltages but fixed ones to measure current fluctuations. This makes it possible to measure quick density fluctuations having no information about electron temperature.

3 – the measured current changes its sign: in this case, full analysis of the plasma characteristics is possible.

2. Space experiments results: some CLP measurement problems

The satellite experiments continue to the end of the satellite's life and the measurements are integral. This makes it possible, on the one hand, to carry out scientific research and, on the other hand, to perform statistical analysis. An ideal V-A curve is shown in Fig. 1. It consists of three typical parts [2]: *а* - ion saturation, *б* - electron retarding and *в* - electron saturation.

The V-A curves from many experiments are shown in Figs. 2, 3 and 4.

Here, two problems can be formulated:

- strong influence of the φ_S on the measurements;
- U with constant amplitude and continuance.

In paper [3], the authors present a method for periodical measurement and control of φ_{clp}.

The method is practically based on two principles:

- From time to time, 16-bit precision measurement and control of φ_{clp} for a zero probe current (testing cycle).
- CLP electrodes control by ($U - \varphi_{clp}$) at the time of the next measuring cycle.

3. CPL collector current measurement: algorithm and computer simulation.

The structural graph of the CPL collector current measurement algorithm is shown in Fig.5. It includes a testing and a measurement cycle.

In the figure: Io – the current for the analyzing voltage $U=\varphi_{clp} - 4$ V; I_1 and I_2 – currents from the electron retarding part of the V-A curve; U_1 and U_2 – corresponding voltages; c_1 , c_2 , c_3, c_4 – constants (determined by digital experiments); U_{start} , U_{end} , U_{slope} – start, end and limits of U variations.

The next figures 6 (a-f) show a computer simulation of the algorithm operation.

Let plasma density at the start of operation be $N_i=N_e=10^8$ m^{-3}, plasma temperature T_e=1000 K and ion mass M_i =16 a.m.u. (O^+) where the satellite's potential is $\varphi_s = 0$ V. In the beginning, we change U from –8 V to +8 V to determine φ_{clp} (Fig.6a). φ_{clp} is determined on 0,25 V, so we change U from (φ_{clp} – 4V) to (φ_{clp} + 4V), i.e. from –4,25 V to +3,75 V (Fig.6b). The ion current amplitude is used to determine the two levels of I_1 и I_2 whose corresponding voltages U_1 and U_2 will be measured. Now U_{start}= –4,25 V and U_{end}= +1,28 V (Fig.6b, 6c). The parameters of the next U (U_{start}= –1V, U_{end} = +1.28V) already ensure an optimal result (Fig.6b, 6d) and will be repeated unless plasma parameters are not changed critically.

Let the satellite now enter into a region where plasma parameters change suddenly: $N_i=N_e=10^9$ m^{-3}, Te=10000 K, M_i =1 (H^+) and as a result φ_{clp} =3V. Naturally, U course will be determined as with the previous curves, i.e. U_{start} = –1,0V, U_{end} = +1,28V (Fig. 6c). The algorithm again operates in the same way: ion current is measured at U_{start}, the two levels of currents I_1 and I_2 are determined and the corresponding levels of U_1 and U_2 are measured. The parameters of the next U are computed: U_{start} = –5,82V, U_{end} = +4,11V.

Only one step is enough to compute U, covering all three parts of the curves (Fig.6f).

4. Results and discussion

An algorithm and computer simulation are developed for:

- a new high-precision method for φ_{clp} periodical measurement and control;
- adaptive control of the CLP collector current measurement.

From future space experiments with CLP we expect:

- periodic measurement of the highly-informative parameter φ_{clp};
- ultra sensitivity of the measurement tract;
- no switching scales transition processes;
- real V-A curves.

The use of active methods eliminates the necessity of physical phenomena monitoring. So we consider that the presented solutions, which pertain to the passive methods, will be further developed and approved in future. The CLP is included as an important component of the SPACE WEATHER program [4] at the International Space Station, where φ_S floats within a wide range ± 300 V.

References

1. Riedler W., K. Torkar M., Pedersen A. et al. Spacecraft potential experiment RON/RSA - IKI- CNES. Interball mission and Payload, 1995.
2. Gousheva M.N., P.S. Angelov, P.L. Hristov, B.B. Kirov, K.Y. Georgieva. Some problems in systems using cylindrical electrostatic probe for electron density and temperature measurement on spacecraft board. The Eleventh International Scientific and Applied Science Conference ELECTRONICS ET'2002, 25-27 September 2002, Sozopol, Book of Abstracts, p. 48.
3. Gousheva M.N., P.S. Angelov, P.L. Hristov, B.B. Kirov, K.Y. Georgieva. A method for measurement and control of the cylindric probe floating potential. An algorithm for control and measurement of the V-A curve. The Eleventh International Scientific and Applied Science Conference ELECTRONICS ET'2002, 25-27 September 2002, Sozopol, Book of Abstracts, p. 47.
4. Klimov V.A. et al. The use international space station infrastructures for space weather research. Presented at the COSPAR Colloquium "Plasma processes in the near-earth space: INTERBALL and beyond", 5-10 February, 2002, Sofia, Bulgaria, Abstracts, pp.76.

ЕЛИМИНИРАНЕ ВЛИЯНИЕТО НА ПЛАВАЩИЯ ПОТЕНЦИАЛ НА КОСМИЧЕСКИЯ АПАРАТ ПРИ ИЗСЛЕДВАНЕ НА СТРУКТУРНИТЕ ПАРАМЕТРИ НА ЙОНОСФЕРНАТА ПЛАЗМА С ЦИЛИНДРИЧНА СОНДА НА ЛЕНГМЮИР

Марияна Гушева[1], *Пламен Ангелов*[1], *Пламен Христов*[1]
Боян Киров[2], *Катя Георгиева*[2]

[1] Институт за космически изследвания
[2] Централна лаборатория за слънчево-земни въздействия

Резюме

В настоящата работа са анализирани проблемите от влиянието на плаващия потенциал на космическия апарат и анализиращото напрежение при изследване на структурните параметри на йоносферната плазма с цилиндрична сонда на Ленгмюир. Показана с компютърна симулация, използваща нов високоточен метод за периодично измерване на плаващия потенциал на цилиндрична сонда на Ленгмюир при измерване на тока от колектора на сондата. Дискутирани са преимуществата на предложения метод за измерване на всички участъци от волт-амперната характеристика на сондата.

Bulgarian Academy of Sciences. Space Research Institute.
Aerospace Research in Bulgaria. 18. 2003. Sofia

SIMPLE ADAPTIVE METHOD FOR USE OF CYLINDRICAL LANGMUIR PROBE IN A WIDE RANGE OF SATELLITE SKIN POTENTIAL

Bankov L.G., Vassileva A.K.

Space Research Institute – Bulgarian Academy of Sciences

Abstract

Spacecraft charging effects have been studied since the beginning of the first satellite-borne experiments in space. Here, both skin and internal dielectric charging effects are meant. The first high-altitude flights showed that these effects could become of great importance for the proper operation of onboard electronic equipment. In some cases, satellite skin potential could reach relatively high levels, for example at geostationary orbits. Completely new type of problems could appear when large bodies like manned spacecrafts, space stations at docking procedures etc. have to operate for a long period on orbit with high reliability of the onboard equipment for reason of crew safety. Here, we propose very simple equipment for wide range measurements of the satellite skin potential using Langmuire probe in a special operation mode.

INTRODUCTION

The skin potential of the charged body in space depends on the balance of the inflow and outflow currents to its surface. The physical characteristics of the surrounding plasma and the different materials of the surface have considerable input to this balance. Large bodies in space like manned spacecrafts, space stations or large geostationary satellites can form significant potential drops between different parts of their constructions. Very often this could be a problem for onboard electronics and/or other charge-sensitive devices. A simple solution could be a distributed system for skin potential measurement and control sensors spread on the surface of the spacecraft unit. Here, the proposed Langmuir probe for spacecraft skin potential measurements is working close to a zero detection system mode, which simplifies the measuring techniques and onboard electronics.

INSTRUMENTATION

The cylindrical Langmuir probe (**CLP**) is a very extensively used instrument for electron density N_e, electron temperature T_e and satellite skin potential U_{sat} measurements because of its simplicity and relatively high accuracy [1,2,3]. Here, we will discuss the basic aspects of the CLP application for ionospheric plasma diagnostics. I.Langmuir and H.Mott-Smith were the first to postulate plasma probe measuring technique in laboratory plasma in 1924 [4]. Briefly described, plasma probe diagnostics is based on electrometer measurements of the current from the conductive electrode in plasma as a function of the sweep voltage applied to it, which is often called volt-ampere curve. In Fig.1, a sketch of a typical V/A curve (J_{clp} vs U_g) from a cylindrical Langmuir probe operating onboard the satellite is shown. Four important regions could be identified on the volt-ampere curve, denoted by A,B,C,D, accordingly. Region A represents the ion saturation current from CLP at enough negative U_g at which all attracted ions reach the collector surface while the electrons are repelled from it. The relative changes in total ion current with U_g represent the changes in the effective ion collection surface of the probe. In the retardation zone B, the electrons with sufficient energy reach the probe surface. The probe potential at which J_{clp} becomes zero as a superposition of equal electron and ion currents to the probe surface is called floating potential U_{fl}. Near U_{fl} the rapid change in the probe current is a function of the effective retardation U_g for electrons where the Te determines the power of exponent in the theoretical expression of the V/A curve. A large Te value corresponds to a large retardation zone. In a close area of point C, the probe potential becomes positive in respect to the plasma and as a result, the probe current is almost caused by electrons attracted to the probe. This value of the U_g sweep, at which the probe potential becomes zero compared to the undisturbed plasma far from the probe is called satellite skin potential U_{sat}. A large positive potential U_g in the saturation region D causes the probe current to be ..... only by the attracted electrons on the CLP surface. To obtain T_e, N_e and U_{sat} values from the experimental C/V curve, a least square technique could be used to fit the theoretical expression for J_{clp}. It is important to note that large T_e values correspond to a large retardation zone and as a consequence on large U_{sat}-U_{fl} difference. In the Earth's ionosphere $|U_{sat}-U_{fl}|$ does not exceed 0.5÷0.6v. In the case of wide range measurements of the satellite potential U_{sat}, for example, from –200v to +200v, the $|U_{sat}-U_{fl}|$ difference becomes less than 0.5% of the desired range. Therefore, if we measure accurately U_{fl}, this in fact corresponds to a U_{sat} value with less than 0.5% accuracy in the whole targeted (-200v÷200v) dynamic region.

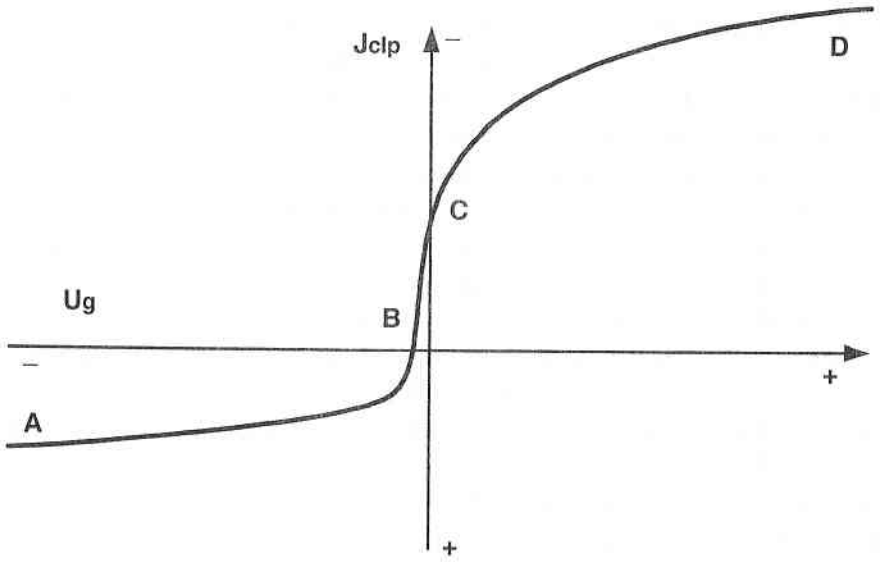

Fig.1

The basic assumption of the measuring technique proposed here is to measure U_{fl} as a zero J_{clp} current level detector with fixed sensitivity current-to-voltage converter. In the beginning of the operation cycle we use a CLP only as a rough zero current detector. In Fig.2, we show the schematic solution of the proposed instrument. CLP output is connected to the input of a current-to-voltage converter (**CVC**) with appropriate sensitivity. The output voltage of the CVC through a zero crossing voltage comparer (**COMP**) provides an opto-isolated logical output signal. This logical signal is used as an up/down switch of the counter (**COUNT**) whose output through a digital-to-analogue converter forms the U_g voltage sweep. The wide dynamic range of U_g is a function of the gain of the voltage amplifier (**AMP**). The high output voltage of the AMP stage is connected to the floating ground of the CVC to provide voltage offset in respect to the plasma. The DC/DC converter and the opto-isolated telemetry buffer output are used to protect onboard electronics. The operation principle of this instrument is quite simple. If the input CLP current passes through zero level at some $U_g=U_{fl}$ the output logical signal from the comparer reverses the counting direction of the counter, gain of the output amplifier stage and starts analog to digital conversion of the ADC block. Every passing through zero level current repeats this process in the downward direction and in fact

a current-to-voltage characteristic with a fine voltage sweep from the CLP in a digital form to the TM output. This part of the C/V curve could be successfully processed for N_i, N_e, T_e and U_{sat} [5]. When the bottom level of the counter is reached, logic control changes the gain and output voltage step to search for next $U_g=U_{fl}$ level. To minimize the error caused by the difference between Usat and Ufl some a shift in the zero level adjustment of the comparer can be applied. Time resolution of the method is limited from the clock (**CLK**) frequency and frequency band of the CVC. The input stage of the current-to-voltage converter has to be overload protected. A differential pair of high voltage transistors could be used. The dynamic range of this instrument could be extended by the special HV protected construction of the electronic block. The main objectives of this schematic solution could be realized in some part by a micro-controller unit (counter, DAC, TM output). This will not reduce significantly the used measuring algorithm. In some cases, low integration chips are better protected from the influence of high voltage static discharge, high level radiation etc. Either way, the electronics and CLP could be small enough to be spread at different locations on the surface of large body spacecrafts, space stations etc.

CONCLUSION

In the present paper a simple method of CLP application within a wide range of satellite skin potential values is proposed. This measuring technique could be an effective tool as a part of onboard control and safety systems.

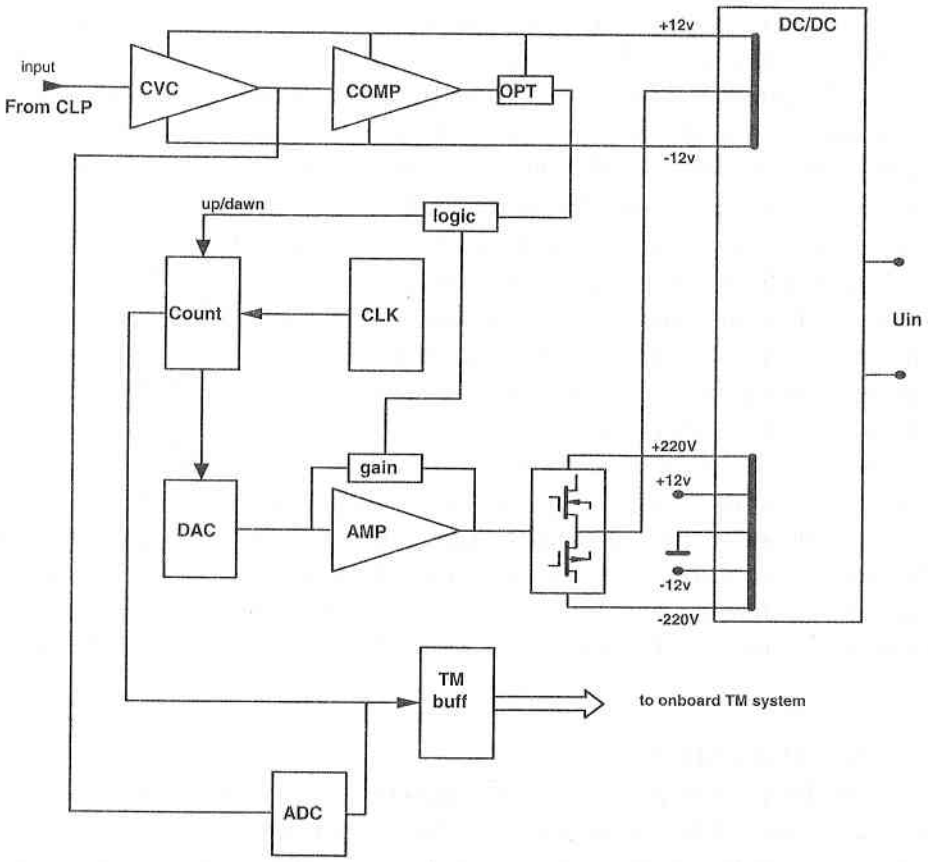

Fig.2

References

1. Brace L.H., R.F. Theis, and A.Dalgarno. The cylindrical electrostatic probes for Atmosphere Explorer-C,D,E , Radio Science,vol.8, 4, p.341, 1973.
2. Krehbiel J.P.et al., The Dynamics Explorer Langmuir probe instrument, Space Science Instrumentation, 5, 4, 493, 1981.
3. Bankov L.G. et al., An instrument for electron density and electron temperature measurements, N36160/reg. N61371/1983.
4. Langmuir I., Mott-Smith H.M., Sdudies of electric discharges in gases at low pressures, General Electrical Review, 27, 616, 1924.
5. Krehbiel J.P. et al., Pioncer Venus orbiter electron temperature probe, IEEE, 18, 1, 49, 1980.

ПРОСТ АДАПТИВЕН МЕТОД ЗА ИЗПОЛЗВАНЕ НА ЦИЛИНДРИЧНА СОНДА НА ЛЕНГМЮР В ШИРОК ДИАПАЗОН НА ИЗМЕНЕНИЕ НА ПОТЕНЦИАЛА НА СПЪТНИКА

Л.Банков и А.Василева

Резюме

Ефектите от зареждане на космическите апарати са били изучавани още с първите спътникови експерименти в космоса. Този проблем се разделя на външен и вътрешен (диелектричен) ефекти на зареждане. Първите високо апогейни полети показват, че тези ефекти биха могли да бъдат от изключителна важност за правилното функциониране на бордовата електроника на спътника. В някои случаи, потенциалът на повърхността на спътника може да достигне относително високи нива, например за геостационарни орбити. Напълно нов тип проблеми могат да се появят, когато големи тела като пилотируеми космически кораби, космически станции по време на процедури за скачване и т.н. трябва да функционират за дълъг период на орбита с висока надеждност на оборудването, гарантиращо безопасността на екипажа. В тази работа ние предлагаме много прост прибор за измерване на потенциала на повърхността на спътника в широк диапазон, като се използва сонда на Ленгмюр, като се използува специфичен режим на работа.

Bulgarian Academy of Sciences. Space Research Institute.
Aerospace Research in Bulgaria. 18. 2003. Sofia

SOME APPROACHES TO THE RESEARCH MODELS OF CHAOTIC PHENOMENA IN THE SOLAR SYSTEM

Kostadin Sheiretsky

Space Research Institute-Bulgarian Academy of Sciences

Abstract

Our solar system provides a plethora of examples of chaotic motion. The giant planets in our solar system are chaotic, as are the inner planets (independently). In extreme cases, chaos can disrupt some orbital configurations, resulting in the loss of a planet. The spin axes of planets may also evolve chaotically. Despite the variety and complexity of applications, we can introduce many of the concepts in solar system dynamics using the pendulum: phase space structure, periodic motion, and stability.

The physical basis of chaos in the solar system is now better understood: in all cases investigated so far, chaotic orbits result from overlapping resonances.

A series of remarkable features in the asteroid belt vividly illustrates the importance of dynamical chaos in the solar system. The distribution of semi-major axes of asteroid orbits contains a number of distinct gaps. These are called Kirkwood gaps, in honor of Daniel Kirkwood, who first identified them and noted that they occur at locations where the orbital period, T, which depends on the semi-major axis, would be of the form $(p/q)T_J$, where T_J is the orbital period of Jupiter and p and q are integers. The paper that ignited the modern era of work on the Kirkwood problem was Jack Wisdom's (1982) - first contribution to the study of the 3:1 mean-motion resonance at a = 2.50 AU. His startling results showed that an orbit at this resonance could remain quiescent, with a low eccentricity, e < 0:1, for more than 100,000 years, but also showing occasional surges lasting for about 10,000 years that would lift to a maximum value of about 0.35. Such a value is just sufficient to allow crossing of Mars' orbit, resulting in an eventual collision or a close encounter.

Further afield, about one new "short-period" comet is discovered each year. They are believed to come from the "Kuiper Belt" (at 40 AU or more) via chaotic orbits produced by mean-motion and secular resonances with Neptune. Finally, the planetary system itself is not immune from chaos. For example, Mercury, in 10^{12} years, may suffer a close encounter with Venus or plunge into the Sun. In the outer solar system, three-body resonances have been identified as a source of chaos, but on an even longer time scale of 10^9 times the age of the solar system.

The first striking example of chaotic behavior in the solar system was given by the chaotic tumbling of Hyperion, a small satellite of Saturn whose strange rotational behavior was detected during the encounter of the Voyager spacecraft with Saturn.

The equations of motion for the orientation of a satellite S orbiting around a planet P on a fixed elliptical orbit of semi-major axis a and eccentricity e (Figure 1) are given by the Hamiltonian:

$$H = \frac{y^2}{2} - \frac{3}{4}\frac{B-A}{C}\left(\frac{a}{r(t)}\right)^3 \cos 2(x - v(t)) \tag{1}$$

where $r(t)$ is the distance from the planet to the satellite, x gives the orientation of the satellite with respect to a fixed direction, $y = \frac{d}{dt}x$ is its conjugate variable, v is the true anomaly of the satellite, and A < B < C are the principal inertia moments of the satellite

When expanding the Hamiltonian with respect to eccentricity (e), which is supposed to be small, and retaining only the first order terms in eccentricity, one obtains:

$$H = \frac{y^2}{2} - \frac{\alpha}{2}\cos 2(x-t) + \frac{\alpha e}{4}\left[\cos(2x-t) - 7\cos(2x-3t)\right],$$
$$\alpha = \frac{3(B-A)}{2C}. \tag{2}$$

As a result of the transition between librational motion and rotational satellite motion, small chaotic zones appear. When perturbation size ε increases, resonant zones corresponding to the various possible resonant terms *cos* 2(*x*-*t*), *cos* (2*x*-*t*), *cos* (2*x*-3*t*) will overlap, giving rise to large-scale chaotic motion.

This is the case for Hyperion, where □e = 0,039. The resulting effect is that the rotational motion of Hyperion is not regular, and it becomes impossible to adjust any periodic or quasi-periodic model to its light curve.

They briefly recall a mathematical model introduced in (Celletti, 1990) to describe the "spin–orbit" interaction in Celestial Mechanics. Let S be a tri-axial ellipsoidal satellite orbiting around a central planet P (Figure1). Let T_{rev} and T_{rot} be the periods of revolution of the satellite around P and the period of rotation about an internal spin–axis. A p:q spin–orbit resonance occurs whenever:

$$T_{rev} / T_{rot} = p / q,\ p,q \in N, q \neq 0.$$

The equation of motion may be derived from the standard Euler's equations for a rigid body. In normalized units (i.e. assuming that the mean motion is one, 2□ / T_{rev} = 1) we obtain:

$$\frac{d^2x}{dt^2} + \varepsilon\left(\frac{1}{r}\right)^3 \sin(2x - 2v) = 0, \varepsilon = \frac{3(B-A)}{2C}. \quad (3)$$

We investigate numerically the stability of the periodic orbits. We denote by □*(p/q) the value of the perturbing parameter at which transition occurs.

The plot of □ (p/q) (Figure 2) shows that for low eccentricity values there is only a marked peak corresponding to the 1:1 commensurability (occurring when the periods of revolution and rotation are the same). Increasing the eccentricity, other resonances appear. Indeed, the 3:2 resonance can be observed at eccentricities larger than 0.01.

Prof. Damgov introduces a heuristic model for the discrete distribution of Solar system planets and the satellites' mean distances from the primaries.

Herewith, as a general model we take a periodical motion, that is the rotation of a charge at which an electromagnetic wave falls along the x-axis.

The charge motion equation is

$$\ddot{x} + 2\beta\dot{x} + \omega_o^2 x = eE_x \sin(\nu t - kx), \quad (4)$$

where E_x is the x-axis electrical field component and k is the wave modulus.

The solution of Eq. (10), describing a linear oscillator under wave action, is written in the form of a quasi-harmonic function

$$x(t) = a\sin(\omega t + \alpha),$$

where $a(t)$ and $\alpha(t)$ are the slowly changing amplitude and phase, $\omega = \nu / N$ is the charge periodic motion frequency, and N =1,2,3,... is an integer.

The examination of the stability solutions reveals that the stable oscillations amplitude a satisfies condition $J'_N(ka) = 0$.

Hence, the stationary charge oscillations can be realized for amplitudes a_i, belonging to a strictly defined set of amplitude values. The a_i values are determined by the Bessel function extremes, and may be presented as $ka_i = j_{N,i}$, where $j_{N,i}$ is the N-th order Bessel function argument value ka_i at the i-th extremum point. The Solar system planets' mean distances are presented on Table 1.

The unsolved problems in solar system chaotic dynamics are many. As yet, we have no relation for secondary resonances, where ejection time is a function of the Lyapunov time. Unlike the outer planets, the source of inner planets chaos has not been convincingly established.

References

1. Дамгов, В., Нелинейни и параметрични явления в радиофизически системи. Академично издателство "Проф. Марин Дринов" София, 2000
2. Celletti, A., Chierchia, L., Hamiltonian Stability of spin-orbit Resonances in Celestial Mechanics, CeMDA, 2000.
3. Murray, N., Holman, M., The role of chaotic resonances in the solar system. Astro-ph/0111602 v2, 2001.

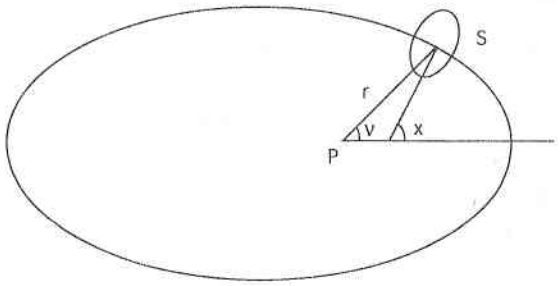

Fig. 1: The spin–orbit geometry.

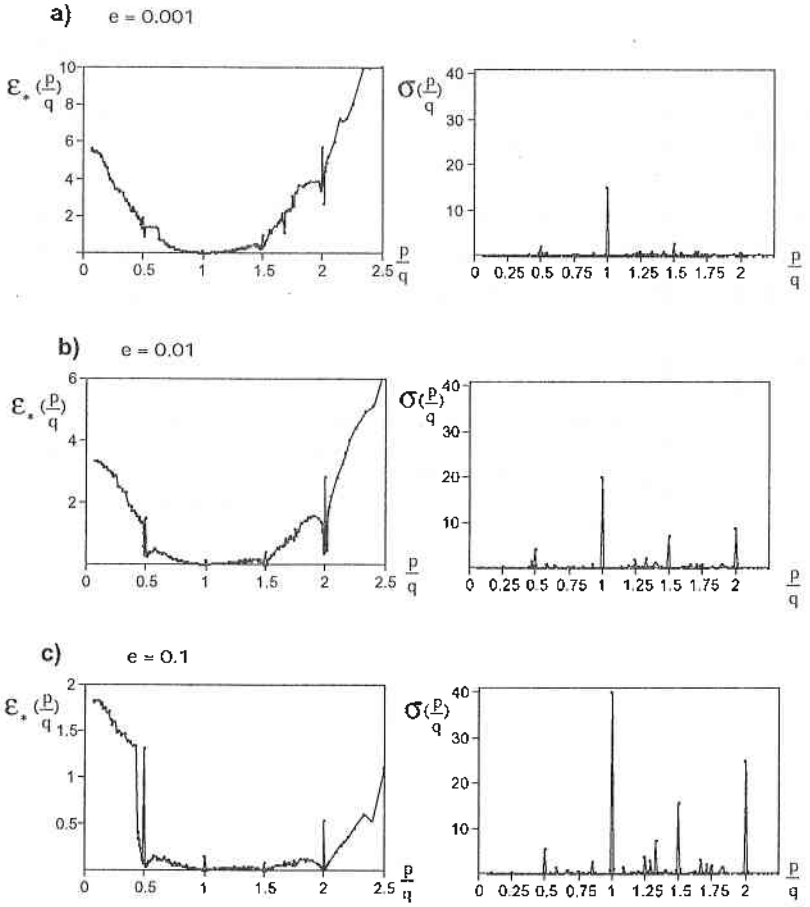

Fig. 5: Left panel: plot of □*(p/q) vs. p/q for the frequencies listed in the text; right panel: plot of the CSI □(p/q) vs. p/q for the same frequencies as in the left panel. a) e = 0.001, b) e = 0.01, c) e = 0.1.

Planets in the Solar system	Data from direct astronomical measurements of planet distances from the Sun (Allen, 1973) A.U.	Computed planet distances using Equation (65) of the "Oscillator-wave" model	
		i	a/j
Mercury	0.39	1	0.392
Venus	0.72	3	0.723
Earth	1.00	5	1.000
Mars	1.52	9	1.530
Asteroids	2.78	19	2.824
Jupiter	5.2	37	5.132
Saturn	9.55	71	9.474
Chiron (Collewll's objects)	13.71	104	13.689
Uranus	19.18	147	19.180
Neptune	30.03	232	30.035
Pluto	39.67	307	39.598

Tab. 1: Mean planet distances in the Solar system

НЯКОИ ПОДХОДИ ПРИ МОДЕЛНОТО ИЗСЛЕДВАНЕ НА ХАОТИЧНИТЕ ЯВЛЕНИЯ В СЛЪНЧЕВАТА СИСТЕМА

Костадин Шейретски
Институт за Космически изследвания – БАН

Резюме

Нашата слънчева система представя множество от примери за хаотични движения. Гигантските планети, както и вътрешните планети са подвластни на хаоса. В някои случаи хаосът може да разруши някой орбитални конфигурации, водейки до загуба на планета. Оста на въртене на планетите може също да еволюира хаотично. Независимо от разнообразието и сложността на хаотичните явления, ние можем да представим много от концепциите на динамиката на слънчевата система използвайки махало: Структурата на фазовото пространство, периодично движение и стабилност.

Bulgarian Academy of Sciences. Space Research Institute.
Aerospace Research in Bulgaria. 18. 2003. Sofia

COMPUTER PROCESSING OF THE MEASURED ELECTRON WORK FUNCTION ON THE SURFACE OF ANTIFRICTION MATERIALS

Yu.Simeonova, L.Dinkova, T.Grozdanova

Space Research Institute-Bulgarian Academy of Sciences

Abstract

The architecture of an automatic system for precise measurement of the contact potential difference with antifriction materials is represented in this work. Automating of this process provides the possibility to make experiments with different materials under the same conditions that on the one hand leads to simple comparability of the results and significant increase of the precision of the experiment.

Regardless of the great development of thribological science, a series of questions related to the nature of friction and wearing of materials remain obscure which is due to the complex character of the process of their mutual contact, most strongly manifested when working in extreme conditions and particularly with friction and space surroundings [1]. Here, alongside with the traditional frictional surface indices such as micro-geometry and micro-hardness, some physical and chemical parameters that determine its energy state have to be taken in mind. In this sense, the work function of the electron in metals can be used as energy state parameter determining the traditional method of measuring the contact-potential difference between the surface being researched and standard metal surface with constant electron work function [2].

The research of G.P.Shpenkov [3], D.N.Gorkunov [4], as well as some of our studies show that there is connection between surface wear resistance and electron work function in metals, alloys and more complex thribotechnical systems on a metal base. Our research experiments for thribocouples of metal-metal alloy and lead bronze-metal alloys show that when materials are in contact wear increases with increase of the electron

work function, and with decrease of their contact potential difference, accordingly.

There are a great variety of factors influencing the physico-chemical state of surface and electron work function. These factors are frequency and smoothness, microstructure and element composition in the presence of oxides and other secondary structures on the surface. To achieve the required precision in determining the contact potential difference and electron work function, especially in complex thribo-technical materials containing a great number of components, it is necessary to use precise registration methods and process large data array in measuring the contact potential difference [5].

In the present work, the architecture of an automatic system for precise measurement of the contact potential difference with antifriction materials is offered. The automatic system is based on a system determining the energy state of surface friction [6]. The recording device used so far in the methods for experimental determining of the electron work function and the antifrictional material surface is oscilloscope. We have introduced an analogue recorder and a personal computer in the accomplished automatic system. The structural diagram of the system is shown in Fig. 1, where: 1 - variable force of outer generator (F~); 2 - electromechanical fluctuating system (EMFS); 3 – electronic-measurement circuit; 4 - oscilloscope; 5 - analogue multiplexer; 6 – monitoring-storage circuit; 7 - analogue-to-digital converter and 8 - personal computer.

In the measurement process, digital ensemble accomplishments of the random process with sufficiently long accomplishment are recorded to be statistically correct. Some measurements have been made, whereas the length of one accomplishment is equal to 255 discrete values of the contact-potential difference, a couple of them for one and the same test specimen. This boosts the statistical fidelity of the signal's automatic digital processing.

The digital processing of measurements is accomplished in the following steps:

1. Scaling of the measured values. The scaling coefficient conforms to the coefficient of amplification and scaling of the scale in spectral measurements.

2. Two types of values are obtained in the process of measuring, stable and unstable. The stable are the real ones, that give us the correct measurement and the unstable are called noise. The noise value is eliminated from the digital signal by means of a filter. The filter sets a window, whose dimensions depend on the mean value of the contact

potential difference. The filter operates in following way: if, for a given specimen, the values are over twice greater or much less than the mean value, they are removed from the spectrum and they are not processed. The next operation is averaging of the values obtained after filtration and their graphic representation. Increasing the number of processing iterations results in increasing the precision of the result. This is achieved because of the fact that, with each subsequent iteration, more and more digital noise values are removed. The conditions under which measurement has been carried out are also important (room temperature; type of the generator - Functional generator 3325A, HEWLETT PACKARD; a source of constant voltage).

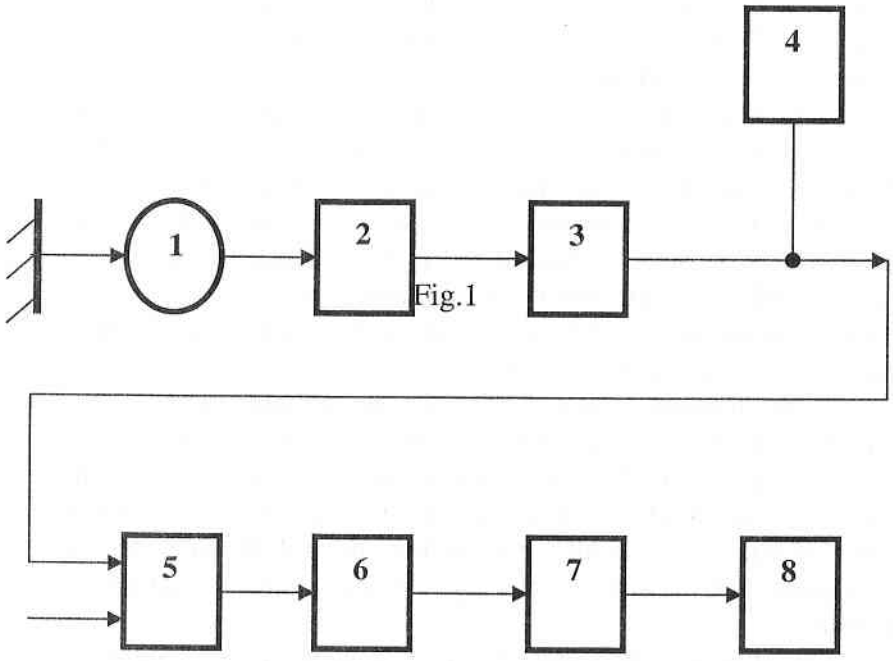

Fig.1

Fig.1

Conclusions:

Automating the process of measurement of the potential contact difference allows to perform experiments with different antifriction

materials under one and the same conditions. This provides a possibility for simple comparability of the measurement results. Besides, high precision of the results is achieved because the subjective factor (measurement by oscilloscope) is eliminated and in practice, a sufficient number of accomplishments for achieving the required statistic fidelity of the measurement results can be written.

References

1. Симеонова, Ю., М.Аструкова, Т.Грозданова, Л.Динкова, Характерни особености на трибологичните процеси във висок вакуум, Контакт 97, София, 1997.
2. Astrukova, M. On the Contact Potential Difference and Measurement for the Purposes of Space Thribology. Aerospace Research in Bulgaria, 2000, No.16.
3. Шпеньков, Г. Физико-химия трения, Минск, БГУ, 1978.
4. Гарькунов, Д. И др., Способ определения антифрикционных свойств материалов, Авт. Св. No.179975, 1966.
5. Симеонова, Ю., М.Аструкова, Г.Мардиросян, Р.Недков, Т.Грозданова, Г. Чолаков. Определяне износоустойчивостта на антифрикционни материали за космически приложения. "30 години организирани космически изследвания в България", Сб. доклади, Окт. 1999 г., 274-277.
6. Аструкова, М., Т.Грозданова, Р.Недков, Г.Мардиросян, Ю. Симеонова, Г. Чолаков. Устройство за определяне на енергетичното състояние на триеща се повърхност. Патент No.103270/23.03.1999г. Официален бюлетин на Патентно ведомство на Р. България, 08/1999г.

КОМПЮТЪРНА ОБРАБОТКА НА ИЗМЕРЕНАТА ОТДЕЛИТЕЛНА РАБОТА НА ЕЛЕКТРОНА НА ПОВЪРХНОСТТА НА АНТИФРИКЦИОННИ МАТЕРИАЛИ

Ю.Симеонова, Л.Динкова, Т.Грозданова

Резюме

В работата е представена архитектура на автоматизирана система за прецизно измерване на контактната потенциална разлика при антифрикционни материали. Автоматизирането на този процес дава възможност да се извършват експерименти с различни материали при едни и същи условия, което от своя страна води до еднозначна сравнимост на резултатите и значително повишаване точността на експеримента.

Bulgarian Academy of Sciences. Space Research Institute.
Aerospace Research in Bulgaria. 18. 2003. Sofia

MODEL OF ACCRETION FLUX IN THE PRESENCE OF MAGNETIC FIELD

K.Iankova, L.Filipov

Space Research Institute-Bulgarian Academy of Sciences

Abstract

We consider a geometrically thin disk. The material accretes on a star with magnetic field. We study the MHD behaviour of the disk-magnetosphere system and their interaction. Are these conditions related to corona generation?

1. Introduction

Quite often, accretion on a magnetic star is accompanied by a corona. The observations reveal hard X-ray of the corona and soft X-ray of the cold disk incorporated in it. The presence of a corona and the magneto-hydrodynamic (MHD) processes in such a system is considered by a number of authors, such as [1,2,10]. Other authors study a disk-magnetosphere system (DMS) without a corona [4,5,9]. Our objective is to reveal the possible continual transition between these models.

2. Formulation of the problem

Let us consider the second case, i.e. a thin disk (H<<r) in the presence of magnetic field (MF), where H and r are corresponding half-thickness of disk and the distance from the rotation axis z (DRA). We shall choose dipoler MF, which is normal to the plane of disk and we shall use cylindrical coordinates (r, φ, z).

$$(1) \qquad r\frac{\partial \Sigma}{\partial t} + \frac{\partial}{\partial r}(r\Sigma v_r) = 0,$$

$$(2) \qquad \frac{\partial v_r}{\partial t} + v_r\frac{\partial v_r}{\partial r} - \frac{v_\varphi^2}{r} = -\frac{1}{\Sigma}\frac{\partial P}{\partial r} - \frac{\partial \Phi}{\partial r},$$

(3) $$r\frac{\partial}{\partial t}(\Sigma\omega r^2)+\frac{\partial}{\partial r}(r\Sigma v_r\omega r^2)=\frac{\partial}{\partial r}(r\Sigma\vartheta r^2\frac{\partial\omega}{\partial r})+r^2B_zB_\varphi\ ,$$

(4) $$Q^+ + Q_{mag} = Q^-\ ,$$

(5) $$P = P_r + P_g + P_m\ ,$$

where v_r - radial velocity; $v_\varphi = r\omega$ is linear velocity on φ; Φ - gravitational potential; $\Sigma = 2H\rho$ is surface density; $\vartheta = \alpha v_s H$ - kinematic viscosity; $v_s^2 = P/\rho$ - sound velocity ; P - pressure (5); $B_r << B_z, B_\varphi$ are the field components; Q^+ - viscosity dissipation; Q_{mag} - magnetic dissipation; Q^- - radiative cooling.

This is a basic MHD equation of the model. In such a disk, as a result of the physical conditions, four layers with different accretion regimes are formed. The can be seen best in profile $v_r(r)$.

3. Profile of $v_r(r)$

1. $R > r > R_{co}$, where $\omega(R_{co}) = \omega_s$ [6]. In this layer, when we ignored the MF, because it is far enough we shall have time-dependent disk accretion (6).

(6) $v_r \sim t^{-1}r^{-0.25}$ or $v_r \sim t^{-1}r^{-0.4}$,

depending on opacity law $\chi(\rho, T)$.

2. $R_{co} > r > R_m$, where $\omega(R_m) = \omega_a$. Here, it is necessary to solve the full equations, taking into account the instabilities' influence on the parameters in layer [8,11].

There are alphenic waves in the layer, because the values of the velocity on the flow and the alphenic velocity are very close. These waves along with differential rotation are the reasons for the appearance on magneto-rotary instabilities of Balbus-Houly (BHI) and supersonic accretion – for thermal instability (TI).

3. $R_m > r > R_d$ where disk destruction starts when $Q_{mag}/Q^+ \sim 1$ [7]. The layer is viscously unstable. There, the MF (or ML) lines are closed, they press firmly the disk, forcing plasma to rotate like a solid, i.e. the equation do not dependent explicitly on time, but only through the changes

in MF. Therefore, the derivatives in (1)-(5) disappear and the parameters are expressed by r and α (7) only, where $\alpha = \alpha(B)$ [3].

(7) $$v_r \sim \frac{\alpha(B) r}{\alpha^2(B) + r^2}$$

4. The quick decrease of v_r corresponds to plasma motion along the ML.

4. Comments

Here, the basic laws and assumptions for the system's evolution are presented. The birth of the corona is directly related with the disk-magnetosphere interaction in layers 2 and 3. BHI creates MF in the disk and TI assists ML to emerge outwards until the field envelops the entire disk.

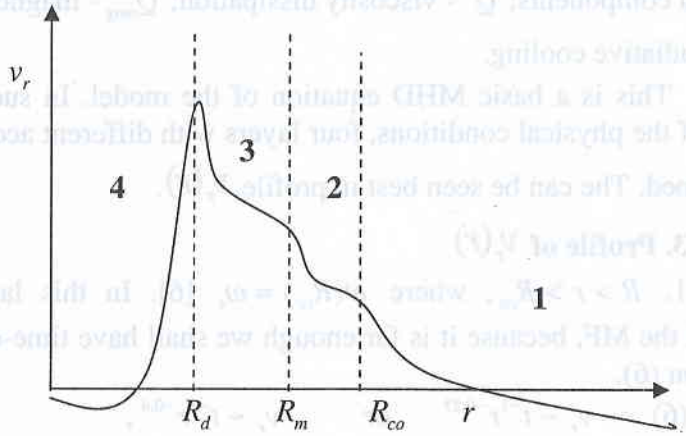

Fig. 1 Profile of $v_r(r)$.

References

1. Bardou A., Heyvaerts J., A&A, 307, 1009-1022, 1996

2. Beloborodov A. M., arXiv: astro-ph/9901108, 1999

3. Brandenburg A., Disk Turbulence and Viscosity, preprint

4. Brandenburg A., Campbele C. G., MNRAS, 298,223-230, 1998

5. Brandenburg A., Donner K. J., MNRAS, 288,L29-L33, 1997

6. Campbele C. G., MNRAS, 301,754-758, 1998

7. Campbele C. G., Heptinstall P. M., MNRAS, 299,31-41, 1998

8. Gammie C. F., Accretion Disk Turbulence, preprint

9. Lee S. M., Hong S. S., arXiv: astro-ph/9909118, 1999

10. Matteo T. Di, MNRAS, 299, L15-L20, 1998

11. Papaioizou J. C. B., Lin D. N. C., A&A, 33, 505-540,1995

МОДЕЛ НА АКРЕЦИОНЕН ПОТОК В ПРИСЪСТВИЕ НА МАГНИТНО ПОЛЕ

К.Д.Янкова, Л.Г.Филипов

Резюме

Разглеждаме геометрично тънък диск. Веществото акрецира върху звезда с магнитно поле. Изследваме магнито-хидродинамичното поведение на системата диск-магнитосфера и тяхното взаимодеиствие. Свързани ли са тези условия с появата на корона?

Bulgarian Academy of Sciences. Space Research Institute.
Aerospace Research in Bulgaria. 18. 2003. Sofia

EULER COMPUTATIONS OF AN AIRFOIL USING FINITE VOLUME METHOD AND RUNGE - KUTTA TIME STEPPING SCHEME

Konstantin Metodiev

Space Research Institute - Bulgarian Academy of Sciences

Abstract.

Finite volume method for spatial discretization of two-dimensional Euler equations is used to describe flow of an inviscid gas among structural elliptic grid. A four step Runge-Kutta scheme is also applied for time integration. A non-linear artificial viscosity is added to suppress numerical oscillation of solution. The boundary conditions at inflow and outflow are based on the method of characteristics. The results for some subsonic cases are presented and collated with experimental data.

Introduction.

For the several decades past a wide number of methods for simulation of viscous compressible flow have been developed. One of them, a finite volume method, is proved simple and efficient for calculation of such cases. The choice of this method is determined by these factors.

It is possible to apply the method for various cases of space discretization. This fact determines two forms of numerical flux implementation – the so called cell and node centering. It is useful to apply cell centering while structural quadrilateral grid is used. Otherwise, in case of triangular meshes, both ways of centering are permitted but in case of node centering an overlapping of two adjacent cells occurs. In the case when the grid is generated by solving a system of Laplace equations, a solution among curves extremely close to the flow equipotential and stream lines is asked.

When the spatial discretization is done, the considered partial differential equation is reduced to ordinary one. There are different numerical methods for solving space – discretized Euler equations but most frequently applied are Runge – Kutta schemes. These schemes use

information from only one previous iterative stage. Their advantage is the increased accuracy. Actually, when high accuracy is not required, it is possible to adjust the current iterative step size. This fact allows acceleration of the numerical process.

Theoretical background.

Conservative system equations, describing compressible gas flow among Cartesian coordinates (2D), is consisting of continuity, Euler and energy equations. It has the form:

$$(1)\qquad \frac{\partial}{\partial t}\vec{q}(x,y,t)+\frac{\partial}{\partial x}\vec{f}\left[\vec{q}(x,y,t)\right]+\frac{\partial}{\partial y}\vec{g}\left[\vec{q}(x,y,t)\right]=$$

$$=\frac{\partial}{\partial t}\begin{Vmatrix}\rho\\ \rho u\\ \rho v\\ E\end{Vmatrix}+\frac{\partial}{\partial x}\begin{Vmatrix}\rho u\\ \rho u^2+p\\ \rho uv\\ (E+p)u\end{Vmatrix}+\frac{\partial}{\partial y}\begin{Vmatrix}\rho v\\ \rho uv\\ \rho v^2+p\\ (E+p)v\end{Vmatrix}=0$$

where ρ is density, u, v are Cartezian velocities, p is static pressure and E is the total internal energy per unit mass. Then the following problem is formulated: find out the monotonous scalar functions ρ, u, v, E and p, initially defined in space of states, with initial conditions

$$\vec{q}(x,y,0)=\vec{q}_0(x,y)$$

and boundary conditions

$$B\left(\vec{q}(x,y,t)\right)=0$$

Here B is operator for determination

$$\vec{q}(x,y,t)=\left\|\rho \quad \rho u \quad \rho v \quad E\right\|^T$$

and p is replaced with the following expression:

$$p(\rho,e)=\rho RT=\rho R\frac{e}{c_v}=\rho\frac{c_p-c_v}{c_v}e=(\kappa-1)\rho e=$$

$$=(\kappa-1)\left[E-\frac{1}{2}\rho\left(u^2+v^2\right)\right].$$

Here κ is the Poisson adiabatic constant, R is universal gas constant and c_p, c_v are the specific heats. The unknown quantities are included in the governing equations with their dimensionless values

$$p=\frac{p}{p_0}\qquad T=\frac{T}{T_0}\qquad u,v=\frac{u,v}{\sqrt{RT_0}}\qquad \rho=\frac{\rho}{p_0/RT_0}$$

where the subscript $(\ )_0$ denotes stagnation parameter.

Numerical solution.

The finite volume method is applied for solving of equations (1). For this purpose the physical space around the rigid body is discretized to quadrilateral cells (finite volumes - fig. 2). As explained in Ref. [1] the basic idea of the method is to satisfy the integral form of equations (1) for each control volume. It is necessary to find out total flux of vectors $\vec{f}(\vec{q})$ and $\vec{g}(\vec{q})$ on each face of the cell separately and so on along the entire grid. Then, as proposed in Ref. [2], for the present time step, the system (1) is discretized for the current cell like this:

$$
\begin{aligned}
&\frac{\partial}{\partial t}(J\rho)+\sum_{k=1}^{4}(U_k\rho_k)=0\\
&\frac{\partial}{\partial t}[J(\rho u)]+\sum_{k=1}^{4}\left[U_k(\rho u)_k+(-1)^k\Delta y_k p_k\right]=0\\
&\frac{\partial}{\partial t}[J(\rho v)]+\sum_{k=1}^{4}\left[U_k(\rho v)_k+(-1)^{k+1}\Delta x_k p_k\right]=0\\
&\frac{\partial}{\partial t}(JE)+\sum_{k=1}^{4}\left[U_k(E+p)_k\right]=0
\end{aligned}
\qquad (2)
$$

The J symbol means the cell area and

$$U_k=(-1)^k\Delta y_k u_k+(-1)^{k+1}\Delta x_k v_k$$

corresponds to a contravariant velocity component. The sign replacement in front of an individual additive is conformed to normal vector sign variation while shifting to the adjacent cell. Each quantity, in system (2), is evaluated as the average of the values in the cells on the two sides of the cell's face (fig. 1), for example:

$$U_1(\rho u)_1=\frac{1}{2}\left[U_{i,j}(\rho u)_{i,j}+U_{i,j-1}(\rho u)_{i,j-1}\right]$$

Thus the scheme is an analog of a central difference scheme on a Cartezian grid.

Time – depending derivative discretization scheme, for space-discretized equations

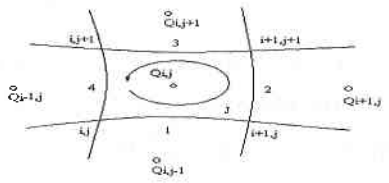

Fig. 1. Flux calculation sequence about cell i, j.

$$\frac{dq_i}{dt} + \frac{1}{J_i} Q(q_i) = 0,$$

$i = 1,2,3,...$

is 4th order Runge – Kutta

$$q^{(0)} = q^n$$

$$q^{(1)} = q^{(0)} - \frac{\Delta t}{2} Q\left(q^{(0)}\right)$$

$$q^{(2)} = q^{(0)} - \frac{\Delta t}{2} Q\left(q^{(1)}\right)$$

$$q^{(3)} = q^{(0)} - \frac{\Delta t}{2} Q\left(q^{(2)}\right)$$

$$q^{(4)} = q^{(0)} - \frac{\Delta t}{6} Q\left(q^{(0)}\right) - \frac{\Delta t}{3} Q\left(q^{(1)}\right) - \frac{\Delta t}{3} Q\left(q^{(2)}\right) - \frac{\Delta t}{6} Q\left(q^{(3)}\right)$$

$$q^{(n+1)} = q^{(4)}$$

Here the flux $Q(q_i)$ is computed over again at each time step where the following initial conditions are considered:

$$\kappa = 1.4 \quad \rho_0 = 1 \quad p_0 = 1 \quad a_0 = \sqrt{\frac{\kappa p_0}{\rho_0}}$$

$$u_0 = M_\infty a_0 \cos\alpha \quad v_0 = M_\infty a_0 \sin\alpha$$

Here symbol a denotes speed of sound, α means the angle of attack and M denotes Mach number.

To suppress non-physical oscillations of the results, according to Ref. [2], the last time step is augmented by addition of the filter:

$$q^{(n+1)} = q^{(4)} + \Delta t D_x^+ \mu_x D_x^- q^{(4)} + \Delta t D_y^+ \mu_y D_y^- q^{(4)}$$

In the expression above the superscripts + and – denoted forward and backward difference operators. The coefficients μ_x and μ_y are made proportional to

$$\mu_x \sim \frac{Q_{i+1,j} - 2Q_{i,j} + Q_{i-1,j}}{Q_{i+1,j} + 2Q_{i,j} - Q_{i-1,j}}$$

$$\mu_y \sim \frac{Q_{i,j+1} - 2Q_{i,j} + Q_{i,j-1}}{Q_{i,j+1} + 2Q_{i,j} - Q_{i,j-1}}$$

The boundary conditions, in accordance with placement, are reduced to the following kinds: along the rigid body contour and along the outer boundary of the physical domain. In regard to the first group, it is truth that

all fluxes across contour are identically zero (impermeable condition). Exception is numerical contribution to the momentum flux.

The second kind boundary conditions, computation of which is based upon one-dimensional characteristic method, is divided on inflow and outflow. Because wave propagation normal to the boundary is dominant, variations parallel to the boundary may be neglected and the linearized one-dimensional Euler equations can be written as:

$$\frac{\partial U}{\partial t} + A \frac{\partial U}{\partial x} = 0$$

$$U = \begin{Vmatrix} \rho \\ u \\ v \\ p \end{Vmatrix} \qquad A = \begin{Vmatrix} u & \rho & 0 & 0 \\ 0 & u & 0 & \frac{1}{\rho} \\ 0 & 0 & u & 0 \\ 0 & \rho a^2 & 0 & u \end{Vmatrix}_{ref}$$

The reference state for evaluating the matrix A will be the state on boundary at the old time step. To make the matrix A constant, the average value of the state vector on the boundary will be used to evaluate A .

For subsonic inflow, there are three incoming waves and one outgoing wave. The last one is computed by the algorithm using quantity conservation of corresponding Riemann invariant among the same wave while for the incoming waves the prescribing quantities for nozzle inflow (total enthalpy, entropy and flow angle) are used:

$$H = \frac{\kappa}{\kappa - 1}\frac{p}{\rho} + \frac{1}{2}\left(u^2 + v^2\right)$$

$$s = \ln\left(p\right) - \kappa \ln\left(\rho\right)$$

$$\alpha = arctg \frac{v}{u}$$

For subsonic outflow the linearized analysis shows that there are three outgoing waves and one incoming wave. In such case it is classic to prescribe the static pressure at outflow nodes.

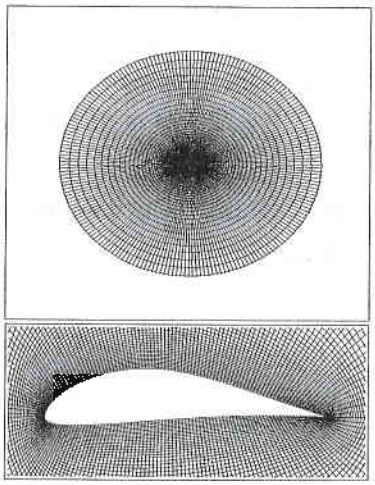

Fig. 2. An "O"-type computational grid (above) and its expanded center (below) surrounding Eppler387 wing section

Computational grid.

As was mentioned above, the physical domain surrounding wing section is discretized into finite cells. In the

current case of study this fact is achieved by curvilinear elliptic coordinate system generation by solving system Laplace equations. As mentioned in Ref. [3] the iterative act of synthesis uses initial coordinates of the grid nodes, which are evaluated previously by interpolating the interior of the physical domain. The grid coordinates at the boundaries of the field import the boundary conditions. The interpolation used is one-dimensional (normally to boundary curves) and includes hyperbolic tangent function. In this way the derived initial "ordinate" axis allocation corresponds well to the Laplace operator "effect of smoothness": the closing in of the "abscissas" curves to the convex boundary. The construction of the interpolation, as proposed in Ref. [4], is made as follows: let arc length s varies from 0 to 1 and arc's points number ξ varies from 0 to I in such way so $s(0) = 0; s(I) = 1$. Initially assigning values of the first derivatives

$$\frac{\partial}{\partial \xi} s(\xi = 0) = \Delta s_1$$

$$\frac{\partial}{\partial \xi} s(\xi = I) = \Delta s_2$$

the following expressions are defined:

$$A = \sqrt{\frac{\Delta s_2}{\Delta s_1}}$$

$$B = \frac{1}{I\sqrt{\Delta s_1 \Delta s_2}}$$

$$B = \frac{sh\ \delta}{\delta}$$

Then these equations are valid:

$$u_1(\xi) = \frac{1}{2}\left\{1 + \frac{th\left[\delta\left(\frac{\xi}{I} - \frac{1}{2}\right)\right]}{th\ \frac{\delta}{2}}\right\}$$

$$s(\xi) = \frac{u_1(\xi)}{A + (1 - A)u_1(\xi)}$$

If the equations above are applied to curve for which $\vec{r}(\xi) \in [\vec{r}(0); \vec{r}(I)]$ then for the curve point distribution follows:

$$\vec{r}(\xi) = \vec{r}(0) + [\vec{r}(I) - \vec{r}(0)]s(\xi), \xi = 0,1,2,3,\ldots, I$$

The derived in the described manner initial grid quantities are "smoothed" by solving the Laplace equations about $\vec{r}$

$$\Delta\xi = 0$$

$$\Delta\eta = 0$$

which are previously transformed into curvulinear basis (Ref. [3]). The new system equations looks like:

$$g_{22}r_{\xi\xi} + g_{11}r_{\eta\eta} - 2g_{12}r_{\xi\eta} = 0$$

$$g_{11} = x_\xi^2 + y_\xi^2$$

$$g_{22} = x_\eta^2 + y_\eta^2$$

$$g_{12} = x_\xi x_\eta + y_\xi y_\eta$$

It is solved, after aproximation with finite defferences, by successive overrelaxation method with corresponding coefficient $\omega = 1.8$.

Results.

An "O" - type elliptic grid has been generated with 200 points along tangent and 100 points along normal directions of Eppler 387 wing section. Thus the physical domain around the foil has been discretized with 20000 cells (fig. 2).

With the developed numerical algorithm serial calculations has been implemented with various Reynolds numbers and angles of attack. The results, verified with experimental data (published in Ref. [5]), are shown below. There are not a good coincidence with the experiment at the Reynolds numbers Re~60000. The reason of this is inability of the algorithm to predict transient flows.

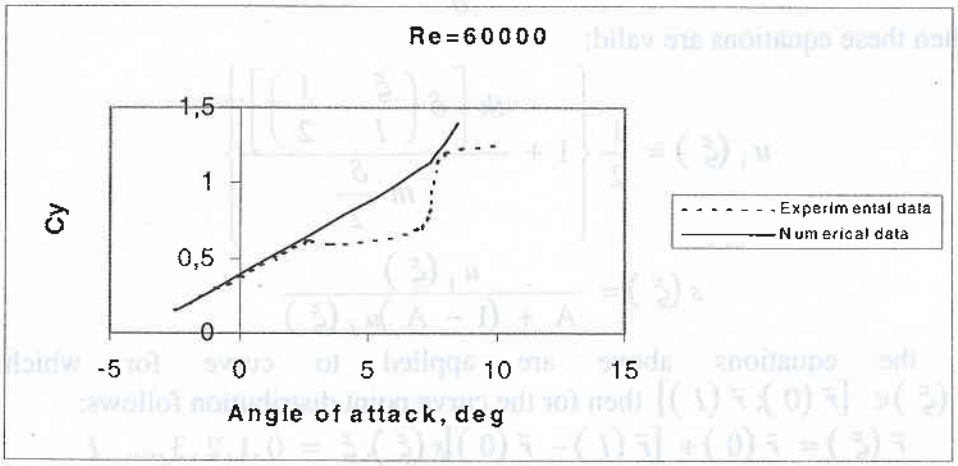

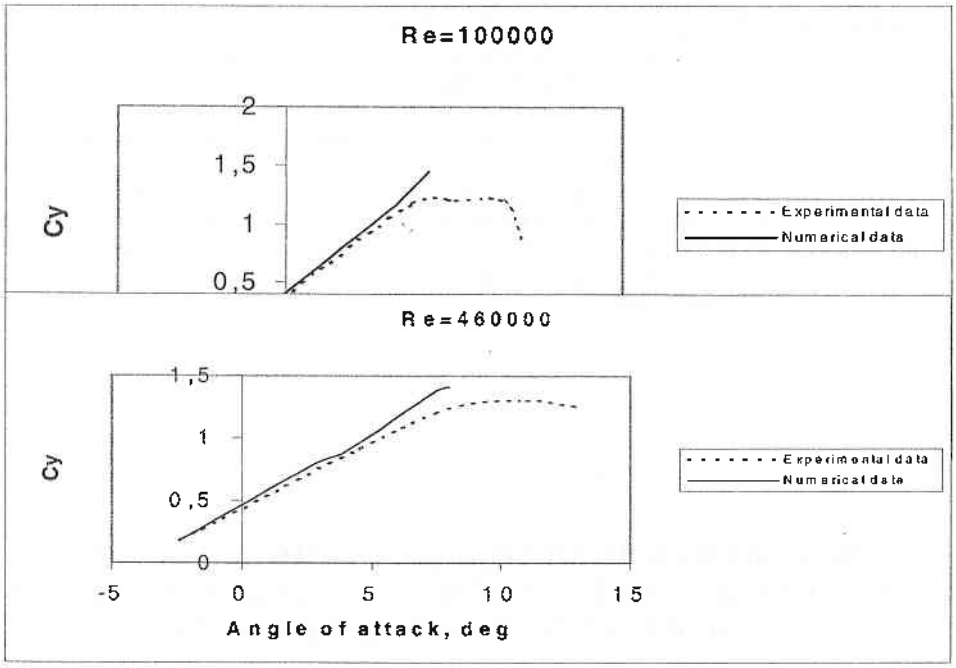

Conclusion.

A finite volume method has been used to solve partial differential equations of Euler, describing a motion of an ideal gas in two-dimensional space. A steady-state solution has been achieved using a 4^{th} order Runge – Kutta scheme. The numerical oscillations of solution were suppressed by augmenting artificial viscosity. The boundary conditions were derived using method of characteristics. An elliptic grid has been generated while solving a system of Laplace equations. The ability of the algorithm has been demonstrated to simulate a subsonic flow over a wing section.

References.

1. Lomax, H., T. Pulliam, D. Zingg, *Fundamentals of Computational Fluid Dynamics*, NASA Ames Research Center, 1998
2. Jameson, A., W. Schmidt, E. Turkel, Numerical Solutions of the Euler Equations by Finite Volume Methods Using Runge Kutta Time Stepping Schemes, *AIAA Paper 81-1259*, 1981, AIAA 14th Fluid and Plasma Dynamic Conference, Palo Alto, June 1981
3. Thompson, J., Z. Warsi, C. Mastin, *Grid Generation Techniques*, Mississippi State University, 1985
4. Vinokur, Marcel, On One – Dimensional Stretching Functions for Finite – Difference Calculations, *Journal of Computational Physics*, 1983, No 50, p. 215
5. Mc Ghee, R., B. Walker, B. Millard, Experimental Results for the Eppler 387 Airfoil at Low Reynolds Number in the Langley Low – Turbulence Pressure Tunnel, *NASA TM-4062*, 1988

ПРИЛОЖЕНИЕ НА МЕТОДА НА КРАЙНИТЕ ОБЕМИ И СХЕМА РУНГЕ - КУТА ЗА АЕРОДИНАМИЧЕН АНАЛИЗ НА ОБТИЧАНЕТО НА КРИЛЕН ПРОФИЛ

Константин Методиев

Резюме

В работата е използван метода на крайните обеми за дискретизация на уравненията на Ойлер, описващи движението на идеален газ върху структурна елиптична координатна система. Използвана е също схема Рунге–Кута от 4-ти ред за последващо интегриране по време. Добавен е нелинеен изкуствен вискозитет за да се подтиснат нефизически числени осцилации на решението. Определянето на граничните условия е базирано на метода на характеристиките. Резултатите от приложението на алгоритъма върху случай на дозвуково обтичане на двумерно тяло са сверени с експериментални данни.

Bulgarian Academy of Sciences. Space Research Institute.
Aerospace Research in Bulgaria. 18. 2003. Sofia

A MODEL OF THE INTERNAL CONTOUR OF HELICOPTER NAVIGATING SYSTEM

D. Jordanov, R. Radushev, N. Stoykova

Space Research Institute – Bulgarian Academy of Sciences

Abstract

In this project propose methodology for mathematic modelling and research the internal navigation channel of helicopter on the basis of testing the helicopter, the autopilot and pilot models

For the purpose of modelling the helicopter Mi – 8T has been chosen, with a performance aggregate in the navigation channel – combined hydro aggregate, type RA-60. While modelling the internal contour for navigation it is necessary to create in advance sub models of the object of navigation, the control system, the pilot and external disturbance. The assembly of the models in a contour should account for the real special features of the construction and the restriction. In this particular case we choose the following purpose of research: the reaction of the system "helicopter – autopilot" under strong external disturbance and operation of the performance aggregate RA-60 in regimes, which brings the steering-machine up to its working capacity limit.

1. A model for helicopter

The starting parameters in modelling the dynamics of the object are: common general features of the helicopter performance under disturbance and ruling commands; data for maximum possible angular acceleration, as well as the time for this acceleration's reduction to zero, as a result of the damping moment. The starting regime for the concrete modelling tasks is the "hang on" regime. The maximum theoretical angular acceleration of the helicopter, achieved through step-like pedal-fed commands from neutral position to the end is $\varepsilon_y = 1.5\ (1/s^2)$ [5]. Under the damping moment, in the

process of motion, the angular acceleration of helicopter Mi-8 reduces till zero within 12 *s* [5]. The model of the helicopter's motion within the tail channel is shown in Fig.1.

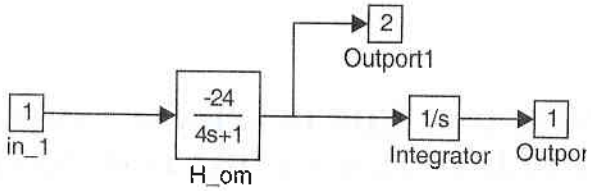

Fig.1. A model of isolated motion of course

2. Model of the control system

The control system of the helicopter is a mechanic chain including combined hydro accelerators connected in an irreversible scheme with a mechanical entrance form the pilot and electrical entrance from the autopilot. The aggregate of performance in the tail wind channel RA-60 features variable dynamics, depending on the strength of disturbance, which the autopilot tries to neutralize in the process of stabilization (the "peregonka" regime). This main feature is accounted for in a manner similar to the one described in [8]. The transmission coefficients of the autopilot have been chosen by data for autopilot AP-34B and have been broken down along the chain in the "peregonka" regime.

3. Model of the pilot

To neutralize the disturbance in the tail wind channel of the helicopter, we have to choose the simplest model of transmission function for the pilot, which is typical for the elementary regime of stabilization under conditions of disturbance: $W_p=Ke^{-\pi}$. The parameters are adjusted by taking into consideration the specifics of the helicopter – joint operation with the autopilot in the "damping" regime. In Fig. 2, the model of the pilot is shown. The transmission coefficient $K=0.6$ *[mm/deg]* is consistent with the limit of the contour resistance (Klim=0.9) and the condition for maximum possible speed of the pedals movement with the pilot's reaction under strong disturbance. The delay of τ= 0.3s is typical for most pilots. Both quantities are random, but in this particular case, the average parameters are studied. Typical parameters for the pedals and the chain leading to aggregate RA-60 are added to the pilot's model.

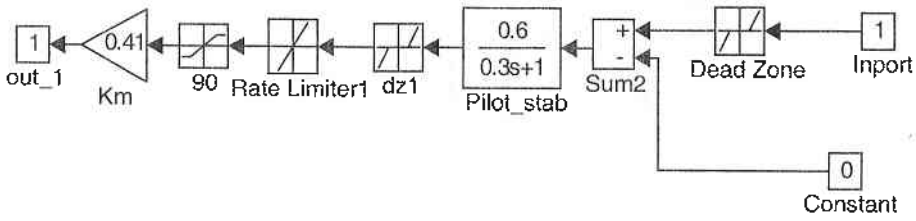

Fig.2. A model of the pilot and the mechanic chain leading to aggregate RA-60

4. Model of the disturbance

Except for uncoordinated control, the most typical cases are those under influence of side wind while in the "hang on" regime. All kinds of disturbances produce angular acceleration, based on the moments' balance disturbance around axis OY. Such disturbances could be modulated through deliberate changes in the step tail screw, whereas these changes are of various natures corresponding to the external disturbance. With this model, the background of the disturbance-caused route could be also modelled. The side wind changes the velocity triangle and the stream-line conditions of the tail propeller (changes in axis velocity).

5. Model of the "helicopter-autopilot-pilot" contour

The model of the "helicopter-autopilot-pilot" contour is shown in Fig.3. Different navigation conditions are formulated through keys "Key_AP", "Key_Pst" (with the coefficients 0 and 1): from autopilot, pilot in a combined regime – together with the autopilot. The "Switch" block switches off the autopilot's "stabilization" regime when the pilot is working in combined regime.

The results – angular velocity and course angle are visualized in block "R". The used symbols have the following provisional meaning: – Subsystem "EMB" (Embarrassment) – model of disturbance; "Control_AP"- signals from the autopilot (V),"Control_P"- signals from the pilot's model (mm).

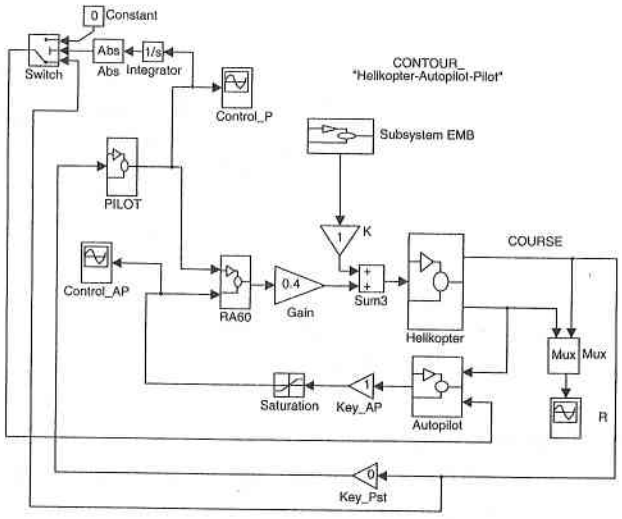

Fig.3. A "helicopter-autopilot-pilot" model

This model has been studied under various disturbances and working conditions of the contour. Figures 4, 4.1 and 5 present the modelling results, which illustrate the work of the "helicopter - autopilot" system.

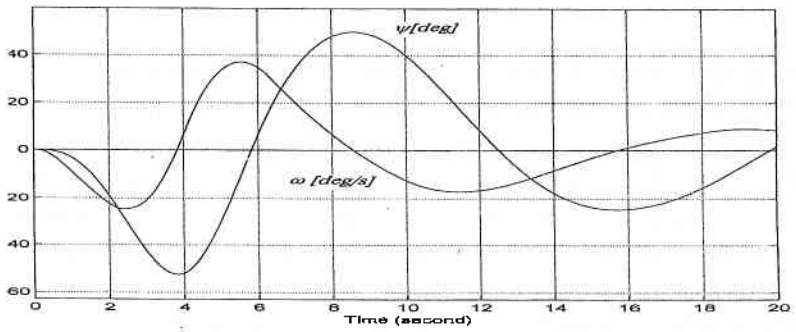

Fig.4. Transitional process in neutralizing a quick damping side-wind surge of the "pulse" type

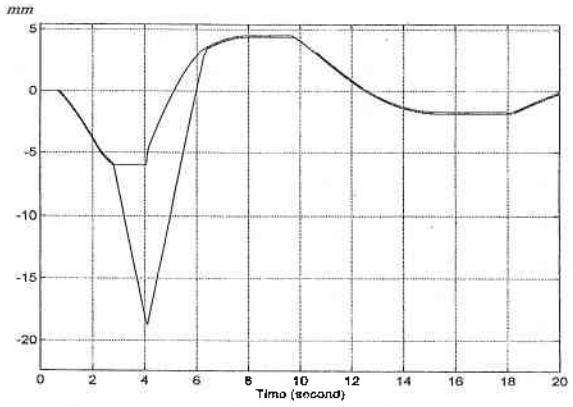

Fig. 4.1. Pace of the executive mechanism PA-60 under "pulse" disturbance.

The steering machine is fluctuating around neutral position, reaching in the beginning
(from 3s to 4s) the restriction of *6mm* and providing conditions for the "peregonka" regime.

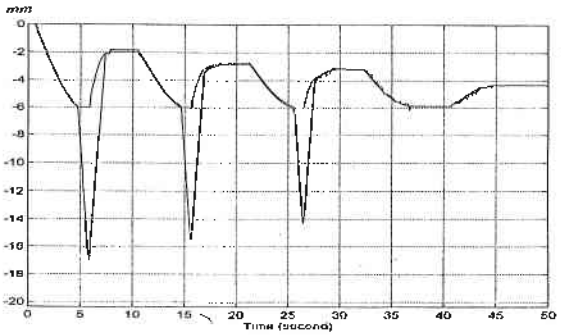

Fig.5. Pace of the executive mechanism PA-60 under constant disturbance – right-hand side wind of 15 m/s. The "peregonka" regime – 6s, 16s, 27s.

6. Conclusions

Considering the modelling results, conclusions for the operation and repair practice could be made as follows:

- The specific "peregonka" regime of aggregate RA-60 is reasonable if implemented for a short time (up to 1..2 s) in the beginning to neutralize the disturbance of constant side wind or strong, but short-lasting surges ("pulses");

The "peregonka" regime resembles the initial stage of the pilot work when neutralizing disturbance and imitates the reflector type of navigation disturbance – with maximum speed of movement of the aggregate of performance;

In "peregonka", long-term stabilization of the process is impossible;

- In repair and diagnostic operations, special attention should be paid to adjustment of the assembly, switching on and off the "peregonka" regime; early switching on in the presence of side wind (before the steering machine reaches its constructive limit pace) could result in strong fluctuations of the helicopter the "hang on" regime;
- The insensitivity area of the steering machine of aggregate RA-60 affects unfavourably the contour's stability under strong external disturbance.
- The potential unfavorable consequences of the "peregonka" regime under strong disturbance have resulted in its elimination in next-generation combined aggregates.

References

1. Агрегаты КАУ-30Б и РА-60Б, Инструкция по эксплуатации. Москва, изд. Транспорт, 1995г.
2. Баженов А.И., И.С.Гамынин, В.И.Карев, А.А.Никулин, А.М.Селиванов, А.А.Суслов Проектирование следящих гидравлических приводов летательных аппаратов, Москва, изд. Машиностроение 1981 г.
3. Браверман А.С., А.П. Вайнтруб, Динамика вертолета-предельные режимы, Москва, изд. Машиностроение 1988г.
4. Гультяев А.К. MATLAB 5.2 Имитационное моделирование в среде Windows; Практическое пособие Санкт Петербург изд. Корона принт, 1999 г.
5. Дмитриев И.С., С.Ю.Есаулов Системы управления одновинтовых вертолетов, Москва, изд. Машиностроение, 1975 г.
6. Данилов В.А., В.М. Занько, Н.П. Калинин, А.И. Кривко Âåðòîëåò Ìè-8МТВ, Москва, изд. Транспорт, 1995 г.
7. Йорданов Д., Кр.Хинков, Р.Радушев, Моделиране и изследване на комбинирани агрегати за управление на хеликоптери, Доклад на юбилейна научно-приложна конференция "30 години Институт по въздушен транспорт",София 12-13 декември 2001 г.
8. Йорданов Д., Р.Радушев, Н.Стойкова, Моделиране и изследване на изпълнителни агрегати с променящи се динамични характеристики от САУ на хеликоптери, Доклад на Юбилейна научна конференция - ВВВУ "Г.Бенковски" април 2002 г.

МОДЕЛ НА ВЪТРЕШНИЯ КАНАЛ ЗА ПОПЪТНО УПРАВЛЕНИЕНА ХЕЛИКОПТЕР

Д.Йорданов, Р.Радушев, Н.Стойкова,

Резюме

В разработката се предлага методология за математическо моделиране и изследване на контура за попътно управление на хеликоптер по данни от изпитание на обекта за управление, модели на автопилота, пилота и изпълнителния агрегат на системата за управление.

Bulgarian Academy of Sciences. Space Research Institute.
Aerospace Research in Bulgaria. 18. 2003. Sofia

FAILURE RESISTANCE ALGORHYTM

*Antonio Andonov, Zoya Hubenova**
Higher School of Transport "T. Kableshkov",

**Space Research Institute – Bulgaran Academy of Sciences*

Abstract:

An important part of the general problem of building up an efficient and reliable control systems is the problem for identification of their dynamic characteristics. The current information about the dynamic status of a functioning system provides for organization of optimum control adapting to the changing external conditions, on the one hand, and for taking timely and proper decisions in case of failure of subsystems, on the other hand.

In the paper, the structure of an adaptive, multiple-connection automated control system with dynamic characteristics identification is proposed, using a combined control principle: adaptive control with relatively slow parameter change, as a result of parameter interference and change of the system's control part structure with leap parameter change, as a result of failures in the individual subsystems.

The modern ACSs are very sophisticated, due to the great variety of problems solved by them. The availability of a great quantity of functionally necessary elements and the relations between them in the system put to the fore the problem for enduring their failure resistance. A system's reliability is its property to preserve with time within certain fixed limits the value of its parameters, characterizing its ability to perform the required functions, i.e., to preserve its efficiency status in preset modes and application conditions.

Efficiency status is the status of an object, where all parameters, characterizing its ability to perform the prescribed functions comply with the requirements of the normative and technical or design documentation. Reliability is a combination of the following properties: failure-free operation, longevity, maintainability and possibility for preservation. Failure-free operation is the system's property to continuously preserve its efficiency status within a fixed period of time. The three remaining aspects

of reliability characterize only the technical properties of the system and the extent to which they depend on the specificity of the ACS' operation. This is the reason why further we shall consider reliability only in the sense of failure-free operation.

There are two main ways to ensure system reliability. The first one suggests preservation of the efficiency status of all ACS elements, i.e., synthesis of a reliable system of reliable elements. This suggests higher requirements for the elements' reliability, which results in drastic increase of the system's cost. That is why, such an approach is expedient only within certain limits.

With the second approach, the system status with failure is regarded as one of the multitude of its possible statuses; in this status, the ACS' reliability is ensured by means of definite system structure building up. In this way, synthesis of a reliable system of non-reliable elements is accomplished.

An important part of the general problem of building up an efficient and reliable control systems is the problem for identification of their dynamic characteristics. The current information about the dynamic status of a functioning system provides for organization of optimum control adapting to the changing external conditions, on the one hand, and for taking timely and proper decisions in case of failure of subsystems, on the other hand.

In the paper, the structure of an adaptive, multiple-connection automated control system with dynamic characteristics identification is proposed, using a combined control principle: adaptive control with relatively slow parameter change, as a result of parameter interference and change of the system's control part structure with leap parameter change, as a result of failures in the individual subsystems.

The structure of such an ACS, from an organizational point of view, has a two level hierarchy. The lower level comprises the system control part, the top one comprises a coordinator, changing the control part of the system at times of failures while readjusting its parameters in the presence of parameter interference on the controlled object. The failure diagnostics, accomplished by the coordinator, provides for the fitting of additional elements or subsystems in the ACS' control part circuit, or to form a new structure, by means of switching to trouble-free systems.

The building of such ACSs calls to determine the identification methods, providing the possibility for carrying out a reliable and timely diagnostics of possible faults in the system's operation, alongside with the assessment of the current status of the operating system. It is obvious, that

these methods shall have certain properties, such as: high speed, noise resistance, high sensitivity, adequacy for high-order complex systems, potential to detect the most typical faults, relatively simple algorithm. All these features determine the diagnostics reliability.

These features are manifested best by the active statistic methods for dynamic characteristics' identification, using pseudo-random test signals with determined parameters and limited intensity, which do not disturb the normal operation mode of the examined system. The passive identification methods are characterized by relatively low speed and low accuracy [1].

For the purpose of simplifying the computing procedures and accelerating operation speed, it is expedient to use recursive algorithms for indirect evaluation of the dynamic characteristics – the decomposition coefficients of the time characteristics in a generalized Fourier series, according to the system of orthogonal functions. Moreover, these algorithms are independent of the series of the examined system:

Let $\mathbf{k} = (k_1, k_2, ..., k_m)$ are the parameters of the controlled object (CO), $\mathbf{c} = (c_1, c_2, ..., c_n)$, $\mathbf{n < m}$, are the readjustable parameters of the controller (C), compensating the change of **n** most substantial parameters of the controlled object; $\mathbf{A} = (a_1, a_2, ..., a_n)$ – the identified parameters of the closed control system, for example, the decomposition coefficients of the pulse transition function in series, according to the system of orthogonal functions. Where needed, the vector space of parameters **A** could be extended to a dimension **n + m** in accordance with the vector space dimension of the closed control system parameters. And the vector **A** components are selected according to the criterion for maximum sensitivity to the change of the corresponding parameters of the closed ACS.

The following assumptions are made, regarding the proposed model for the closed ACS:

1. The identified parameters of the model are constant and even:

$$a_i(k_0, c_0) = a_{i0} \quad ,i = 1, 2,... n ,$$

where:

$$k_0 = (k_{10}, k_{20}, ..., k_{m0}) \quad , c_0 = (c_{10}, c_{20}, ..., c_{n0})$$

2. For an arbitrary population of changing parameters $\mathbf{k(t)}$ there exists such a population of readjustable parameters $\mathbf{c(t)}$, so that at the end of the adjustment cycle the following is valid:

$$a_{ir}(k ,c) = a_{i0} ,$$

where **r** is a discrete time interval, corresponding to the end of the consecutive adjustment cycle.

On the so made proposals for the model, the readjustable parameters of the controller, compensating the changes of the controlled object, as grounded in [1], are determined using the equations:

$$\Delta A_r = B_{r-1}\, \Delta c_r ,$$

where:

$$\Delta A_r = (\Delta a_{1r}, \Delta a_{2r}, ..., \Delta a_{nr}) \ , \quad \Delta a_{ir} = \Delta a_{ir} - \Delta a_{10}$$

Δc_r is the vector, determining the controller parameter changes of the series **nx1**;

$B_{r-1} = \mathbf{bij}$ is a matrix with dimensions **n x n**, $b_{ij} = (\partial a_1 / (\partial c_j)_{r-1}$. The **B matrix** parameters are function of k_{r-1}, c_{r-1} and are calculated at the end of the transition **(r - 1)** self-adjustment cycle. The controller's readjustable parameters are determined by the ratio:

$$c_r = c_{r-1} + \Delta c_r$$

In this way, the status of the control system is defined by the vector of the identified parameters, which changes continuously in the presence of parameter interference, and can also undergo a leap change, as a result of possible failures in the individual subsystems. In this case, the task for the system's classification can be formulated in terms of the theory of pattern recognition: the presented population of identified parameters shall be related to one of the earlier established diagnoses (statuses) The status population of the diagnosticated **R** is broken down to a series of sub-populations Q_i, Q_0 – a population of statuses, corresponding to a faulty system. Q_I , **I = 1, 2, ..., N** - a population of statuses, corresponding to a faulty system, whose fault is caused by the failure of the i subsystem. The diagnostics is performed dependent on the distance of the current vector **A** to the vectors of the corresponding populations A_{Q0}, A_{QI} or on the distance to the references A_{Q0}*, A_{QI}*, whose coordinates are equal to the mean value of the coordinates, included in the specific population. With such an approach, all control solutions for one type of failure or other shall be provided in advance. The design stage of the discussed system class is finalized with training of the coordinator. The issues of the selection of the most informative parameters and their order are specified, as well as the issues of coding the vector components of the identified parameters for the purpose of forming a solving logic function (SLF).

The two tasks – self-adjustment and control of the system's status, carried out by the coordinator, can be solved within the frame of a single specialized digital computing equipment (SDCE). Its operation algorithm contains the following sequence of operations:

- Periodic measurement of the components of vector A of the identified parameters **A**;
- Classification of the system's statuses (formation of the SLF);
- On available failt, a vector of the controlling actions **U** is formed with combined binary components (1,2), switching the control part of the ACS.

The discussed approach is most efficient in constructing digital (microprocessor) ACS with high reliability and operation quality requirements. The digital controller has hardware excess, which means that it has to provide for change of the control system structure at the expense of the connections between the input devices, processors, storage components, and output devices. The coordinator and the control part are organized as a multiprocessor control set.

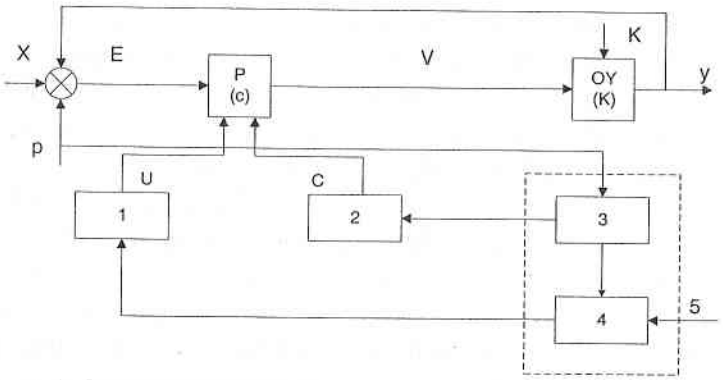

1 - Control action formation unit
2 - Adjustment coefficient forming unit
3 - Identification unit
4 - Solving logic function formation unit
5 - Output information

References

P. Eikhoff, Fundamentals of control system identification, M. Mir,1993.

АЛГОРИТЪМ ЗА ОСИГУРЯВАНЕ НА ОТКАЗОУСТОЙЧИВОСТ

*Антонио Андонов, Зоя Хубенова**

ВТУ"Т. Каблешков", катедра "СОТ

**ИКИ – БАН*

Резюме

Важно място в общия проблем за построяване на ефективни и надежни системи за управление заема проблемът за идентификация на динамичните им характеристики. Познаването на текущата информация за динамичното състояние на функциониращата система позволява, от една страна да се организира оптимално управление с адаптация към изменящите се външни условия, а от друга - да се вземат своевременни и правелни решения при възникване на откази в отделни подсистеми. В настоящата работа се предлага структура на адаптивна многосвързана система за автоматично управление с идентификация на динамичните характеристики, използваща комбиниран принцип на управление: адаптивно управление при относително бавно изменение на параметрите вследствие на параметрически смущения и изменение на структура на управляващата част на системата при скокообразно изменение на параметрите вследствие откази на отделни подсистеми.

Bulgarian Academy of Sciences. Space Research Institute.
Aerospace Research in Bulgaria. 18. 2003. Sofia

CLASS OF DYNAMICAL SYSTEMS WITH NONLINEAR EXCITATION [+)]

V.Damgov, P.Trenchev
Space Research Institute – Bulgaran Academy of Sciences

Abstract

The phenomenon of "quantized" oscillation excitation is presented and discussed. A class of kick-excited self-adaptive dynamical systems is formed and proposed. The class is characterized by non-linear (inhomogeneous) external periodic excitation (as regards the coordinates of excited systems) and is remarkable for its objective regularities: "discrete" oscillation excitation in macro-dynamical systems having multiple branchy attractors and strong self-adaptive stability.

1. Introduction

Our main objective here is to present a phenomenon of highly general nature manifested in various dynamical systems. What is meant here is the display of peculiar "quantization" by the parameter of intensity of the excited oscillations, i.e. given unchanging conditions, it is possible to excite oscillations with a strictly defined discrete set of amplitudes; the rest of the amplitudes being "forbidden". The realization of oscillations with specific amplitude from the "permitted" discrete set of amplitudes is determined by the initial conditions. The occurrence of this unusual property is predetermined by the new general initial conditions, i.e. the non-linear action of the external excited force with respect to the coordinates of the system subject to excitation.

It is well known that the Theory of Non-Linear Oscillations considers mostly the action of external periodic forces on oscillating systems. Those forces are either independent of the coordinates of the

[+)] Research supported by the "Scientific Research" National Council at the Bulgarian Ministry of Education and Science under Contract No.H3-1106/01

system or linear with respect to the coordinates (the latter are in essence the classical parametric systems) (cf, for example [1]). The phenomenon under review is characterized by other initial conditions, i.e. non-linearity of the external action force as regards the coordinate of the system that is being excited. The result is the occurrence of qualitatively new properties ([2, 3, 4]).

A class of phenomena and systems with specific excitation can be formed and proposed. It can be most generally termed a class of kick-excited self-adaptive systems. Kick excitation is represented by a short impact of the external periodic force compared to the basic oscillations period. The self-adaptivity consists in the self-tuning of the system to the external kick excitation, which conditions the super-stability of the oscillations.

We consider a class of systems with specific energy feeding. It is constructed on the basis of non-linear oscillator under external force of special kind:

$$\frac{d^2x}{dt^2} + 2\delta\frac{dx}{dt} + f(x) = \varepsilon(x)\Pi(\nu t) \qquad (1)$$

The external force is presented here as a product of two terms - one is periodic function of time t and the other is a non-linear function of the variable x. The function f(x) can be non-linear or, even, linear function; $\delta = const$. The form and the role of the function $\varepsilon(x)$, which in fact can be regarded as coordinate-dependent amplitude of the driving force, is essential. In general, it can be constructed in an arbitrary complicated form.

In considering the case of non-linear oscillator under wave action [3], the governing equation can be presented in the following form:

$$\frac{d^2x}{dt^2} + 2\delta\frac{dx}{dt} + f(x) = F\sin(\nu t - kx) \qquad (2)$$

where $F, \nu = const$ F and k is the wave number.

This case is remarkable for the fact that the non-linearity of the external action (that is the external wave excitation) is present in a natural way, without arranging any artificial conditions for accomplishment of inhomogeneous excitation. In practice, such systems exist in the outer space and other medium and, generally, those are charged particles moving in a magnetic field under the action of electrostatic waves. The "oscillator-wave" system features the same set of distinctive characteristics, such as the possibility of excitation of stable oscillations with a strong determined set of possible amplitudes, strong self-adaptive stability of stationary modes, etc.

2. Theoretical analysis of the kicked pendulum.

In this section, we present an approximate but simple derivation of a two-dimensional map corresponding to the Poincaré map of kicked pendulum

$$\varepsilon(x)=\begin{cases}1, & |x|\le d'\\ 0, & |x|>d'\end{cases}$$

(3) $$\ddot{x}+2\beta\dot{x}+\sin x=\varepsilon(x)F\sin(\nu t),$$

The fact that Poincaré's map is defined in energy-phase variables suggests that we should examine the energy balance of the system. The external force acts in such a way that the system receives energy only once in a half-period in the form of a very short pulse; therefore, an expression for the incoming energy can be easily obtained. In order to simplify our calculations, we have to make two main assumptions concerning the system parameters. We assume weak positive dissipation ($0<\beta<<1$) and thin active zone, i.e. the phase trajectory crosses it for a time $t_{zone}<<T$, where T is the oscillation half-period. The two map variables will correspond to the total energy and the phase of the external force in the active zone's center (x = 0).

The energy received for one pass through the active zone is:

(4) $$\Delta E_{in}=\int_{-d}^{d}F\sin(\nu t(x))dx$$

Introducing phase variable $\psi=\nu t$ and assuming $\overline{\nu}$ to be the average velocity in the active zone, one can obtain

(5)

$$\Delta E_{in}=\int_{\psi_{in}}^{\psi_{out}}\frac{F}{\nu}\sin\psi\dot{x}d\psi=\frac{F\nu}{\nu}\int_{\psi_{in}}^{\psi_{out}}\sin\psi d\psi=2\frac{F\nu}{\nu}\sin\psi_o\sin\xi=2Fd'\frac{\sin\xi}{\xi}\sin\psi_o$$

Here, we have introduced median phase $\psi_o=(\psi_{in}+\psi_{out})/2$ and phase half-width of the active zone $\xi=(\psi_{out}-\psi_{in})/2=\nu d'/\overline{\nu}$. Expression (5) can be further simplified by assuming small phase half-width $\sin\xi\cong\xi$; in this case, we get:

(6) $$\Delta E_{in}=2Fd'\sin\psi_o.$$

Now we have to determine the energy loss of (3) for the time interval between two passes through the active zone, it will be approximately equal to the energy loss in the case of free damped pendulum, which is given by

$$\Delta E_{out} = 16\beta[E(m) - (1-m)K(m)] \tag{7}$$

Here, $m = E_o / 2$ and $E_o = \dot{x}/2 + (1-\cos x)$ is the full energy of the system, $K(m)$ and $E(m)$ are complete elliptic integrals of first and second kind, accordingly. In case of small amplitudes, (7) can be simplified using the expansions:

$$K(m) = \frac{\pi}{2}\left(1 + \frac{m}{4} + \frac{9}{64}m^2 + \ldots\right)$$
$$E(m) = \frac{\pi}{2}\left(1 - \frac{m}{4} - \frac{3}{64}m^2 + \ldots\right) \tag{8}$$

and keeping only terms of order up to m, one obtains:

$$\Delta E_{out} = 4\beta K(m) E_o = \beta T(m) E_o \tag{9}$$

Here, $T(m)$ is the period of pendulum oscillations expressed as a function of its energy.

Let us now define the map variables precisely. The energy variable is $m = E_o / 2$, and the phase one is the median phase defined in (5): $\theta = \psi_o$. In addition, we assume that m_n does not stand for the moment of the nth pass through the center of the active zone, but for the moment of the $(n-1)^{th}$ leaving the zone; these moments are shown in Fig.1. We used such a complicated notation because it simplifies the equation for the phase variable's evolution. It becomes simply:

$$\theta_{n+1} = \theta_n + \frac{\nu T}{2} + \pi = \theta_n + 2\nu K(m_{n+1}) + \pi \pmod{2\pi} \tag{10}$$

The additional term $+\pi$ is introduced because of the symmetry of (3): it is invariant under transformation $(x, \dot{x}, \psi) \to (-x, -\dot{x}, \psi + \pi)$, and the subsequent passes through the active zone occur for velocities with opposite signs (cf. Fig.1). The balance of m is written as:

$$m_{n+1} = m_n + \Delta\frac{E_{in}}{2} - \Delta\frac{E_{out}}{2} = m_n + Fd'\sin\theta_n - \Delta\frac{E_{out}}{2} \tag{11}$$

Here, we can use either the exact expression for energy dissipation (7) or the small amplitudes' approximation (9). In the first case, combining the

equations for energy and phase variables, we obtain the two-dimensional map:

$$m_{n+1} = m_n - 8\beta[E(m_n) - (1-m_n)K(m_n)] + Fd'\sin\theta_n$$
$$\theta_{n+1} = \theta_n + 2\nu K(m_{n+1}) + \pi \pmod{2\pi} \tag{12}$$

In the case of small amplitudes approximation, expressing T L only with terms of order up to m and assuming m and β are both small, the following approximate map is obtained:

$$m_{n+1} = m_n(1 - 2\pi\beta) + Fd'\sin\theta_n$$
$$\theta_{n+1} = \theta_n + (\nu+1)\pi + \frac{\nu\pi}{4}m_{n+1} \pmod{2\pi} \tag{13}$$

Let us find the fixed points (m^o, θ^o) of the map (12). The equation for m yields:

$$Fd'\sin\theta^o = 8\beta[E(m^o) - (1-m^o)K(m^o)] \tag{14}$$

and from equation for θ it follows that:

$$2\nu K(m^o) = (2l-1)\pi \tag{15}$$

The last result shows that for a fixed value of the frequency ν the system processes discrete set of stationary states m_l^o for various values of l; the condition $K(m) \geq \pi/2$ requires $(2l-1) \geq \nu$. Moreover, Eq.(15) completely determines the energy's stationary values, hence the amplitude of oscillation. Taking into account only the first two terms in the expansion of $K(m)$ according to (8), one can find approximately:

$$m_l^o = 4\left[\frac{2l-1}{\nu} - 1\right] \tag{16}$$

That is the reason for which we call (15) a discretization condition for the system.

Writing the energy balance equation and combining it with the phase equation we arrive at a map identical with the dissipative twist map:

$$E_{n+1} = (1-\delta)E_n + \varepsilon\Pi(\theta_n)$$
$$\theta_{n+1} = \theta_n + 2\pi\alpha(E_{n+1}) \pmod{2\pi} \tag{17}$$

with the following notations introduced:

$$\varepsilon = \gamma Fd'; \quad \alpha(E) = \nu\frac{T(E)}{4\pi} + \frac{1}{2} \tag{18}$$

So, it becomes clear that dissipative twist map (17) models well the general kick-system (1) with symmetric potential, small dissipation and thin active zone.

This is a very important result. It places the class of kick-excited systems in correspondence to the well-studied class of dissipative twist maps. It also highlights the fact that kick-systems inherit their common features from twist maps. So, we can assert that it is convenient to consider system (17) as a general kick-model, which stands for a variety of physical systems and especially for those forced in a pulse way, i.e. the external force acts only through short time pulses.

3. Conclusion

The basis properties characterizing the mechanism of "quantized" oscillation excitation are:

(1) Excitation of oscillations of the quasi-eigenfrequency of the system with a set of discrete stationary amplitudes, depending only on the initial conditions, i.e. a specific "quantization" of the excited oscillation by the parameter of intensity.

(2) The possibility for effective division of the frequency with high-rate frequency of the unary transformation.

(3) Adaptive self-control of the energy contribution in the oscillating process, revealed as maintenance of the amplitude values and the oscillations frequency in the system in case of significant change of the amplitude of external action, the quality factor (Q-factor, load, losses) and other actions, i.e. this is a phenomenon of strong adaptive stabilization of regimes when the parameter changes up to hundreds percent.

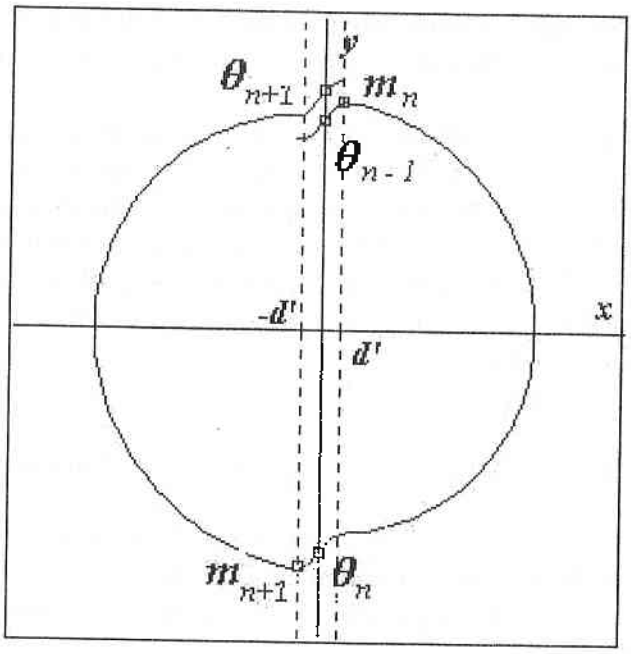

Fig.1 The phase points standing for consecutive iterations of the map variables along the trajectory

References

1. Migulin, V.V., V.Y. Medvedev, E.R. Mustel, V.N. Parigin. Basic Theory of Oscillations, World Scientific Notes in Physics, 1983
2. Damgov, V., I.Popov. "Discrete" Oscillations and Multiple Attractors in Kick-Excited Systems. Discrete Dynamics in Nature and Society (An International Multidisciplinary Research and Review Journal), 2000, v.4, pp.99-124
3. Damgov, V.N. Modeling Systems and Mechanisms of Oscillation Excitation. Earth, Moon and Planets, 1993, v.61, pp.87-117
4. Damgov V.N., D.B. Doubushinsky. The Wave Nature and Dynamical Quantization of the Solar System. Earth, Moon and Planets, 1992, v.56, pp.233-242

ЕДИН КЛАС ДИНАМИЧНИ СИСТЕМИ С НЕЛИНЕЙНО ВЪЗБУЖДАНЕ +)

В. Дамгов, П. Тренчев

Резюме

В статията е описано и изследвано е явлението "квантована" осцилация. Предложен е създаден клас от кик-възбудими самоадаптивни динамични системи, който се характеризира с нелинейно (нехомогенно) външно периодично възбуждане (по отношение на координатите на възбудимите системи) и се отличава с обективните си закономерности: възбуждане на "дикретна" осцилация в макродинамични системи с множество клонови атрактори и силна самоадаптивна устойчивост.

+) Research supported by the "Scientific Research" National Council at the Bulgarian Ministry of Education and Science under Contract No.H3-1106/01

Bulgarian Academy of Sciences. Space Research Institute.
Aerospace Research in Bulgaria. 18. 2003. Sofia

SYNCHRONIZATION IN RADIO COMMUNICATION SPREAD SPECTRUM SYSTEMS

Antonio Andonov , Ilka Stefanova, Kancho Kanchev

Higher School of Transport "T. Kableshkov,

Abstract:

Movable radio-communication systems are known to cause uncertain delay of the received signals as a result of the changing distance between the movable objects. In the promising wide-band systems with leap changing bearing frequency shall establish and maintain synchronization through a combination of autonomous synchronization made possible by the introduction of compact high-stability frequency references, and forecasting methods for the distance between the transmitter and the receiver using auxiliary devices such as dedicated calculating units, which will provide to obtain sufficiently accurate data to compensate for the delay. In view of this setting, here, an algorithm is suggested for autonomous synchronization with forecast of random delay fluctuations.

The problem of communication system synchronization lies in the time combination of periodic processes, describing the operation of the transmitter and the receiver. Even the precise knowledge of the transmitter's starting operation time and the perfect stabilization of the time standard are no complete solution of the synchronization problem. This is especially valid for mobile radio communication, where the change in the distance between the mobile objects generates indefiniteness in the delay of the received signals. Nevertheless, some authors [1,2] consider that in the future, broad band systems with discontinuous variation of the carrier frequency will use a combination of the method of autonomous synchronization in connection with the creation of compact highly stable frequency standards and methods of prognosticating the distance between the transmitter and the receiver by additional means, including special computing facilities and providing the possibility to obtain sufficiently precise information for the purpose of compensating the delay. With a view to this formulation, one of the objectives of this paper is to propose an

algorithm for autonomous synchronization with prognostication of random delay fluctuations.

The most universal approach to the problem of the synthesis of optimal receiving algorithms is based on Markov's nonlinear filtration theory. To compensate the delay τ (t) in the signal propagation medium s(t), the signal should be emitted ahead of time, i.e. it should be of the kind:

$$S_x(t) = s[t+x(t)].$$

When available delay τ (t), the useful signal at the receiver's input is described by the expression:

(1) $S_x[t-\tau(t)] = S\{t-\tau(t)+x[t-\tau(t)]\}$

The problem, whose solution is the subject of this paper, is to determine the value of x(t), at which maximum root-mean-square of the displacement ε(t) is obtained at the time of receiving the signal at the receiver's input with available random delay τ (t), or

(2) $\varepsilon(t) = \tau(t)-x[t-\tau(t)]$.

To determine x(t) the total current information about the random delay can be used, which is contained in the realized w(t) during the time interval [0,t] at the receiver's input. This oscillation is a mixture of useful signal and noise:

(3) $w(t) = S_x[t-\tau(t)]+n(t)$.

The signal emitted by the transmitter at random time t_0 enters the receiver's input through a random delay channel at time t_1, so that the obvious equation:

(4) $T_0 = t_1 - \tau(t)$.

is satisfied.

The described problem could be reduced to determination of the advance x(t), providing minimum root-mean-square of the displacement $\varepsilon(t_1)$ of the signal, received at time t_1, based on the observation of the realization w(t) by the time of the signal's emission $w_0 = \{w(t), 0<t<t_0\}$.

As well known, the optimum root-mean-square estimate coincides with the arbitrary mathematical expectation:

(5) $$X(t_0) = M\{\tau(t_1)|\, w_0\} = \int_{-\infty}^{\infty} \tau_1 P_1(\tau|\, t_0)\, d\tau;$$

$P_1(\tau|\, t_0) = P\{\tau(t_1)|\, w_0\}$.

To avoid considering the process at random times, it is reasonable to introduce the following process:

(6) $\tau_1(t_0) = \tau(t_1)$.

From (4) it follows that

(7) $\tau_1(t_0) = \tau[t_0 + \tau(t_1)] = \tau[t_0 + \tau_1(t_0)]$.

In this case with respect to the probability density $P_1(\tau \mid t)$ it could be said that it is the current presumptive density of the process's probabilities $\tau_1(t)$;

$P_1(\tau \mid t) = P\{\tau(t_1) \mid w_0\} = P(\tau_1(t_0) \mid w_0\}$.

The physical meaning of $\tau_1(t)$ is the delay of the signal emitted at time t_0.

From (7) can be derived an equation, determining the relation between $P_1(\tau, t)$ and $P(\tau, \mid t) = P(\tau(t+l) \mid w_0\}$, or the *a posteriori* probability density of the random delay at the fixed time $\tau(t+l)$. If l is regarded as a random value with probability density P(l), and $\tau(t+l)$ as a function of this value, than based on (6), the following is valid:

$$(8)\quad P\{\tau_1(t) = \tau \mid w_0\} = \int_{-\infty}^{\infty} P\{\tau(t+l) = \tau \mid w_0\} P(l)dl$$

From (7) it follows that $l=\tau_1(t)$, or:

$P(l) = P\{\tau_1(t)\} = l \mid w_0\} = P\{[l \mid t\}$

In this way, a homogeneous Fredholm integral equation of the second type can be defined, providing the possibility to determine $P_1(\tau \mid t)$ at assigned probability density $P\{\tau, \mid t)$.

$$(9)\quad P_1(\tau \mid t) = \int_{-\infty}^{\infty} P(\tau; l \mid t)\, P_1(l \mid t)\, dl.$$

Equation (9) relates the probability characteristics of the $\tau_1(t)$ process to the characteristics of the $\tau(t)$ process. The algorithm of calculating $P(\tau; l \mid t)$ follows from the results of the optimum nonlinear filtration theory. The random delay can assume non negative values, or $\tau_1(t)>0$, $P_1(\tau \mid t)=0$ for $\tau<0$. That is why in (9), only $P(\tau; l \mid t)$ for $l>0$ or only the extrapolated probability density is used. In practice, it can always be assumed that $\tau(t)$ is a Markov process component $\lambda(t) = \{\tau(t), \beta(t)\}$, $\tau(t)$ being separated explicitly.

If S(t) is a synchrosignal, emitted by the monitoring station and the delay is the only random parameter of the $S_x(t)$ signal, then the assignment of τ defines completely the signal:

$S_x[t-\tau(t)] = S\{t-\tau(t)+x[t-\tau(t)]\}$

The realization of $w_0^{t-\tau(t)}$ in formula (1) is known, determined by previous observations.

So, the determination of the a posteriori probability density of the probabilities $P(\tau; l \mid t)$, based on the observation w^t_0, is a problem of the

Markov theory for an optimum linear filtration, that can be solved. The probability density can be determined by the equation

$$\frac{\partial P(\lambda;l|t)}{\partial l} = L\{ P(\tau; l | t)\}, \quad (10)$$

where L(.) is the presumptive operator of Focker – Plank - Kolmogorov [2].

The initial condition in this equation is determined by the expression:

$$P(\lambda;\ v=.0 \mid t) = P(t,\lambda),$$

where $P(t,\lambda)$. $P\{\lambda(t) \mid w^t_0\}$ is the current a posteriori probability density of the $\lambda(t)$ process at the observation y^m_0, determined by the equation for the filtration equation of Stratonovich [2]. In this case it is of the following kind:

$$\frac{\partial P(T,\lambda)}{\partial t} = L\{P(t,\lambda)\} + [F_x(t,\tau) - F_x(t)]\ P(t,\lambda), \quad (11)$$

where

$$F_x(t,\tau) = \frac{2}{N}\ \{w(t)\ S_x(t-\tau) - ½\ S_x^0(t-\tau)\}\ ;\ F_x(t) = \int F_x(t,\tau)\ P(t,\lambda)d\lambda$$

For the purpose of simplifying equations (10), (11) and forming the extrapolated probability density $P(\tau; l \mid t)$ it is reasonable to apply the well known method of the Gaus approximation.

References

1. Andonov, A.V. Optimization of the similar to noise signals structure for the purpose of minimizing of the time of the initial synchronization in systems with discontinuous variation of the working frequency. – Symposium of works of HMTS "T. Kableshkov", 1992.
2. Tihonov, V.I., Kuljman, N.K. Nonlinear filtration and quasi-coherent signal receiving. M. Sov. Radio, 1975.

СИНХРОНИЗАЦИЯ В СИСТЕМИ С РАЗПРЕДЕЛЕН СПЕКТЪР

Антонио Андонов, Илка Стефанова, Кънчо Кънчев
Висше транспортно училище "Т. Каблешков",

Резюме

В системите на подвижната радиовръзка вследствие на промяната на разстоянието между подвижните обекти възниква неопределеност в закъснението на приеманите сигнали. В перспективните широколентови системи със скокообразно изменение на носещата честота, за установяване и поддържане на синхронизация ще е възможно използване на съчетание на метода за автономна синхронизация във връзка с създаването на компактни високостабилни еталони на честота и методи за прогнозиране на разтоянието между предавателя и приемника с помощта на допълнителни средства, включващи специализирани изчислителни устройства и даващи възможност да се получи достатъчно точна информация с оглед компенсиране на закъснението. С оглед на тази постановка в настоящата работа е предложен алгоритъм за автономна синхронизация с прогнозиране на случайни флуктуации на закъснението.

Bulgarian Academy of Sciences. Space Research Institute.
Aerospace Research in Bulgaria. 18. 2003. Sofia

ANTIFRICTION PROPERTIES OF SELF-LUBRICANT COMPOSITE MATERIALS UNDER FRICTION VACUUM CONDITIONS

Yulika Simeonova, Georgi Sotirov

Space Research Institute - Bulgarian Academy of Sciences

Abstract

Two self-lubricant copper-based composite materials, alloyed with Sn or Ni, P, and containing Pb, were studied. The obtained experimental data revealed a small friction coefficient in vacuum (for load of 2 and 10 N, and velocity of 0,2 and 1 m/s) with both materials. The "Cu-P-Sn-Pb" system's friction coefficient was 0,12 - 0,15. The "Cu-P-Ni-Pb" system's friction coefficient was 0,18 - 0,24. The measured wear values for friction in vacuum were also small. For system one wear reached 4.10^{-6} mm^3/Nm, and for system two, 4.10^{-5} mm^3/Nm. An interesting fact is that, by increasing the load 5 times (from 2 to 10N) at 0,2 m/s in vacuum the wear of system one became 6.10^{-6} mm^3/Nm. For system two this value was 5.10^{-5} mm^3/Nm. The obtained results proved the good antifriction properties of these materials at dry friction in vacuum, resulting from the friction surface's enrichment with lead, Pb. During the friction process, Pb diffused from volume to surface and acted as a solid lubricant.

Introduction

Space studies have shown the complex and non-traditional nature of tribological processes in vacuum, where the medium is greatly rarefied, lacking oxygen and humidity, convectional cooling, and traditional contact lubrication. As a result, contact interactions are realised at elevated temperature, increased plastic deformation, destruction of oxides, at strongly increasing adhesive activity of the frictional surfaces, leading to intensive wear [1]. Friction in vacuum usually takes place in dry conditions.

All these peculiarities necessitate the development of materials with improved antifriction properties, since in space practice, failures of tribological character are not quite rare.

Our experience in material research and use in space has shown that self-lubricant copper-based composite materials are suitable for space application. One material of this type was used in the bearings of the space apparatus which operated steadily in vacuum on the MIR Orbital Station for 5 years [1996 - 2001] [2,3].

Properties and parameters of new materials

The object of the study are the properties and triboparameters of two self-lubricant copper-based composite materials, alloyed with Sn or Ni, P, and containing Pb in the form of globular formations.

The materials are as follows:

1. System "(Cu - P) - (Pb -Sn)", to be called provisionally "material 1" and
2. System "(Cu - P - Ni) - Pb", to be called provisionally "material 2."

The main pecularity of this type of materials is the fact that the functions of their structural components are strictly differentiated. Some of the components play the role of the bearing part (the matrix). These are the copper alloys. The other components have antifrictional function as solid lubricant (Pb, Sn, their alloys). An important factor providing for the choice of these components was the interrelation between them in the material structure.

Alloying with Ni and Sn improves the mechanical properties of the alloys and forms a solid solution with Cu, increasing material strength.

Phosphorous increases the wear resistance of materials, forms a solid phase Cu_3P, which limits the formation of intensive plastic deformation at contact and restricts the creation of seizure centres at dry friction vacuum conditions. Pb actually does not interact with Cu, and plays the role of a solid lubricant, decreasing wear and increasing the reliability of the tribo-couple. Pb is present in the materials' structure in the form of isolated formations.

A general technological principle in the creation of this type of antifrictional materials is the formation of strongly heterogeneous structure, ensuring good antifrictional characteristics and parameters (small friction coefficient and high wear resistance).

"Material 1" possesses complex heterogeneous structure built by α-solid solution of Sn in Cu with isolated formations of Pb. At the boundaries of α-solid solution grains, a web of Cu_3P is located with areas of complex eutectics "Cu_3P + Cu_3Sn + (Cu + Sn), and isolated crystals probably of the Pb_2SnO_4 type.

The structure of "material 2" is built of a hard solution of Ni and P in Cu with solid phase Cu_3P, located on the grains in the form of a broken web. Pb formations fill the gaps between the particles of the solid solution.

A high wear-resistance is inherent to these materials, because of the favourable relation between strength and plasticity resulting from the alloying of the bearing part (the matrix) with Ni or Sn, which increases the loading capacity of the materials.

Irrespective of the distinct specifics of triboprocesses in vacuum and especially due to adhesion increasing at dry friction vacuum conditions, the obtained experimental figures for the friction coefficient in vacuum for both materials were small. System's "Cu-P-Sn-Pb" friction coefficient was 0,12 - 0,15 and system's "Cu-P-Ni-Pb" friction coefficient was 0,18 - 0,24 (load 2 N and velocities 1 and 0,2 m/s). The measured wear values for friction in vacuum were also small - for material 1, the wear reached 4.10^{-6} $mm^3/N.m$, and for material 2, 4.10^{-5} $mm^3/N.m$. This result could be explained by the effect of self-lubrication. Our previous studies have shown that under dry friction in vacuum this type of materials certainly demonstrate a self-lubricant effect [3].

As a result of the increased temperature at contact, the plastic deformation and the differences in the diffusion and linear extension coefficients of the material's components, diffusion of Pb towards the friction surface is observed.

Such diffusion is also accomplished with friction in air, but in this case Pb on the surface is oxided, and with friction in vacuum Pb is metallic, acting as solid lubricant. Experience shows that metal Pb features more stable triboparameters than PbO. Metal Pb keeps its own plasticity and the formed thin layer is steady.

In Fig. 1, the dependence of the friction coefficient on distance at dry friction vacuum conditions is shown for material 1 (load 2 N and velocity 0,2 m/s).

With increase of load and velocity, friction power increases, contact temperature rises, the diffusion process is activated and the surface is enriched with Pb acting as lubricant, which decreases further the friction coefficient, as seen in Fig.2 with velocity 1m/s. The case with material 2 is similar, where the value of the friction coefficient decreases with increase of velocity from 0,25 to 0,18.

An interesting fact is that, by increasing the load 5 times (from 2 to 10 N) at velocity 0,2 m/s in vacuum the wear for material 1 was 6.10^{-6}

$mm^3/N.m$. For material 2 this value was 5.10^{-5} $mm^3/N.m$. This result proved the good antifriction properties of the materials under dry friction in vacuum. We assume that the load 10 N at 0,2 m/s is not limiting for both materials. The shown triboparameters are measured at rotation movement with counterbody of steel AISI52100 (100 Cr 6). The tribological study was carried out by the AMTT - Seibersdorf. UHV-tribometer [4].

The structural-morphological peculiarities of the friction surface at dry friction in vacuum are very specific. Wear by friction removes irreversibly oxide structures and cleans the surface. This can be seen in the micrograph of the surface at friction in vacuum for material 1 - Fig.3. This is the beginning of the formation of Pb layer on the surface, where well-outlined formation of Pb (1) is observed, assuming orientations along the direction of movement.

The Pb layer formed on the surface at friction under vacuum for material 2 is shown in Fig.4. The formation of a stable Pb layer depends on the structural-morphological configuration of the composite material, the distribution of lead in the surface layer and the friction regime, which makes the friction surface adaptable while in service. Therefore, the self-lubricant composite materials of this type are steady and reliable under dry friction vacuum conditions, including space environment. Our efforts show that they are suitable for space application as a material for bearings, working continuously in dry friction regime in vacuum.

Conclusions

1. Lubrication effect has been established for two antifriction copper-based composite materials under dry friction vacuum conditions for loads of 2 and 10N and velocities of 0,2 and 1 m/s.
2. The triboparameters friction coefficient and wear of these materials are comparable to those of the material LB9 (Glacier BS 1400 LB4-6).
3. Because of their good triboparameters and great operation stability in vacuum these materials are of interest for space material science and technologies. They are a promising material for space applications, involving continuous dry friction in vacuum.
4. It is purposeful the research to be continued on these materials in order to determine their ultimite potentials with regard to their loading with heavier operation regimes in vacuum.

Upon complete assessment of these materials, they could be proposed for use in space equipment and devices.

Acknowledgments

The authors extend their gratitude to:

- A.G.Kostornov, O.I.Fucshich and T.M.Chevichelova from the Ukrainean National Academy of Sciences for the provided research samples of the antifrictional composite materials.
- the "Improving Human Potential" Program of the European Commission for the obtained funding.
- the Aerospace and Space Materials Technology Testhouse (AMTT) Seibersdorf, Austria, for the provided possibility to carry out studies at high scientific and technical level.

References

1. Silin, A. A., Friction in Space Vacuum. Friction and Wear, Issue No. 1, 1989, 1 (in Russian).
2. Simeonova Yu., T. Nazarsky, Application of Composite Materials in the Design of Space Apparatuses. Intern. Congress "Mechanical Engineering Technologies'97", Sept. 1997, Sofia, Bulgaria. Proceedings V 4(13), 104.
3. Yuga, A., T. Chevichelova, Yu. Simeonova, T. Nazarsky, Application of a New Antifriction Material at Tribological Junctions of Space Research Equipment. 2nd World Tribology Congress, Sept. 2001, Vienna. Ses. Tribology in Extreme Situation, 63-4.
4. Simeonova Yu., G. Sotirov, Study of the Parameters of New Antifriction Materials under Dry Friction Vacuum Conditions, Bulg. Acad. Sciences, ARC Seibersdorf Research GmbH, Studia, 2002.

Captions:

Fig.1. Friction coefficient dependence of distance under dry vacuum friction (load 2N, velocity 0,2 m/s) material 1.
Fig.2. Friction coefficient dependence of distance under dry vacuum friction (load 2N, velocity 1 m/s) material 1.
Fig.3. Micrograph of friction surface of material 1 at dry friction in vacuum (load 2N, velocity 0,2 m/s), (x 1000).
Fig.4. Micrograph of friction surface of material 2 at dry friction in vacuum (load 2N, velocity 1m/s), (x 1000).

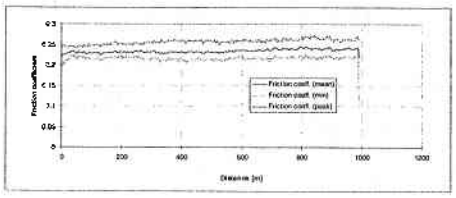

Fig.1

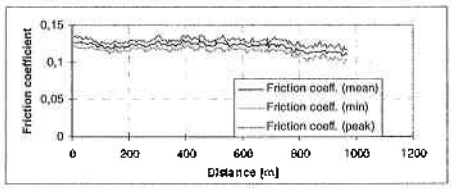

Fig.2

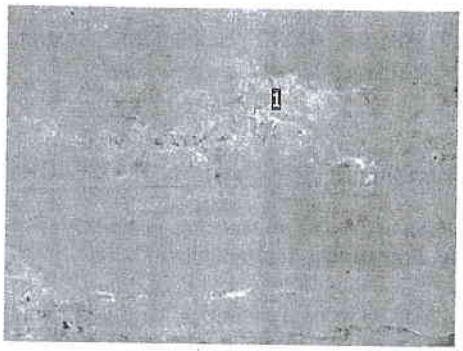

Fig.3

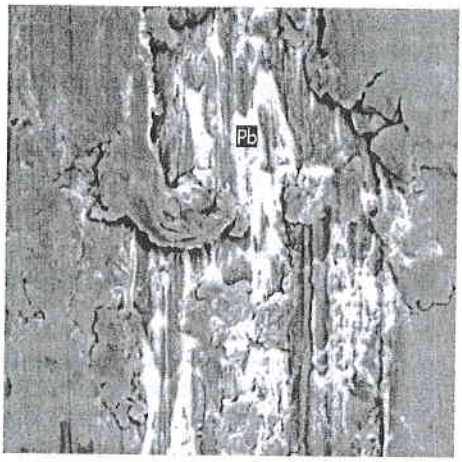

Fig.4

АНТИФРИКЦИОННИ СВОЙСТВА НА САМОСМАЗВАЩИ СЕ КОМПОЗИТНИ МАТЕРИАЛИ ПРИ ТРИЕНЕ ВЪВ ВАКУУМ

Юлика Симеонова, Георги Сотиров

Резюме

Изследвани са два самосмазващи се материала на медна основа, съдържащи олово, сплавени с калай или никел и фосфор. Получените експериментални данни показаха нисък коефициент на триене във вакуум (за товар 2 и 10 N, и скорост 0,2 и 1 m/s) и при двата материала. Коефициентът на триене на системата "Cu-P-Sn-Pb" е 0,12 - 0,15. Коефициентът на триене на системата "Cu-P-Ni-Pb" е 0,18 - 0,24. Измерените стойности на износване при триене във вакуум също са малки. Износването в първата система е 4.10^{-6} mm^3/Nm, а във втората система - 4.10^{-5} mm^3/Nm. Интерес представлява фактът, че увеличавайки товара 5 пъти (от 2 на 10N) при 0,2 m/s във вакуум, износването на първата система става 6.10^{-6} mm^3/Nm. За втората система тази стойност е 5.10^{-5} mm^3/Nm. Получените резултатаи потвърждават добрите антифрикционни свойства на тези материали при сухо триене във вакуум, получени в резултат от обогатяването на фрикционната повърхност с олово Pb. В процеса на триене Pb дифундира от обема към повърхността и действа като твърд лубрикант.

Bulgarian Academy of Sciences. Space Research Institute.
Aerospace Research in Bulgaria. 18. 2003. Sofia

COMPARATIVE ANALYSIS OF PLANT GROWTH IN TWO DIFFERENT SUBSTRATES DURING EARTH EXPERIMENT

Iliana Ilieva

Space Research Institute - Bulgarian Academy of Sciences

Abstract

*One-month, earth-based experiment with onions carried out in the prototype of SVET-2 Space Greenhouse which has operated for 10 years on the MIR Orbital Station is described in this paper. A new substrate (**Ekolin**) is used which is compared with the substrate used before (**Balkanin**) on the biological indications of the grown plants. The equal environmental parameters in the root zone were maintained by automatic substrate moisture control in both Vegetation Modules. **Balkanin's** relatively low water-conductivity is an essential disadvantage as a result of which twice fewer plants were grown; moreover, they were shorter and with twice less biomass compared to that grown in **Ekolin**. For its good water-conductivity **Ekolin** could be used in the future Space Greenhouses.*

1. Introduction

Balkanin is Bulgarian invention and patent and was the first substrate used in five space and many on-earth experiments carried out in the period 1985 - 1997. Because of its high relative weight and radioactive background, low water-capacity and low water-conductivity, the American scientists replaced **Balkanin** with **Turface**.

The aim of this experiment was to use new substrate – **Ekolin** and to compare it to the used before **Balkanin** on the biological indications of the grown plants. As the environmental parameters in the Growth Chamber are the same for all plants we also tried to maintain equal environmental parameters in the two Vegetation Modules by automatically controlling the substrate moisture.

Allium cepa – onion was chosen as a biological material in this experiment because of its fast growth and rich vitamine content. The plant is also a candidate for growth in the Biological Life Support Systems providing food, water and air recovery for the future long-term space

missions. Onion is also a suitable model plant for studding the impact of different environmental stress factors. The plant is especially sensitive to water stress and indication for this is the lowered rate of transpiration, photosynthesis and growth.

The basic biological indications that will be measured and will serve for estimation in this experiment are: germination and plant height, row biomass and root development.

2. Technical description of the experiment

SVET Space Greenhouse consists of Plant Growth Unit and Control Unit. The Vegetation Vessel is divided into two Vegetation Modules (VM), and is mounted on rails (like a drawer) in the Plant Growth Unit [1]. Each VM has independent, automatic moisture control maintained by moisture sensor operating on thermodynamic principle [2].

Ekolin – the new substrate is placed in VM 1 and **Balkanin** – the previously used substrate - in VM 2. The new substrate is developed by NIPRORUDA and consists of natural clinoptilolite in composition with expanded perlite and vermiculite, natural vermiculite, fertilized clinoptilolite and water-soluble polymers, modified and activated by original Know How technology of the firm. Its basic nutritional compounds are shown on Table 1 [3].

Balkanin is natural zeolite enriched with nutrients on original Bulgarian technology Table 2 [4].

T a b.1. Agrochemical characteristics of **Ekolin** for space greenhouse

PH	EC	P_2O_5	K_2O	$N\text{-}NH_4$	$N\text{-}NO_3$
	mS/cm	Water soluble forms		Extraction with KCl solution	
	mg/100g				
6.2	0.79	18.50	7.22	32.38	15.75

T a b. 2. Nutrient content of substrate **Balkanin**

Total content	**%**	**Easy assimilable forms**	**mg/100g**	**Microelements**	**ppm**
N	0.20	NH_4	72	B	2.0 – 4.0
P_2O_5	0.04	P_2O_5	12	Cn	15 - 20
K_2O	2.39	K_2O	1440	Zn	40 - 80
Na_2O	0.58	Na_2O	400		
CaO	3.65	CaO	574		
MgO	1.90	MgO	60		

The two VMs were filled only with substrate, without the linen wicks and the air-pipe system for artificial aeration of the substrate as was in the original construction. The position of the two sensors was different, too. They were situated 2,5 cm off the bottom of each VM, and not 3 cm off the covering lid. This position allowed us to control the moisture so as to avoid gravitational flow out of water – a phenomenon typical for ground-based experiments.

3. Experimental course

The experiment was started on 18 November 2002 and continued till 18 December 2002. It was worked out in another ground-based experiments that it is better to repeat Program 2 – the program for initial substrate moistening for twice better and more even water distribution in the volume with small water doses. So, Program 2 was repeated twice with approximately 13 ml water dose. Program 3 – the program maintaining automatic control of the environmental parameters during plant growth was started on 22 November. Before that the biological material – the onions were planted. Each VM has two beds and 9 onions were planted on each of them or totally 18 onions for each substrate. Analyzing the received data from the twice-repeated Program 2 we decided to set the following initial parameters for Program 3: moisture threshold - 45% and 37 ml water dose for both VMs. Some of the environmental parameters monitored during the experiment are shown on Figure 1. Although we set equal initial parameters one week later twice less water was input in **Balkanin** due to substrate's bad

water conductivity. This led to different conditions in the root zones. **Balkanin** was twice drier than **Ekolin**. To equalize the conditions in the root zones we raised the moisture threshold in **Balkanin** from 45% to 50 % and kept the same water dose – 37 ml.

In the beginning of the experiment when plants have not germinated yet nor grown up enough water consumption is less, being needed only to compensate water loss during evaporation. But the situation was different with **Ekolin** - too much water was consumed without plants. Analyzing the data from the received telemetric frames it was determined that the substrate in VM1 was subject to more intensive evaporation than the substrate in VM2. X-ray photograph was stick on beneath the VV to prevent electronics from damage if some gravitational water flow out occurred. The X-ray photograph gave negative impact on the equal water evaporation from both VMs, but as it was impossible to remove it without interrupting the experiment we decided to leave it. On the 21st day when all of the plants in **Ekolin** and half of the plants in **Balkanin** germinated and twice more water was input in VM1 at one and the same moisture threshold the evaporation from both VMs equalized and remained still till the end of the experiment.

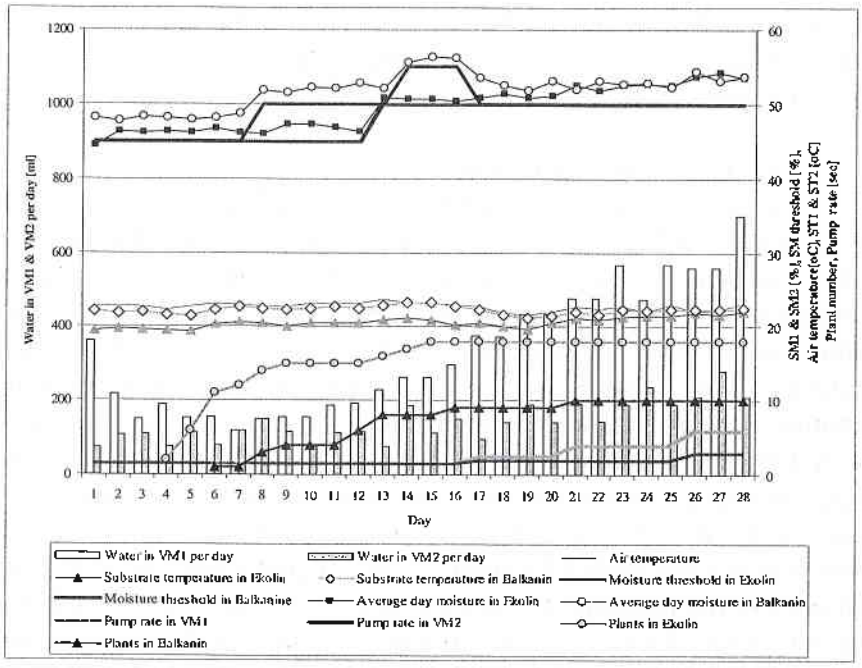

Fig 1. Environmental parameters in VM1 and VM2 during the experiment

The bad **Balkanin** water-conductivity allowed only half of the planted plants to germinate although we raised the moisture threshold to 55% for several days and almost reached the point when gravitational flow out of water was very possible to occur.

The moisture thresholds set during the experiment were as follows: in VM1 - 45% and 50% and in VM2 - 45%, 50%, 55% and 50%. These thresholds were maintained by different doses depending on pump operational time.

4. Results

From the very beginning of the experiment we measured some of the plant biological parameters. The first indication observed was plant germination. With two times less water in **Balkanin** due to its bad water-conductivity two times less plants germinated. Four days after starting Program 3, the first plant in **Ekolin** germinated, and two days later, the first one in **Balkanin** germinated. 100 % germination was achieved on the 15th day of the experiment in **Ekolin** and 51% germination on the 21st day in **Balkanin**. The plants in **Balkanin** were smaller with softer leaves with less biomass compared to those grown in **Ekolin**. The average plant height in substrate **Ekolin** was 49.6 cm in the first row and 53.1 cm in the second row. Approximately 12 cm smaller were the plants in **Balkanin** - 37.4 cm in the first row and 40.3 cm in the second row. The average plant weight in **Ekolin** was 8.375g and almost twice less in **Balkanin** - 4.794g.

Observation of root growth was made after the experiment had finished. The upper layers in **Balkanin** were completely dry; it was wet near the hydroaccumulators and below in the substrate's volume. Approximately 2 cm of substrate from the covering lid were completely dry in **Ekolin**. The whole volume below was evenly wetted. The plants grown in **Ekolin** were with fine, more branched off roots, distributed like a net in the whole volume of the substrate. The strongest roots were mainly near the hydroaccumulators. The plants grown in **Balkanin** were with not so well developed root system. The roots grew downward mainly near the hydroaccumulators.

Both root systems suffered from anoxia as the roots reached the wettest layers of the substrates at the bottom of the VMs. The roots grew through the polyvinylchloride foam and outside the perforations in the VV walls. Artificial aeration of the substrate is necessary on Earth as well to prevent roots from anoxia.

5. Conclusions

Moisture is vital for faster plant germination and normal plant growth. **Ekolin** - the new substrate is with good water-conductivity and thus ensures twice faster germination and better plant growth. **Ekolin** could be used in the future Space Greenhouses after successfully passing the other space-qualified tests.

References

1. Ivanova, T. N., Yu. A. Bercovich, A. L. Mashinskiy, G. I. Meleshko. The first "space" vegetables have been grown in the "SVET" Space Greenhouse using controlled environmental conditions, *Acta Astronautica*, 1993, Vol. 29, No. 8, pp. 639-644.
2. Ivanova, T. N., I. Dandolov. Moistening of the substrate in microgravity, *Microgravity Science and Technology*, 1992, Vol.3, pp. 151-155.
3. EKOLIN – Certificate for quality
4. Ivanova, T. N., I. Stoyanov, G. Stoilov, P. Kostov, S. Sapunova. Zeolite Gardens in Space. *Natural Zeolites SOFIA '95*, PENSOFT Publishers, Sofia-Moscow, 1997, pp.3-10.

СРАВНИТЕЛЕН АНАЛИЗ НА РАЗВИТИЕТО НА РАСТЕНИЯ В ДВА РАЗЛИЧНИ СУБСТРАТА ПРИ НАЗЕ4МЕН ЕКСПЕРИМЕНТ

И. Илиева

Резюме

В статията е описан едномесечен наземен експеримент с кромид лук, проведен с прототипа на космическата оранжерия "СВЕТ", работила успешно 10 години на Орбитална станция "МИР". Използван е нов субстрат (еколин), който е сравнен с биологическите показатели на използвания по-рано субстрат (балканин). Постоянните показатели в областта на корена за двата вегетационни модула бяха поддържани с автоматичен контрол на влагата. Сравнително по-ниската водопроводимост на балканин е основен недостатък, в резултат на който бяха отгледани двойно по-малко растения; освен това, растенията бяха по-ниски и с двойно по-малка биомаса от масата, получена при използването на еколин. Добрата водопроводимост на еколин го прави особено подходящ за използване в бъдещи космически оранжерии.

Bulgarian Academy of Sciences. Space Research Institute.
Aerospace Research in Bulgaria. 18. 2003. Sofia

ASSESSMENT OF FOREST ECOSYSTEMS AND ADJACENT AREAS STATUS FOR ECOLOGICAL AGRICULTURE

Albena Pavlova

Space Research Institute - Bulgarian Academy of Sciences

Abstract:

The impact of forest change is a dynamic process in time and space. Research of the ecosystem's strength and balance is associated with identification of the destructive factors and the growth direction of the influence. The main objective of the proposed study includes assessment of the destructive factors affecting areas with different land cover in regions with similar climatic conditions. The results of the study include application of the NDVI for vitality evaluation of forest and quantity of green biomass and supervised classification for areas with minimum forest biomass on the base of the obtained NDVI values. For more detailed definition of forest status it is necessary to synthesize a model for correlation between different vegetation indexes and destructive factors influence as parameters in such a model.

1. Introduction

Environment has very delicate equilibrium, which is directly dependent on climate changes, natural disasters, and human influence. Research of the ecosystem's strength and balance is associated with identification of the destructive factors and the growth direction of the influence. Modern problem development covers eco-monitoring, specification of trends, and determination of rehabilitation criteria on the basis of satellite technologies. The main objective of remote sensing is to obtain information from received images for the quality of earth objects and the atmosphere with their spatial interaction. It is well known that aerospace methods for remote sensing of the Earth in various spectral ranges are the most efficient ones for expeditious monitoring of geo-ecological conditions. The present level of remote sensing facilities enables acquisition of high-precision data about land parameters with sufficiently high spatial resolution and periodical updating of information. [1]

Corresponding to the project preparation for ecological agriculture and the needs for forest change assessment in the adjacent areas the following tasks were fixed:

- Assessment of the state of natural forest ecosystems and identification of the destructive factors influencing the forest fund;
- Revealing the developmental trends and direction of identified influences;

The objective of the study includes assessment of the destructive factors affecting areas with different land cover in the region with similar climatic conditions.

2. Selection of test polygons

In accomplishing the task for eco-agriculture development in the region southward of Plovdiv it is very important to evaluate the state of the environment in the boundary area surrounding the selected test sites. It features natural forest ecosystems with prevailing coniferous trees, moderate continental climate, and uniform rain distribution.

The test polygons and field measurement sites were identified using a Landsat 5 TM satellite image from August 1992. Visual interpretation and comparative evaluation vs. a topographic map was used to fix a couple of test polygons near the arable areas of the Plovdiv field. [2] The regions were digitized and put in geographical tables using GIS software - ArcView. The database will be expanded with additional information from field measurements about forest cover, soil, and pollution types.

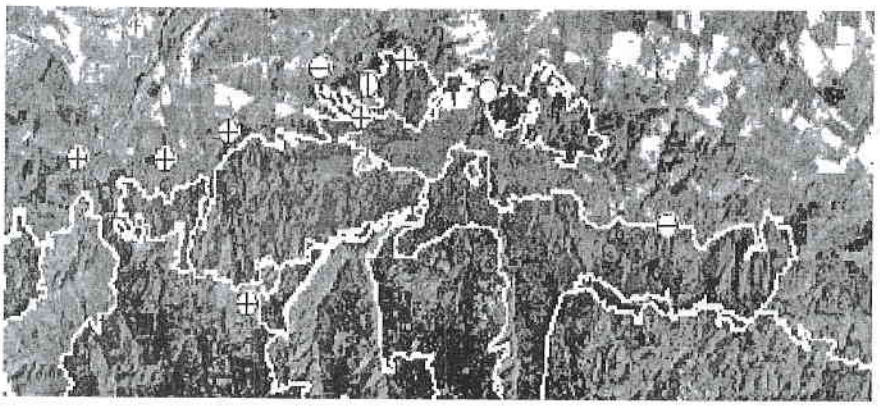

Fig.1 Test polygons

Tab.1 Area of the fixed polygons

Shape	*ID*	*Land cover*	*Area / dca*
Polygon	1	Forest	30092.148
Polygon	2	Forest	5163.340
Polygon	3	Forest	28832.468
Polygon	4	Forest	4319.924
Polygon	5	Forest	7526.470
Polygon	6	Forest	43161.169
Polygon	7	Forest	29620.794
Polygon	8	Forest	2948.970

3. Results

Analysis of vegetation and detection of changes in vegetation patterns are keys to natural resource assessment and monitoring. The detection and quantitative assessment of green vegetation is one of the major applications of remote sensing for decision-making. For these purposes are used vegetation indexes based on the reflection of vegetation in the visible and infrared range of the electromagnetic spectrum, temperature changes, and ratio in water content.

For evaluation of forest vitality and green biomass quantity, the NDVI is used. Based on the obtained values, a supervised classification is made for areas with minimum forest biomass. These classes outline the ground measurement sites where the destructive factor will be evaluated, providing for the deviation from normal biomass distribution.

4. Conclusion

The large area of the studied territory and the approximate homogeneity of the forest cover suggest the use of remote sensing methods for environmental monitoring. The recorded normalized difference vegetation index values and the classification made, reveal forest biomass distribution. For more detailed definition of forest status it is necessary to synthesize a model for correlation between different vegetation indexes and destructive factors' influence as parameters in such a model. The model construction requires complex application of vegetation indexes and high resolution data. [3]

Fig.2 NDVI for vitality assessment of the selected regions

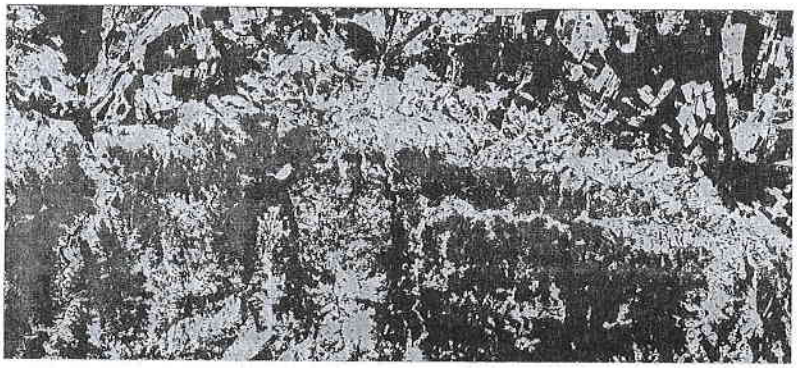

Fig.3 Classification on the NDVI values

References

1. Idrisi 32, Guide to GIS and Image processing J. R. Eastman, 1999
2. C. Travaglia, L. Milenova, et al, Preparation of Land Cover Database of Bulgaria trough Remote Sensing and GIS, FAO, UN, Rome 2001
3. A. Pavlova, R. Nedkov, Satellite and aero image integration for influence assessment of different destructive factors on forest stands, SPIE 9th Annual International Symposium Remote Sensing (in press)

ОЦЕНКА НА СЪСТОЯНИЕТО НА ГОРСКИ ЕКОСИСТЕМИ И ПРИЛЕЖАЩИТЕ ТЕРИТОРИИ ЗА РАЗВИТИЕ НА ЕКОЗЕМЕДЕЛИЕ

А.Павлова

Институт за космически изследвания – БАН

Резюме

Влиянието на горските промени е динамичен процес във времето и пространството. Изследването на издръжливостта и баланса в екосистемите е свързано с определяне на деструктивните фактори и посоката на развитие на оказаното въздействие. Основната цел на предлаганата разработка е свързана с оценка на деструктивните фактори, оказващи влияние върху области с различно земно покритие в райони с подобни климатични условия. Резултатите от изследването включват прилагане на NDVI за оценка на жизнеността на горите и количеството на зелената биомаса и наблюдаваната класификация за области с минимална горска биомаса на базата на получените стойности за NDVI. За по-подробно определяне на горския статус е необходимо да се синтезира модел за корелацията между различните вегетационни индекси и влиянието на деструктивните фактори като параметри в този модел.

Bulgarian Academy of Sciences. Space Research Institute.
Aerospace Research in Bulgaria. 18. 2003. Sofia

SOME FEATURES OF α DISC AND ADVECTIVE-DOMINATED ACCRETION DISC. SELF-SIMILAR SOLUTIONS AND THEIR COMPARISON -II

Lachezar Filipov, Krasimira Yankova, Daniela Andreeva

Space Research Institute - Bulgarian Academy of Science

Abstract

Using the models from part I, we have derived the basic parameters, describing the discs. We have obtained the self-similar solutions of the evolution for both types - ADAD and α discs. The results are expressed quantitatively to demonstrate our conclusion.

1. Introduction

As a continuation of Part I, dedicated to the priority of advection theory and the properties of advection - dominated flow and the comparison with standard accretion theory, here we present the actual results of our calculations. In many problems, the simple self-similar solutions don't correspond to complete solution [12]. They are intervening asymptotically and in a number of cases they give a sufficient idea of the studied physical phenomena with correct boundary conditions. As a result of the required transformation performed in our letter and using work [7] with adequate variables, we will obtain self-similar solutions, too.

2. Equations, describing the evolution of α disc and ADAD.

The last two systems from part I [8] (eq. 3.29 ÷ 3.33; 3.34 ÷ 3.38) enable us to obtain all parameters of the disc, so, we are looking only for Σ in explicit form. To this end we will use the conservation laws; using (eq. 2.10, see [8]) we obtain:

$$(\text{II.1}) \quad \Sigma V_r r = \frac{\dot{M}}{2\pi} = -\left(\frac{\partial h_*}{\partial h}\right)^{-1} \frac{\partial F}{\partial h}$$

which gives respectively:

(II.2) $\dot{M} = -2\pi \frac{\partial F}{\partial h}$

(II.3) $\dot{M} = -\frac{2\pi}{c_2} \frac{\partial F}{\partial h}$

From (eq. 2.9, see [8]) and (II.1) come after:

(II.4) $\frac{\partial \Sigma}{\partial t} = \frac{1}{2} \frac{(GM)^2}{L^3} \frac{\partial}{\partial h} \left\{ \left(\frac{\partial h_*}{\partial h} \right)^{-1} \frac{\partial F}{\partial h} \right\}$

as we apply (eq. (3.33) and eq. (3.38) see [8]) and the relation $\frac{\overline{\nu}}{h} = \left(\frac{2\alpha c_3}{3c_2} \right)$ we obtain the follows diffusion equations:

(II.5) $\frac{\partial F}{\partial t} = \Pi \frac{F^m}{h^n} \frac{\partial^2 F}{\partial h^2}$

(II.6) $\frac{\partial F}{\partial t} = \frac{\Pi_a}{h} \frac{\partial^2 F}{\partial h^2}$

where:

$$\Pi = \frac{AF^{\frac{1}{A}}}{2}(GM)^2 \qquad \Pi_a = \frac{\alpha}{2}\frac{c_3}{c_2}(GM)^2$$

$$m = \frac{4 + 2a_1}{10 + 2a_1 - 2b_1 - c_1} \qquad n = \frac{12 + 6a_1 + 2b_1 - 5c_1}{10 + 2a_1 - 2b_1 - c_1}$$

From (II.4) we get:

(II.7) $\Sigma = \frac{(GM)^2 F^{1-m}}{2(1-m)\Pi h^{3-n}}$

(II.8) $\Sigma = \frac{(GM)^2}{2\Pi_a} \frac{F}{h^2}$

3. Self – Similar Solutions.

First we will define the role of self-similar solutions and then we will give an example for their application. Such an example is the examination of the temperature diffusion equation for stationary conductive medium, presented in [7]:

$$\frac{\partial T}{\partial t} = D\nabla T$$

D - diffusion constant.

We will determine the temperature at successive moments of time, when the initial distribution is: $T = Kr^x$, r - the distance to the centre of the coordinate system.

If we define the scale of the temperature U, the distance Λ and the time η, then we can determine the dimensions D and K:

$$[D] = \eta^{-1}\Lambda^2 \quad \text{and} \quad [K] = \Lambda^{-x}U$$

D independent of U

Sometimes, after the beginning of the process, the typical length scale depending on time may be defined as:

$$\Lambda_c(t) = (Dt)^{1/2}$$

The time-dependant temperature scale may be defined in a similar way:

$$T_c(t) = K\Lambda_c(t)^x$$

The solution should yield T as a function of t and r. In non-dimensional form:

$$\frac{T}{T_c} = \frac{T}{K\Lambda^x}$$

This form should be a function of $\frac{r}{\Lambda_t(t)}$ and $\frac{t}{t}$.

So we obtain the solution in the form :

$$T = K\Lambda_c{}^x T_*\left(\frac{r}{\Lambda_c(t)}\right)$$

T_* - dimensionless function composed of its dimensionless arguments.

The obtained result is a self-similar solution, since time dependent scales are used. The temperature scale ia always the function of scale featuring the length. This is the self-similarity of the problem which denotes that variable scales of Λ_c and T_c may be selected. Because of this, it is possible to represent the scale of characteristics by a single variable function.

Therefore, the presence of several dimensions for the independent constants, including the boundary conditions of the problem, defines the neccessity of self-similar solution.

Let us examine the problem where the self-similar solution is of the first order. The time behavior of a thin disc is defined by (II.5) under the assumption that for the initial moment $t = 0$ the distribution is:

$$F = Kh^{\gamma}$$

The dimensions of all values in (II.5) and initial conditions are:

$$[h] = \Lambda^2\eta^{-1}; [t] = \eta\ ;\ [F] = M\Lambda^2\eta^{-2};$$

$$[\Pi] = M^{-m}\Lambda^{-2(n-m+2)}\eta^{2n-m-3};$$

$$[K] = M\Lambda^{2(1-\gamma)}\eta^{\gamma-2}.$$

Now we have to determine the typical scale of the total angular momentum $h_c(t)$ and typical scale of friction $F_c(t)$ for each moment $t > 0$.

The first value is obtained from the dimensional analysis of (II.5):

$$h_c(t) = \left(\Pi F_c(t)^m t\right)\frac{1}{n+2}$$

For $F_c(t)$ we use the initial distribution:

$$F_c(t) = Kh_c(t)^{\gamma}$$

Subtituting the last equation in the upper one, we obtain for h_c:

$$h_c(t) = \left(\Pi K^m t\right)\frac{1}{n+2-\gamma m}.$$

The solution of the problem yields F as a function of h and t and may be expressed in dimensionless form:

$$\frac{F}{F_c} = \frac{F}{Kh_c(t)^{\gamma}} = F_*\left(\frac{h}{h_c}, \frac{t}{t}\right) = F_*\left(\frac{h}{h_c}\right)$$

Then function F will take the form:

$$F(h.t) = Kh_c{}^{\gamma}(t)F_*\left(\frac{h}{h_c}\right).$$

Using the present above [7], we divide the variables in (II.5) and (II.6):

$$F(th) = F(t)f(\xi),\ \xi = \frac{h}{h_0} = \sqrt{\frac{r}{r_{out}}};\quad h_0 = \sqrt{GMr_{out}}$$

r_{out} is the edge of the disc.

Then:

$$(\text{III.1})\quad F(t)=\left[\frac{h_0^{\,n+2}}{-\lambda m\Pi(t+t_0)}\right]^{\frac{1}{m}}$$

$$(\text{III.2})\quad F(t)=F_0e^{\beta t};\quad \beta=\frac{\lambda_a\Pi_a}{h_0^{\,3}}$$

$$(\text{III.3})\quad \frac{\partial^2 f}{\partial\xi^2}=\lambda\xi^n f^{1-m}$$

$$(\text{III.4})\quad \frac{\partial^2 f}{\partial\xi^2}=\lambda_a\xi f$$

Also, we can search the function in polynomial form:

$$(\text{III.5})\quad f(\xi)=a_0\xi+a^{'}\xi^{l}+a_2\xi^{l_1}$$

$$l=3+n-m,\quad a^{'}=\frac{\lambda a_0^{\,1-m}}{l(l-1)},\quad a_2=\frac{\lambda^2 a_0^{\,1-2m}(1-m)}{2l(2l-1)(l-1)^2}$$

$$a_0=\frac{2l+1}{2(l-1)},\quad \lambda=l(2l-1)a_0^{\,m-1}-2l(l-1)a_0^{\,m}$$

and the boundary conditions are:

$$f(1)=1$$
$$f^{'}(1)=0\qquad f(0)=0$$

finally we replace (III.1), (III.2), (III.5) in (II.7) and (II.8)

Then we replace the result in ((eq. 3.29 ÷ 3.32,) and (eq. 3.34 ÷ 3.37), see [8]). As a result, the parameters of two discs are obtained in explicit form of time and dimensionless coordinate ξ.

Standard accretion disc:

$$\dot{M}=\frac{\dot{M}_k f^{'}}{\Psi^{\frac{1}{m}}};\qquad \dot{M}_k=\frac{-2\pi}{h_0}\left(\frac{h_0^{\,n+2}}{-\lambda m\Pi t_\phi}\right)^{\frac{1}{m}};\quad \Psi=\frac{t+t_0}{t_\phi}$$

$$\frac{\Sigma}{\Sigma_k}=\Psi^{\frac{m-1}{m}}f^{1-m}\xi^{n-3};\qquad \Sigma_k=\frac{1}{2}\frac{(GM)^2}{h_0^{\,3-n}}\frac{1}{\Pi(1-m)}\left(\frac{h^{n-2}}{-\lambda m\Pi t_\phi}\right)^{\frac{1-m}{m}}$$

$$\frac{T}{T_k}=\Psi^{2N_1\frac{m-1}{m}}f^{2N_1(1-m)}\xi^{2N_1(n-3)-6N_2};\qquad T_k=T_0\Sigma_k^{\,2N_1}\omega_{k0}^{\,2N_2}$$
$$\omega_{k0}=\omega_k(r_{out})$$

(III.6)

$$\frac{V_s}{V_{sk}} = \Psi^{N_1\frac{m-1}{m}} f^{N_1(1-m)} \xi^{N_1(n-3)-3N_2}; \qquad V_{sk} = V_{s0}\Sigma_k{}^{N_1}\omega_{k0}{}^{N_2}$$

$$\frac{W_{r\varphi}}{W_{r\varphi}{}^k} = \Psi^{(2N_1+1)\frac{m-1}{m}} f^{(2N_1+1)(1-m)} \xi^{(2N_1+1)(n-3)-6N_2};$$

$$W_{r\varphi}{}^k = W_{r\varphi 0}\Sigma_k{}^{2N_1+1}\omega_{k0}{}^{2N_2}$$

$$\frac{P}{P_k} = \Psi^{(N_1+1)\frac{m-1}{m}} f^{(N_1+1)(1-m)} \xi^{(N_1+1)(n-3)-3(N_2+1)}; \qquad P_k = P_0\Sigma_k{}^{N_1+1}\omega_{k0}{}^{(N_2+1)}$$

$$\frac{\tau}{\tau_k} = \Psi^{q_1\frac{m-1}{m}} f^{(1-m)q_1} \xi^{q_1(n-3)-3q_2};$$

$$\tau_k = k_1 T_0{}^{b_1} V_{s0}{}^{c_1}\Sigma_k{}^{q_1}\omega_k{}^{q_2}$$

$$q_1 = a_1 + 1 + (2b_1 + c_1)N_1$$

$$q_2 = (2b_1 + c_1)N_2 - c_1$$

$$L = \sigma\dot{M}(0,t)c^2; \quad \frac{L}{L_E} = \frac{\sigma\dot{M}_k[M_\odot / day]}{L_E}\frac{a_0 c^2}{\Psi^{\frac{1}{m}}}$$

Advection - dominated discs:

$$\dot{M} = \dot{M}_a e^{\beta t} f^{'}; \qquad \dot{M}_a = \frac{-2\pi}{c_2}\frac{F_0}{h_0}$$

$$\frac{\Sigma}{\Sigma_a} = e^{\beta t} f\xi^{-2}; \qquad \Sigma_a = \frac{F_0}{c_3\alpha h_0{}^2}$$

$$\frac{T}{T_a} = \xi^{-2}; \qquad T_a = T_0{}^a\omega_{k0}{}^2 r_{out}{}^2$$

$$\frac{V_s}{V_{sa}} = \xi^{-1}; \qquad V_{sa} = V_{s0}{}^a\omega_{k0} r_{out}$$

(III.7)

$$\frac{W_{r\varphi}}{W_{r\varphi a}} = e^{\beta t} f\xi^{-4}; \qquad W_{r\varphi a} = W_{r\varphi 0}{}^a\Sigma_a\omega_{k0}{}^2 r_{out}{}^2$$

$$\frac{P}{P_a} = e^{\beta t} f\xi^{-6}; \qquad P_a = P_0{}^a\Sigma_0\omega_{k0}{}^2 r_{out}$$

$$\frac{\tau}{\tau_a} = e^{\beta t} f\xi^{-2}; \qquad \tau_a = \chi_0\Sigma_a$$

$$\frac{L}{L_E} = \sigma_a \frac{\dot{M}_a[M_\odot / day]}{L_E} a_a c^2 e^{\beta_a}$$

Using Tables 1 and 2 (Appendix 1), and from (III.6) we obtain the parameters of the disc for two regimes: Thompson's opacity and frec-to-free transition.

To obtain the parameters of the advective disc we must define the constants c_2, c_3. Using the equations

$$\omega = c_2 \omega_k; \quad h = \omega_k r^2; \quad h_* = \omega r^2; \quad \frac{\partial h_*}{\partial h} = c_2$$

we can find c_2.

But the valuc of c_3 cannot be defined precisely, we can give an appreciation only and taking into account physically and mathematically conditions. To keep the slim disc formation it is necessary $\frac{H}{r}$ doesn't exceed 10^{-2} . But the disc is advective hot and then H/r is in maximum, that is why we consider $\frac{H}{r} = 10^{-2}$.

4. Comments

A comparison has been made between the standard and the advective model of the accretion disc and as a result, the main parameters of both discs in dimensionless quantities are obtained. We have used hydrodynamical equations, as we have added the terms describing the advection. The obtained solutions are self-similar.

The results (Appendix 2) lay down the field of action for the second theory. They prove that the new advective theory can be used, while the main advantage of the standard theory - the slim disc approximation, remains.

The presentation enables us to obtain the full approximation solution for disc parameters at non-stationary accretion. Although the self-similar solution doesn't fit in accurately, it displays good quality estimation for the physical processes in a given astrophysical disc.

References

1. Abramowicz M. A., Igumenshchev I. V., Lasota J.P., 1998, MNRAS, 293, 443-446.
2. Barenblatt G. I., Podobie, avtomodelnost, promezhutochnaja asimptotika / in Russian /, 1978, Leningrad
3. Beloborodov A.M., 1999, arxiv: astro-ph/ 9901108
4. Chen X., Abramowicz M. A., Lasota J.P., 1997, ApJ, 476, 61-69
5. Dibai E. A., Kaplan S. A., Razmernostiipodoble astrophysicheskih velichin / in Russian /, 1976, Nauka, Moskva
6. Fillpov L. G., Non-stationary disc accretion / in Russian /, 1993, Moscou
7. Fillpov L. G., 1990, Space Research in Bulgaria, 6, 21-28
8. Fillpov L. G., Yankova K. D., Andreeva D. V., Some features of α disc and advective-dominated accretion disc. Self-similar solutions and their comparision - I, Aerospace Research in Bulgaria, 17, 2003, 23-33
9. Lipunova G.V., Shakura N. I., 2000, A&A, 356, 363-372
10. NakamuraK. E., MatsumotoR., Kusunose M., Kato S., 1996, PASJ,48, 761-769
11. Narayan R., Yi I., 1994, ApJ, 428, L13-L16
12. Samarskli A. A., GalaktIonov V. A., Rezhimi s obostreniem v zadachah dlja kvazilineinih parabolicheskih uravnenii / in Russian /, 1987, Nauka, Moskva
13. Wu X.B., 1997, MNRAS, 292, 113-119
14. YamasakiT., 1997, PASJ, 49, 227-223

НЯКОИ ОСОБЕНОСТИ НА α ДИСК И АДВЕКТИВНО - ДОМИНИРАЩ АКРЕЦИОНЕН ДИСК. АВТОМОДЕЛНИ РЕШЕНИЯ И ТЯХНОТО СРАВНЕНИЕ - II

Лъчезар Филипов, Красимира Янкова, Даниела Андреева

Резюме

На базата на структурираните модели в част I, са изведени основните параметри, характеризиращи двата диска. Получени са автомоделни решения за еволюцията на двата типа - Адвективно-доминиращ и α диск. Резултатите са представени и количествено за да потвърдят нашите изводи.

APPENDIX 1

Table No.1

Regime	a_1	b_1	c_1
χ_0	0	0	0
χ_{ff}	1	-3,5	-1
α	$M/M_\circ$	r_{out}/R_0	μ
0,3	3	1	0,5

Table No.2

Regim ежим	m	n	λ	a_0	a'	a_2	l	l_1	N_1	N_2	q_1	q_2
χ_0	2/5	1,2	3,482	1,376	-0,39	0,02	3,8	6,6	1/3	1/6	1	0
χ_{ff}	0,3	0,8	3,137	1,430	-0,46	0.03	3,5	6,0	3/14	1/7	2/7	-1/7

Table No.3

c_1	c_3	λ_a	a_a	a''	a_3	γ	γ_1	$\beta\left[1/d\right]$
1	10^{-4}	-5,33	1,5	-0,66	0.08	4	7	$7{,}46.10^{-3}$

APPENDIX 2

Table No.4

Σ_T/Σ_k	Σ_{ff}/Σ_k	Σ/Σ_{ad}	ξ	$lg\Sigma/\Sigma_k$	$lg\Sigma/\Sigma_{ad}$	Δ
517,15		150,00	0,01	2,71	2,18	0,8
32,73		14,99	0,1	1,51	1,18	0,08
14,18		7,47	0,2	1,15	0,87	0,07
	7,73	4,94	0,3	0,89	0,69	0,05
	4,96	3,64	0,4	0,70	0,56	0,04
	3,49	2,93	0,5	0,54	0,47	0,03
$\Delta=10^{-2}$	2,59	2,27	0,6	0,41	0,36	0,03
	1,99	1,83	0,7	0,30	0,26	0,03
	1,57	1,48	0,8	0,19	0,17	0,03
	1,25	1,18	0,9	0,10	0,07	0,03
	1,00	1,00	1,0	0,00	0,00	0,03

Table No.5

T_t/T_k	T_{ff}/T_k	T/T_{ad}	ξ	lgT/T_k	lgT/T_{ad}	Δ
6445,6		10^4	0,01	3,81	4,00	0,8
102,14		10^2	0,1	2,01	2,00	0,08
29,30		25,00	0,2	1,47	1,40	0,07
	6,74	11,11	0,3	0,83	1,04	0,05
	4,36	6,25	0,4	0,64	0,80	0,04
	3,09	4,00	0,5	0,49	0,60	0,03
$\Delta=10^{-2}$	2,33	2,78	0,6	0,37	0,44	0,03
	1,82	2,04	0,7	0,26	0,31	0,03
	1,46	1,56	0,8	0,17	0,19	0,03
	1,20	1,23	0,9	0,08	0,09	0,03
	1,00	1,00	1,0	0,00	0,00	0,03

Table No.6

V_s^T/V_{sk}	V_s^{ff}/V_{sk}	V_s/V_{sad}	ξ	lgV_s/V_{sk}	lgV_s/V_{sad}	Δ
80,03		10^2	0,01	1,90	2,00	0,8
10,07		10	0,1	1,00	1,00	0,08
5,40		5,00	0,2	0,73	0,70	0,07
	2,60	3,33	0,3	0,41	0,52	0,05
	2,09	2,50	0,4	0,32	0,40	0,04
	1,76	2,00	0,5	0,24	0,30	0,03
$\Delta=10^{-2}$	1,53	1,67	0,6	0,18	0,22	0,03
	1,35	1,43	0,7	0,13	0,15	0,03
	1,21	1,25	0,8	0,08	0,10	0,03
	1,10	1,11	0,9	0,04	0,04	0,03
	1,00	1,00	1,0	0,00	0,00	0,03

Table No.7

$W_{r\varphi k}^T/W_{r\varphi}$	$W_{r\varphi k}^{ff}/W_{r\varphi}$	$W_{r\varphi}/W_{r\varphi}^{ad}$	ξ	$lgW_{r\varphi k}/W_{r\varphi}$	$lgW_{r\varphi}/W_{r\varphi}^{ad}$	Δ
$3,3.10^6$		$1,4999.10^6$	0,01	6,52	6,18	0,8
3301,0		1498,3	0,1	3,52	3,18	0,08
411,51		186,84	0,2	2,61	2,27	0,07
	52,13	54,90	0,3	1,72	1,74	0,05
	21,62	22,78	0,4	1,33	1,38	0,04
	10,80	11,74	0,5	1,03	1,07	0,03
$\Delta=10^{-2}$	6,04	6,30	0,6	0,78	0,80	0,03
	3,63	3,74	0,7	0,56	0,57	0,03
	2,30	2,31	0,8	0,36	0,36	0,03
	1,50	1,46	0,9	0,18	0,16	0,03
	1,00	1,00	1,0	0,00	0,00	0,03

Table No.8

P_T/P_k	P_{ff}/P_k	P/P_{ad}	ξ	lgP/P_k	lgP/P_{ad}	Δ
$4{,}09.10^{10}$		$1{,}4999.10^{10}$	0,01	10,61	10,18	0,8
$3{,}25.10^{5}$		$1{,}4993.10^{5}$	0,1	5,51	5,18	0,08
9453,30		4671,00	0,2	3,98	3,67	0,07
	743,48	6,	0,3	2,87	2,78	0,05
	161,85	142,39	0,4	2,21	2,15	0,04
	49,10	46,96	0,5	1,69	1,67	0,03
$\Delta=10^{-2}$	18,31	17,50	0,6	1,26	1,24	0,03
	7,84	7,63	0,7	0,89	0,88	0,03
	3,90	5,61	0,8	0,59	0,56	0,03
	1,88.	1,80	0,9	0,27	0,25	0,03
	1,00	1,00	1,0	0,00	0,00	0,03

Table No.9

τ_T/τ_k	τ^{ff}/τ_k	τ/τ_{ad}	ξ	$lg\tau/\tau_k$	$lg\tau/\tau_{ad}$	Δ
517,15		150,00	0,01	2,71	2,18	0,8
32,73		14,19	0,1	1,51	1,18	0,08
14,18		7,47	0,2	1,15	0,87	0,07
	1,07	4,94	0,3	0,03	0,69	0,05
	1,07	3,64	0,4	0,03	0,56	0,04
	1,06	2,93	0,5	0,03	0,47	0,03
$\Delta=10^{-2}$	1,05	2,27	0,6	0,03	0,36	0,03
	1,04	1,83	0,7	0,02	0,26	0,03
	1,03	1,48	0,8	0,02	0,17	0,03
	1,02	1,18	0,9	0,01	0,07	0,03
	1,00	1,00	1,0	0,01	0,00	0,03

Table No.10

$(\Sigma_k/\Sigma_0)_\tau.10^{-2}$	$(\Sigma_k/\Sigma_0)_{ff}.10^{-4}$	Σ_{ad}/Σ_a	t_ϕ[d]
1,12	9,30	0,86	20
0,61	3,62	0,80	30
0,40	1,85	0,74	40
0,28	1,10	0,69	50
0,22	0,72	0,64	60
0,17	0,50	0,59	70
0,14	0,37	0,55	80
0,12	0,28	0,51	90
0,10	0,22	0,47	100

Bulgarian Academy of Sciences. Space Research Institute.
Aerospace Research in Bulgaria. 18. 2003. Sofia

POSSIBILITIES FOR APPLYING PHASE-MANIPULATED COMPLEMENTARY SIGNALS IN SPACECRAFT-BASED RADARS

Borislav Bedzhev

National Military University, Artillery Department, Air-Defence and Communication and Information Systems

Abstract

In spacecraft-based radar systems, high-quality images of the planet, satellite, and comet surface are obtained using the Synthetic Aperture Radar (SAR) method. Moreover, to provide both wide performance range and great distance resolution, complex radar signals with inner pulse modulation are applied.

Currently, space SARs use mostly linear frequency modulation (LFM) signals. However, alongside with their positive features, they also possess some disadvantages. At the same time, in the recent dozen years or so, signals with internal pulse phase manipulation (PM) became widely applied.

The results of the paper may be summarized as follows:

1. A mathematical method for synthesizing a new class of PM signals called generalized complementary signals (GCS), whose ACF features close-to zero side lobe level has been developed.

2. Through computer simulation of radiolocation systems with inverse synthesized aperture, the applicability of GCS in prospective spacecraft-based radar systems has been proven.

1. Introduction.

As it is known [1], in spacecraft-based radar systems, the method of synthetic aperture is widely used in order to obtain high-quality images of planet, satellite and comet surfaces. In this process, complex radar signals with inner pulse modulation are applied because they provide both wide performance range and great distance resolution.

The most important feature of the autocorrelation function (ACF) of synthetic aperture radar (SAR) signals is the level of their side lobes, because they determine the dynamic range of the image and the possibility to identify small objects. At present, in spacecraft-based radars, signals with linear frequency modulation are widely applied. They were proposed fifty

years ago, but despite their positive qualities, they have some disadvantages as well, such as a relatively high level of ACF's side lobes and complex generating and processing hardware [2]. In this regard, it should be emphasized that, recently, signals with inner pulse phase manipulation (PM) have found wide application in wireless communications. For instance, PM signalling is the basis of the so-called "Direct Sequence Spread Spectrum" techniques [3]. As a result, the PM signal generating and processing hardware has improved drastically.

In view of the above-mentioned facts, this paper aims:

- to suggest mathematical methods for synthesis of a new class of PM signals, named generalized complementary signals, featuring ACF with close-to-zero level of the side lobes;
- to illustrate the advantages of the usage of generalized complementary signals in prospective SARs.

2. Method of phase manipulated complementary signals synthesis

It is known [4], that PM (or DS-SS) signals represent sequences of n equivalent elementary pulses which are described by:

$$(1) \qquad v(t) = \sum_{j=1}^{n} U_j . u_0(t - t_j).\cos[\omega_0.(t - t_j) + \theta_j],$$

where:

- U_j **are the amplitudes of the elementary pulses;**
- $\omega_0 = 2\pi f_0$; f_0 **is the carrier frequency;**

$$u_0(t) = \begin{cases} 1, & if \quad 0 \le t \le \tau_0 \\ 0, & if \ t < 0, \ or \ t > \tau_0 \end{cases}.$$

To simplify the practical accomplishment of the complex process of PM signal receiving, the following limitations in formula (1) are made [3, 4]:

- $\tau_0 = const$; $\quad U_j = U_0 = const$; $\quad j = 1,2,...,n$;
- $\theta_j \in \{(2\pi l)/m; \quad l = 0,1,...,m-1\}$.

In this case, the PM signal can be described as a sequence of complex amplitudes of elementary signals [4]:

$$V(t) = \sum_{j=1}^{n} U_0 . \zeta(j) . u_0(t - t_j),$$

where $\{\zeta(j)\}_{j=0}^{n-1}$ is the set of complex amplitudes of the elementary pulses and the elements of the set are the m-th roots of the unity:

$$(2) \qquad \zeta(j) \in \{\exp(2\pi i l / m); l = 0,1,...,m-1\}.$$

It is known that complementary series are a pair of two special PM signals, whose aggregated non-periodical auto-correlation function (ACF) resembles a delta pulse. The classical Golay's definition of the complementary series [5] is:

Definition 1: *The sequences* $\{\mu(j)\}_{j=0}^{n-1}$, $\{\eta(j)\}_{j=0}^{n-1}$, *consisting of n elements with values +1 and -1:* $\mu(j) \in \{-1,+1\}$; $\eta(j) \in \{-1,+1\}$; $j = 0,1,...,n-1$, *are called pair of complementary series, if:*

$$(3) \qquad R_c(k) = R_\mu(k) + R_\eta(k) = \begin{cases} 2n; & k = 0 \\ 0; k = \pm 1, \pm 2, ..., \pm(n-1) \end{cases}.$$

In (3), the non-periodical ACFs $R_\mu(k)$ и $R_\eta(k)$ are defined by the well known formula [3, 4]:

$$(4) \qquad R_\varsigma(k) = \begin{cases} \sum_{j=0}^{n-1-|k|} \varsigma(j)\varsigma^*(j+|k|), & -(n-1) \le k \le 0 \\ \sum_{j=0}^{n-1-k} \varsigma^*(j)\varsigma(j+k), & 0 \le k \le n-1 \end{cases}.$$

Here, the symbol "*" means a complex conjugation. The above definition of complementary series will be clarified in Fig. 1 by an example of sequences of code-length n=10:

$\mu(0) = -1, \mu(1) = -1, \mu(2) = -1, \mu(3) = -1, \mu(4) = -1, \mu(5) = 1, \mu(6) = -1, \mu(7) = 1, \mu(8) = 1, \mu(9) = -1;$

$\eta(0) = 1, \eta(1) = -1, \eta(2) = 1, \eta(3) = -1, \eta(4) = -1, \eta(5) = -1, \eta(6) = 1, \eta(7) = 1, \eta(8) = -1, \eta(9) = -1.$

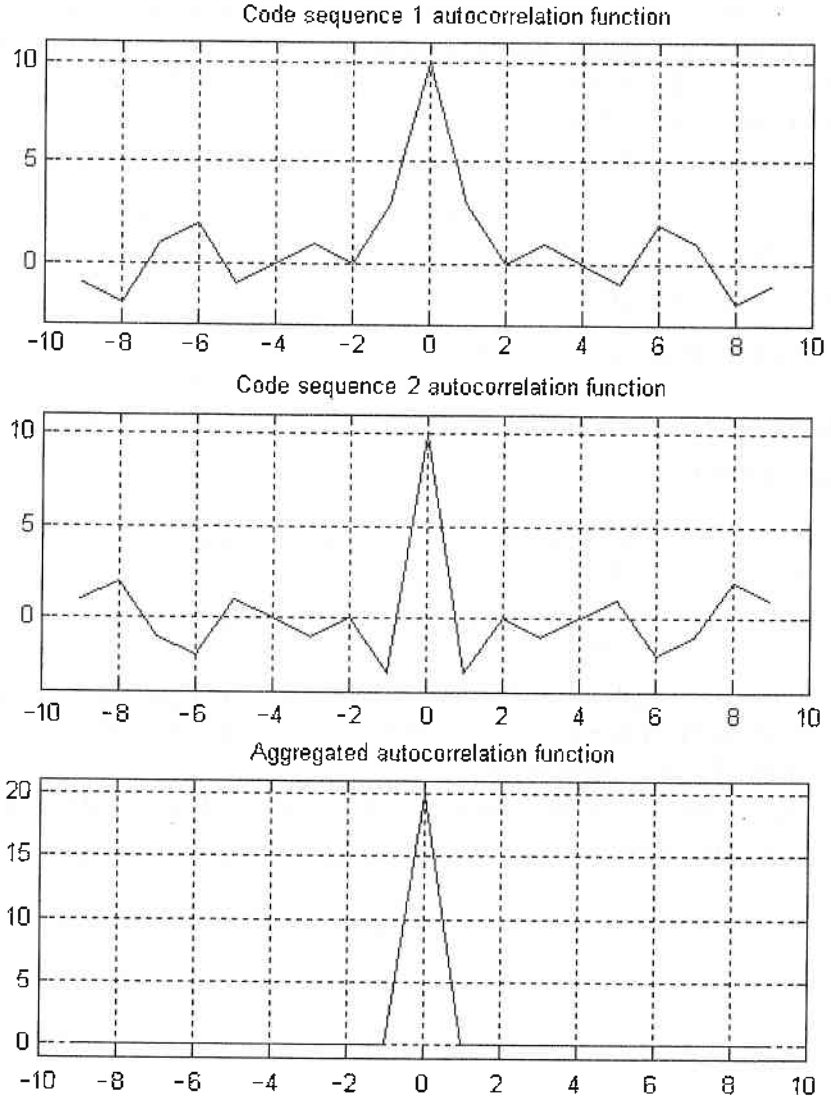

Fig.1. Autocorrelation functions of complementary sequences with $n = 10$ elements.

The complementary series are unique among all PM signals for the following features:

- their aggregated ACF has an ideal shape resembling a delta pulse;
- if a pair of complementary series, consisting of n elements, is known, then it is easy to create an infinite set of pairs with unlimited code-length.

With respect to the second feature, it is necessary to emphasize that most PM type signals with close to ideal ACF have limited code-length. For instance, Barker codes exist only for $n \le 13$, if n is an odd integer.

In the original Golay's paper, two theorems are proved [5], which show the way we can obtain derivative complementary series with code-length 2n.r if two pairs of code-length n and r are known. The theorems are similar and in order to simplify the explanation, they will be combined as follows.

Theorem 1 (Golay's Theorem): If the two pairs of complementary series $A = \{\mu(j)\}_{j=0}^{n-1}$, $B = \{\eta(j)\}_{j=0}^{n-1}$; *and* $C = \{\xi(j)\}_{j=0}^{r-1}$, $D = \{\zeta(j)\}_{j=0}^{r-1}$ *of code-length n and r respectively, are known, then the derivative pairs of sequences:*

(5a)

$$K = \{\xi(0).A, \xi(1).A, ..., \xi(r-1).A, \zeta(0).B, \zeta(1).B, ..., \zeta(r-1).B\};$$
$$L = \{\zeta(r-1).A, \zeta(r-2).A, ..., \zeta(0).A, -\xi(r-1).B, -\xi(r-2).B, ..., -\xi(0).B\};$$

(5b)

$$M = \{\xi(0).A, \zeta(0).B, \xi(1).A, \zeta(1).B, ..., \xi(r-1).A, \zeta(r-1).B\};$$
$$N = \{\zeta(r-1).A, -\xi(r-1).B, \zeta(r-2).A, -\xi(r-2).B, ..., \zeta(0).A, -\xi(0).B\};$$

are complementary sequences of code-length 2nr.

Complementary series of code-length $n = 2,10,26$ are known at present. Using them and Golay's theorem makes it possible to create infinite number of complementary series of code-lengths:

(6) $n = 2^{s_1}.10^{s_2}.26^{s_3}$.

It is necessary to emphasize that Golay's definition of complementary codes is not useful in some important cases. This situation has motivated some theoreticians like Tseng, Liu, Suehiro, Ignatov [6, 7, 8], to extend the classical definition. Namely, they have proposed the so-called "generalized complementary codes" which constitute a set of p elements (PM signals), the aggregate ACF of all sequences having an ideal shape resembling a delta pulse. Consequently, Golay's codes are a particular case of Tseng-Liu codes, where p=2. Now it ought to be seen, that:

- the PM generating hardware is drastically enhanced;
- the binary phase modulation isn't appropriate quite often, because it restricts the rate of information translation and/or the possible variants in the process of developing communication devices.

With regard to this, in the next part of the paper, we shall "correct" Definition 1 as follows.

Definition 2: *The set of p sequences (PM signals), whose elements are complex numbers, belonging to the multiplicative group of the m-th ($m > 2$) roots of unity:*

$$(7)\quad \begin{aligned} &\{A_1 = \{\xi_1(j)\}_{j=0}^{n_1-1}; A_2 = \{\xi_2(j)\}_{j=0}^{n_2-1}; \ldots; A_p = \{\xi_p(j)\}_{j=0}^{n_p-1}\}; \\ &\xi_k(j) \in \{\exp(2\pi i l / m_k); l = 0,1,\ldots,m_k - 1\}; k = 1,2,\ldots,p. \end{aligned}$$

are a set of generalized complementary codes (sequences) if and only if their aggregate ACF has the ideal shape, resembling a delta pulse:

$$(8)\quad R_c(r) = \sum_{k=1}^{p} R_{A_k}(r) = \begin{cases} n = n_1 + n_2 + \ldots + n_p; & \text{if } r = 0; \\ 0; & \text{if } r = 1,2,\ldots,\max\{n_k\}. \end{cases}$$

This definition will be illustrated by the following so-far-unknown complementary codes ($m = 4$ in (2), $p = 2$):

$$(9)\quad \begin{aligned} &\{\mu(j)\}_{j=0}^{2} = \{1,i,1\}; \qquad \{\eta(j)\}_{j=0}^{2} = \{1,1,-1\}; \\ &\{\mu(j)\}_{j=0}^{4} = \{-i,i,1,1,1\}; \quad \{\eta(j)\}_{j=0}^{4} = \{1,i,-1,1-i\}. \end{aligned}$$

Now we shall see whether it is possible to create sets of complementary sequences of unlimited code-length, using some initial sets of complementary sequences of short code-length. In order to reach this goal, we shall prove a theorem, whose particular case is Golay's theorem.

It should be emphasized that a common theorem couldn't be developed based on Theorem 1, because the method of Golay, Tseng and Liu is not applicable for the situation of generalized complementary codes, according to Definition 2. Therefore, we shall use a new algebraic method [9]. At the beginning, we shall introduce some terms, used in the common theorem.

Definition 3: The matrix $H_{q,p} = \{h_{k,l}(x)\}; k = 1,2,\ldots,q; l = 1,2,\ldots,p$ *will be called generalized column orthogonal matrix, if:*

$$(10)\quad \sum_{k=1}^{q} h_{k,j}(x).h_{k,s}^{*}(x^{-1}) = \begin{cases} c_j; & c_j = const, \quad \text{if } j = s; \\ 0, & \text{if } j \neq s; j = 1,2,\ldots,p; s = 1,2,\ldots,p \end{cases}.$$

The entries of the matrix $H_{q,p}$ in (10) are polynomials with equivalent maximal power of x in each column: $\deg h_{k,j}(x) = r_j - 1$.

It is easy to see that the column orthogonal matrices satisfy the equation:

$$(H^*)^T.H = \begin{bmatrix} c_1 & 0 & \dots & 0 \\ 0 & c_2 & \dots & 0 \\ \dots & \dots & \dots & \dots \\ 0 & 0 & \dots & c_p \end{bmatrix}.$$

Here:

- the superscript "T" means "changing the places of the rows and columns";

- the subscripts are omitted in order to simplify the expression.

Examples of the matrix H when $\deg h_{j,k}(x) = 0$ are:

$$\begin{bmatrix} 1 & 1 & 1 \\ 1 & \omega & \omega^2 \\ 1 & \omega^2 & \omega \end{bmatrix}, \begin{bmatrix} \omega & 1 & 1 \\ 1 & \omega & 1 \\ 1 & 1 & \omega \end{bmatrix}, \text{ i.e., where: } \omega = -\frac{1}{2} + i\frac{\sqrt{3}}{2};$$

$\omega^2 = -\frac{1}{2} - i\frac{\sqrt{3}}{2}$, $1 + \omega + \omega^2 = 0$.

Now we are able to prove the following common theorem.

Theorem 2: Let $H_{p,q}$ *be generalized orthogonal column matrix, and let* $\{A_k = \{\xi_k(j)\}_{j=n_1+\dots+n_{k-1}}^{n_k-1}\}_{k=1}^{p}$ *be a set of generalized complementary sequences. Then the set:*

(11)

$$\{h_{11}.A_1, h_{12}.A_2, \dots, h_{1p}.A_p\}; \{h_{21}.A_1, h_{22}.A_2, \dots, h_{2p}.A_p\}; \dots; \{h_{q1}.A_1, h_{q2}.A_2, \dots, h_{qp}.A_p\};$$

is a set of generalized complementary codes, too. Here, multiplications in (11) mean:

(12) $h_{ij}.A_k = \zeta_{ij}(0).A_k, \zeta_{ij}(1).A_k, \dots, \zeta_{ij}(r_{ij}-1).A_k,$

if:

(13) $h_{ij}(x) = \zeta_{ij}(r_j - 1).x^{r_j-1} + \zeta_{ij}(r_j - 2).x^{r_j-2} + \dots + \zeta_{ij}(1).x + \zeta_{ij}(0).$

Proof: The proof will be made using the so-called creative functions method [10]. According to this method, the ACF of the PM signal will be presented by the following polynomial:

(14)

$$P(x) = F(x).F^*(x^{-1}) = R_{\zeta\zeta}(-(n-1)).x^{-(n-1)} + R_{\zeta\zeta}(-(n-2)).x^{-(n-2)} + ... + R_{\zeta\zeta}(0) +$$

$$+ ... + R_{\zeta\zeta}(n-2).x^{n-2} + R_{\zeta\zeta}(n-1).x^{n-1} = \sum_{k=-(n-1)}^{n-1} R_{\zeta\zeta}(k).x^k$$

.

Here:

(15) $F(x) = \zeta(n-1).x^{n-1} + \zeta(n-2).x^{n-2} + ... + \zeta(1).x + \zeta(0)$,

is the polynomial, corresponding to the sequence $\{\zeta(j)\}_{j=0}^{n-1}$ of complex amplitudes of the elementary pulses of the PM signal, $R_{\zeta\zeta}(k)$ are the ACF values and $F^*(x^{-1})$ is the polynomial:

(16)

$$F^*(x^{-1}) = \zeta^*(n-1).x^{-(n-1)} + \zeta^*(n-2).x^{-(n-2)} + ... + \zeta^*(1).x^{-1} + \zeta(0).$$

Applying (14)-(16) in (11) yields:

(17)

$$R_c(x) = \sum_{i=1}^{q}\left[\sum_{j=1}^{p} h_{ij}(x^{n_j}).x^{r_1n_1+r_2n_2+...+r_{j-1}n_{j-1}}.A_j(x)\right]\left[\sum_{j=1}^{p} h_{ij}^*(x^{-n_j}).x^{-(r_1n_1+r_2n_2+...+r_{j-1}n_{j-1})}.A_j^*(x^{-1})\right] =$$

$$= \sum_{i=1}^{q}\sum_{j=1}^{p} h_{ij}(x^{n_j})h_{ij}^*(x^{-n_j})A_j(x).A_j^*(x^{-1}) + \sum_{i=1}^{q}\sum_{j=2}^{p}\sum_{k=1}^{j-1}\left[h_{ij}h_{ij-k}^*.x^{r_{j-k}n_{j-k}+...+r_{j-1}n_{j-1}}A_j(x)A_{j-k}^*(x^{-1}) +\right.$$

$$\left. + h_{ij-k}h_{ij}^*x^{-(r_{j-k}n_{j-k}+...+r_{j-1}n_{j-1})}A_{j-k}(x)A_j^*(x^{-1})\right].$$

It is easy to see, that in (17):

$$\sum_{i=1}^{q}\sum_{j=1}^{p} h_{ij}(x^{n_j})h_{ij}^*(x^{-n_j})A_j(x).A_j^*(x^{-1}) = \sum_{j=1}^{p} A_j(x).A_j^*(x^{-1})\sum_{i=1}^{q} h_{ij}(x^{n_j})h_{ij}^*(x^{-n_j}) =$$

$$= \sum_{j=1}^{p} c_j.A_j(x).A_j^*(x^{-1}) = (c_1n_1 + c_2n_2 + ... + c_pn_p);$$

$$\sum_{i=1}^{q}\sum_{j=2}^{p}\sum_{k=1}^{j-1}\left[h_{ij}(x^{n_j})h_{ij-k}^*(x^{n_{j-k}}).x^{r_{j-k}n_{j-k}+...+r_{j-1}n_{j-1}}A_j(x)A_{j-k}^*(x^{-1}) +\right.$$

$$\left. + h_{ij-k}(x^{n_{j-k}})h_{ij}^*(x^{n_j}).x^{-(r_{j-k}n_{j-k}+...+r_{j-1}n_{j-1})}A_{j-k}(x)A_j^*(x^{-1})\right] = 0,$$

because: $\sum_{i=1}^{q} h_{ij}(x^{n_j}).h^*_{ij-k}(x^{-n_{j-t}}) = 0$, $\sum_{i=1}^{q} h_{ij-k}(x^{n_{j-t}}).h^*_{ij}(x^{-n_j}) = 0$, according to (10).

The last equations show that in (11), condition (8) is satisfied. Hence, set (11) is a set of generalized complementary sequences.

Theorem 2 reduces the problem for synthesis of complementary sequences to two steps: first, finding an arbitrary "initial" complementary set $\{A_k\}_{k=1}^{p}$, and, second, constructing an appropriate "creative" matrix $H_{p,q}$. As the above-shown sets (9) are appropriate initial sets, it is enough to concentrate our efforts on solving the second problem. With regard to this, it is easy to verify that the following matrices H(x) satisfy condition (10) [9]:

(18) $$H(x) = \begin{bmatrix} B_1(x^n); B_2(x^n) \\ \tilde{B}^*_2(x^n); -\tilde{B}^*_1(x^n) \end{bmatrix}, \quad H(x) = \begin{bmatrix} B_1(x^{2n}); & B_2(x^{2n}) \\ x^n.\tilde{B}^*_2(x^{2n}); & -x^n.\tilde{B}^*_1(x^n) \end{bmatrix},$$

where:

(19) $$B_k(x) = \zeta_k(r-1).x^{n(r-1)} + \zeta_k(r-2).x^{n(r-2)} + ... + \zeta_k(1).x^n + \zeta_k(0),$$

(20) $$\tilde{B}^*_k(x^{-n}) = \zeta^*_k(r-1).x^{-n(r-1)} + \zeta^*_k(r-2).x^{-n(r-2)} + ... + \zeta^*_k(1).x^{-n} + \zeta^*_k(0),$$

and $\{\zeta_k(j)\}_{j=0}^{r-1}; k = 1,2$ is an arbitrary set of generalized complementary sequences of length r and p=2.

Construction (11), proven in the paper, will be illustrated by two examples, where sets (9) of generalized complementary series, will be used. Let the first one be as follows:

$$A_1 = B_1 = \{\mu(j)\}_{j=0}^{2} = \{1, i, 1\}; \qquad A_2 = B_2 = \{\eta(j)\}_{j=0}^{2} = \{1, 1, -1\}.$$

Applying the construction of Theorem 2, the derivative set of generalized complementary series of length $2.n.r = 2.3.3 = 18$ is obtained:

$K = \{1,i,1,i,-1,i,1,i,1,1,1,-1,1,1,-1,-1,-1,1\}$; $L = \{-1,-i-1,1,i,1,1,i,1,-1,-1,1,i,i,-i,-1,-$

.

In the second example, the sets of generalized complementary series:

$$A_1 = B_1 = \{\mu(j)\}_{j=0}^{4} = \{-i, i, 1, 1, 1\}; \qquad A_2 = B_2 = \{\eta(j)\}_{j=0}^{4} = \{1, i, -1, 1-i\},$$

are used to develop a set of generalized complementary series of length $2.n.r = 2.5.5 = 50$. The complex parts of the initial and derivative sequences are shown in Fig.2 and Fig. 3, respectively.

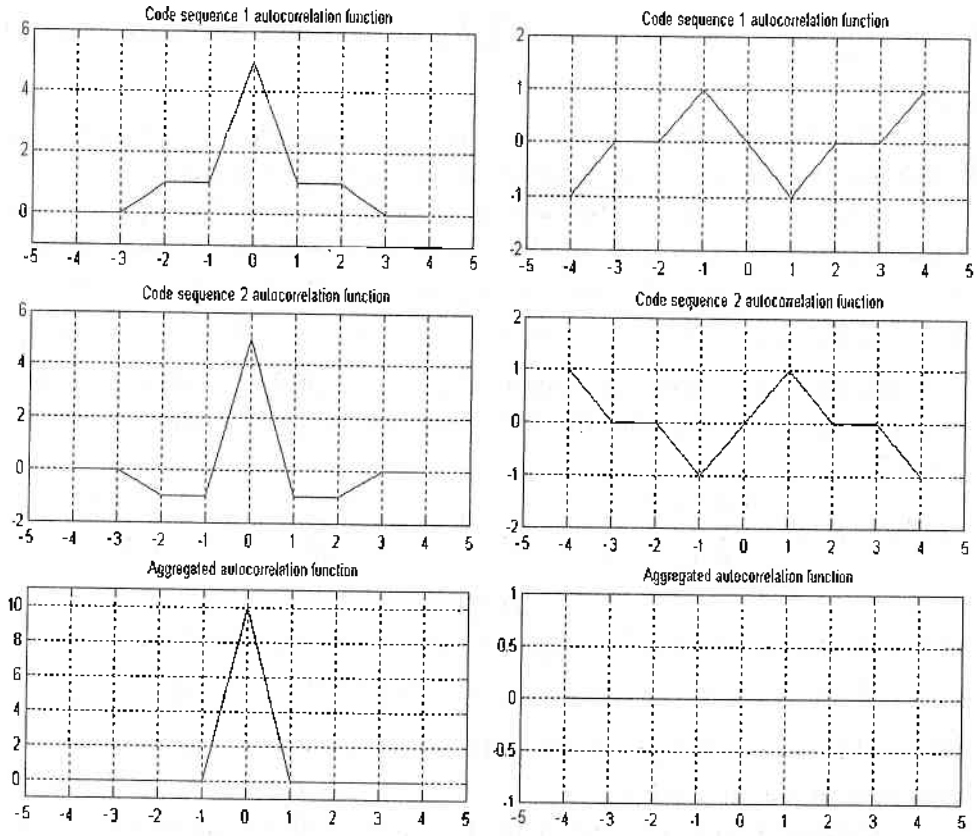

(a)

(b)

Fig.2. Real (a) and imaginary (b) components of the autocorrelation functions of complementary sequences with $n = 5$ elements and $m = 4$.

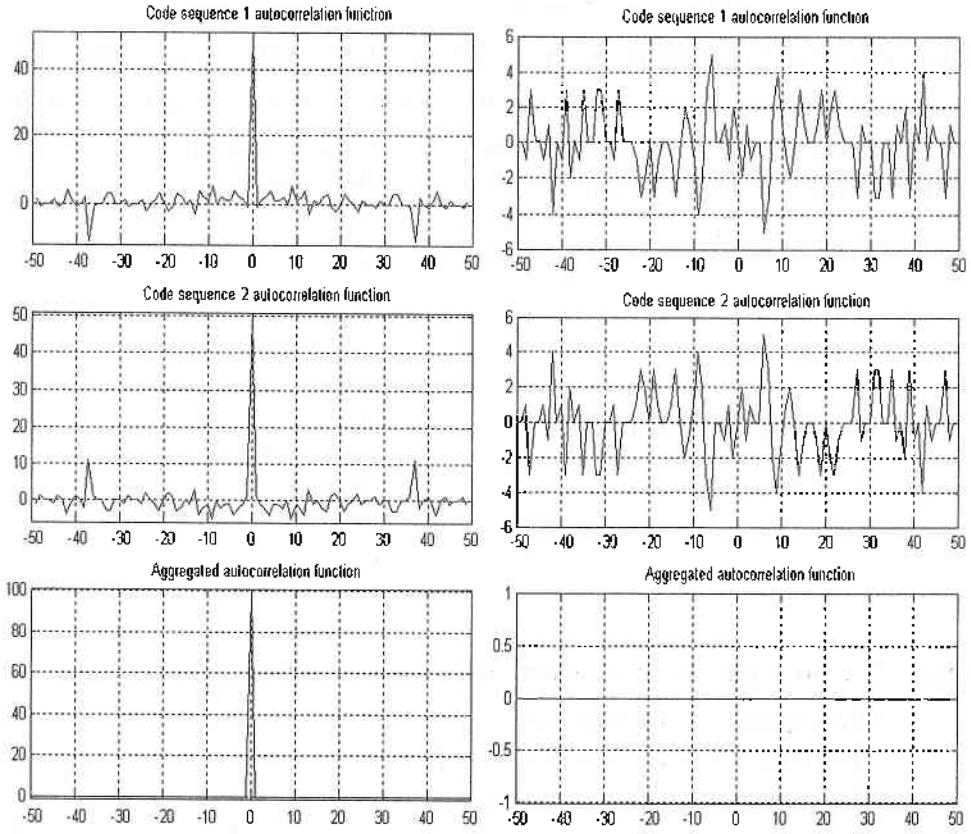

(a) (b)

Fig.3. Real (a) and imaginary (b) components of the autocorrelation functions of complementary sequences with $n = 50$ elements and $m = 4$.

3. Possibilities for applying phase-manipulated complementary signals in spacecraft-based radars

The possible advantages of applying sets of generalized complementary sequences are verified by computer experiments. The operation of a radar using the method of inverse synthetic aperture in the process of target identification is simulated.

The experiments are based on the geometrical model, proven in [11]. It is assumed that the object is radiated by a pulse sequence of pulse duration T, repeat period T_p and carrier frequency f_0. During the experiments, the impact of the type of the inner pulse phase modulation on the quality of the object image is examined. Namely, the pulses of the radar transmitter are described by the following formula:

$$(21) \quad u(t) = U_0 \exp\{i[\omega t + b\pi + \varphi_0]\},$$

where U_0 is the amplitude of the carrier frequency, $\omega = 2\pi f_0$ - the angle frequency; φ_0 - the initial phase, and the parameter b determines the type of phase modulation. For instance, in the case of phase modulation with 13-element Barker code, the parameter b assumes the values:

$$(22) \quad b = \begin{cases} 0 \ , & t = \overline{1,5}\tau_0 ; \\ 1 \ , & t = \overline{6,7}\tau_0 ; \\ 0 \ , & t = \overline{8,9}\tau_0 ; \\ 1 \ , & t = 10\tau_0 ; \\ 0 \ , & t = 11\tau_0 ; \\ 1 \ , & t = 12\tau_0 ; \\ 0 \ , & t = 13\tau_0 , \end{cases}$$

where τ_0 is the duration of the elementary pulses (chips).

The trajectory parameters are:

- the object velocity $V = 400\,[m/s]$;
- the course parameter $\alpha = \pi\,[rad]$;
- the measure of the object space grid cells $\Delta X = 0.6\,[m]$; $\Delta Y = 0.6\,[m]$;
- the initial coordinates of the object $x_0 = 0\,[m]$; $y_0 = 5.10^4\,[m]$.

The parameters of the radiated pulse sequence are:

- the duration of an PM radiated pulse (in the case of Barker code, phase modulation) $T = 5{,}2.10^{-8}\,[s]$;
- the duration of an elementary pulse (chip) $\tau_0 = 4.10^{-9}\,[s]$;
- the carrier frequency $f = 10^{10}\,[Hz]$;
- the number of pulses reflected from the object $N_p = 500$.

In the case of modulation with complementary codes, the following sequences are applied:

$$(23) \quad \{\mu(j)\}_{j=0}^{7} = \{+1,+1,+1,-1,+1,+1,-1,+1\};$$
$$\{\eta(j)\}_{j=0}^{7} = \{+1,+1,+1,-1,-1,-1,+1,-1\}.$$

In the odd periods, the first sequence is used, and in the even periods, the second one. The duration of each sequence ("concatenated" pulse) is $T = 3{,}2.10^{-7}\,[s]$.

In Fig. 4-7, the numerical results of the experiments with models of the aircrafts Boeing-707 (Fig.4), Falcon-2000 (Fig.5), MiG-29 (Fig.6) and MiG-35 (Fig.7) are shown.

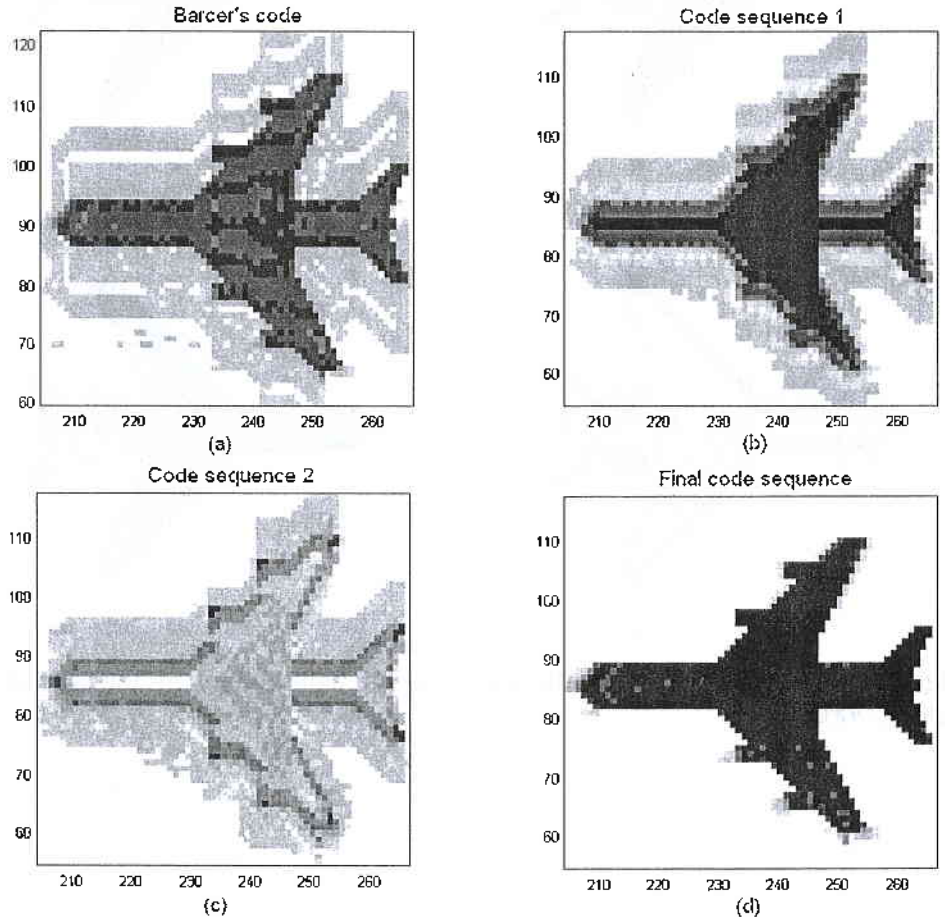

Fig. 4. Numerical results of the experiments with model of the aircraft Boeing-707.

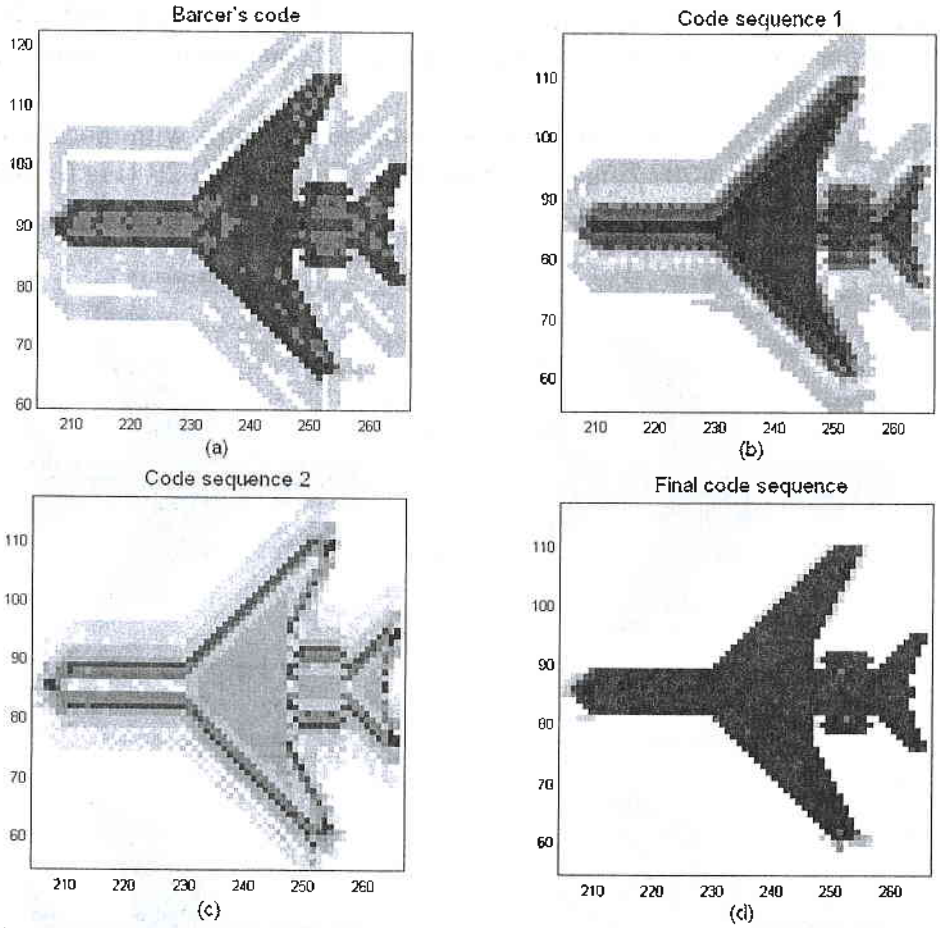

Fig. 5. Numerical results of the experiments with model of the aircraft Falcon-2000 .

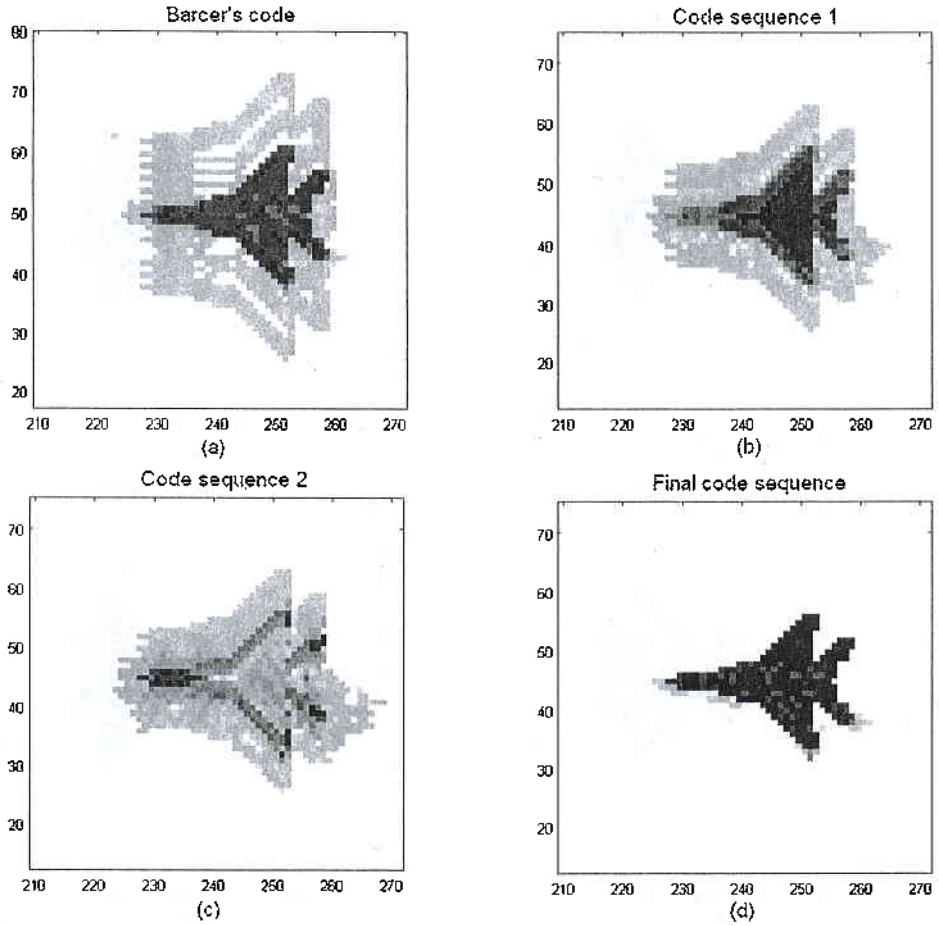

Fig.6. Numerical results of the experiments with model of the aircraft MiG-29.

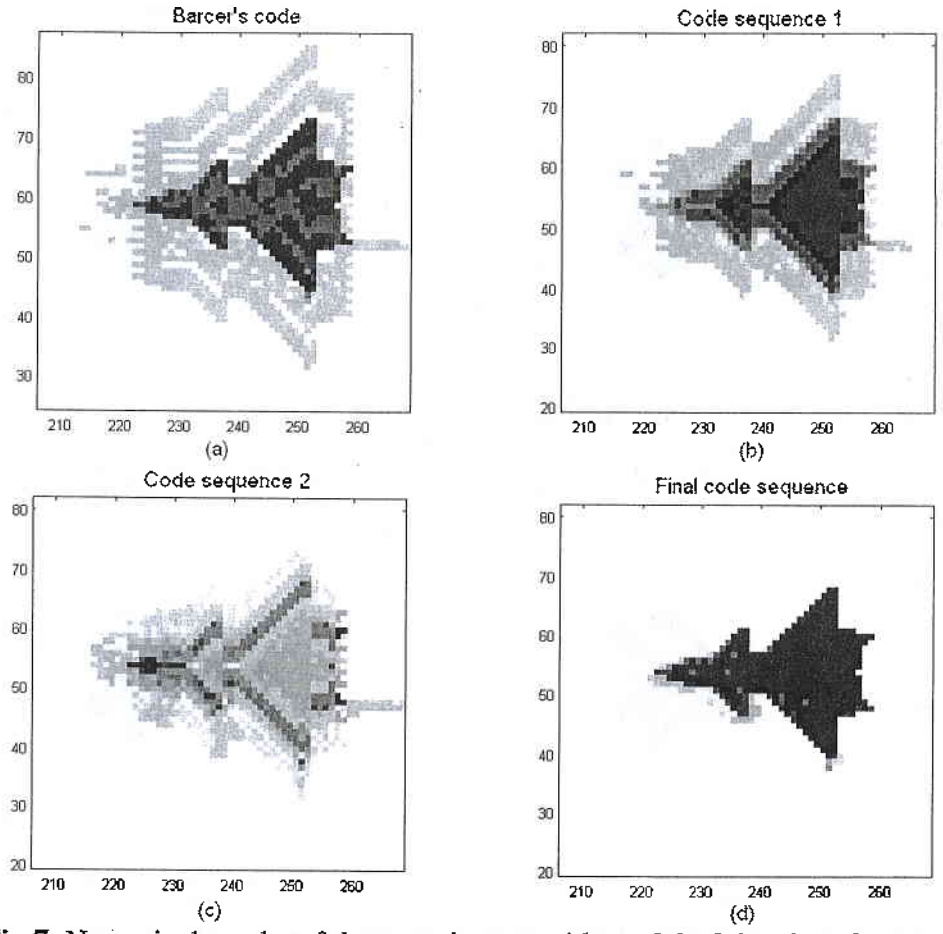

Fig.7. Numerical results of the experiments with model of the aircraft MiG-35.

On the basis of the experimental results, it is easy to see that:

1) If sequences (23) are applied separately, the structural noise is bigger than the noise in the case of modulation with Barker's codes (Fig. 4a,b,c – Fig. 7a,b,c).

2) If sequences (23) are applied together (in "aggregate"), the structural noise decreases practically to zero, which results in ideal shape of the ACF (Fig. 4d – Fig. 7d).

4. Conclusions

From everything stated above, it can be easily seen that Theorem 2 generalizes Golay's [5], Liu's, Tseng's, Suehiro's and Ignatov's constructions [6, 7, 8]. This was revealed upon investigating the common case where the phase of the PM signals can take $m \geq 2$ values. As a result,

Theorem 2 construction accelerates the process of synthesis of complementary series with unlimited code-length $2^s.n^u.r^v$ using complementary series with short lengths n and r. The advantages in the design of modern communication devices are also increased because systems with PM signals with modulated phase according to a set of generalized complementary series make effective use of the electromagnetic spectrum.

Having in mind the above-mentioned positive features, the construction for synthesis of complementary series proven in the paper could be used successfully in prospective spacecraft-based radar systems, where PM signals allow enhancing of the ranging distance without loosing measurement accuracy and target resolution.

References

1. Мардиросян Г., Аерокосмически методи и средства в екологията и изучаването на околната среда – С.: Академично издателство "Проф. М. Дринов", 2003г., 208 с.

2. Шияновский Э. Н., Применение Д-кодов для фазовой манипуляции сигналов РСА, Радиотехника, 1998, № 4, с. 79 – 86

3. Dinan E. H., Jabbari B., Spreading codes for direct sequence CDMA and wideband CDMA cellular networks, IEEE Communications Magazine, 1998, vol. 36, № 9, pp. 48 – 54

4. Варакин Л. Е., Системы связи с шумоподобными сигналами - М.: Радио и связь, 1985. – 384 с.

5. Golay M. Y. E., Complementary series, IRE Trans. on Information Theory, 1961, vol. IT – 7, №2, pp. 82 – 87

6. Tseng C. C., Liu S. L., Complementary sets of sequences, IEEE Trans. on Information Theory, 1972, vol. IT- 18, №5, p. 644 – 652

7. Игнатов В. В., Добровольский С. А., Гужва А. Ю., Матричные системы сигналов для использования в системах CDMA, Электросвязь, 2003, № 9, с. 41-42

8. Chen H.-H., Yat-Sen S., Yeh J.-F., Suchiro N., A multi-carrier CDMA architecture based on orthogonal complementary codes for new generations wideband wireless communications, IEEE Communication Magazine, 2001, vol. 39, № 10, pp. 126 – 135

9. Bedzhev B. Y., Tasheva Zh. N., Mutkov V. A., CDMA codes for the next generation mobile communication systems, XII International symposium of theoretical electrical engineering ISTET 03, Warsaw, Poland, 6-9 July, 2003, Conference Proceedings, vol.I, pp. 78-82.

10. Берлекэмп Э., Алгебраическая теория кодирования, Пер. с англ. - М.: Мир, 1971. – 477 с.

11. Lazarov A. D., Minchev Ch. N., ISAR image reconstruction and autofocusing procedure over phase modulated signals, IEE Conference RADAR 2002, Edinburg, UK, 15-17 October, 2002

12. Гецов Н., Теория на управление полета на летателни апарати – ВТС, 215 стр., 1983.

13. Гецов Н., Изследване на някои възможности за стабилизация на безпилотен самолет при полет по зададена линия на пътя, Пловдив, 1990.

14. Гецов Н., Полунатурно конструиране на системи за управление полета на безпилотни летателни апарати, София, 2002.

ВЪЗМОЖНОСТИ ЗА ИЗПОЛЗВАНЕ НА ФАЗОВО МАНИПУЛИРАНИ КОМПЛЕМЕНТАРНИ СИГНАЛИ В КОСМИЧЕСКИТЕ РАДИОЛОКАЦИОННИ СИСТЕМИ

Борислав Йорданов Беджев

В радиолокационните системи (РЛС), базирани на космически апарати, за получаване на висококачествени изображения на повърхността на планетите, спътниците и кометите, широко се прилага методът на изкуствената синтезирана апертура (Synthetic Aperture Radar - SAR). При това за едновременното реализиране на голям радиус на действие и на висока разделителна способност по разстояние се използват сложни радиолокационни сигнали с вътрешно импулсна модулация.

На настоящия стап в космическите SAR основно приложение намират сигналите с линейна честотна модулация (ЛЧМ). Въпреки положителните им свойства, за тях с характерни и някои недостатъци. В същото време сигналите с вътрешно импулсна фазова манипулация (ФМ) намериха през последните десет години изключително широко разпространение.

Предвид на изложените факти, в настоящата статия са получени следните резултати.

1. Разработен е математически метод за синтез на нов клас ФМ сигнали, наречени обобщени комплементарни сигнали (ОКС), чиято АКФ има страничпи листи с практически нулево ниво.

2. Чрез компютърни симулации на работата на РЛС с инверсна синтезирана апертура е обоснована приложимостта на ОКС в перспективните РЛС с космическо базиране.

NEW BOOKS

AEROSPACE METHODS IN ECOLOGY AND ENVIRONMENTAL STUDIES

In the end of 2003, the *Prof. Marin Drinov* Publishing House issued Part 1 of the Book AEROSPACE TECHNIQUES IN ECOLOGY AND ENVIRONMENTAL STUDIES by Dipl. Eng. Garo Mardirossian, DSc. The book reveals the potentials and application of aerospace techniques and instrumentation in solving one of the essential problems of modern mankind, namely, ecological and environmental studies. Part 1 of the book, entitled TECHNIQUES AND INSTRUMENTATION FOR REMOTE AEROSPACE STUDIES OF THE EARTH is dedicated to the techniques and instrumentation used to acquire data and information by remote sensing of the Earth on board of aerospacecraft.

Aerospace studies and their major trends are considered, emphasis being placed on the physical methods of remote aerospace studies of the Earth from space; various earth orbits are described, in particular, those used in remote sensing. Attention is focused on remote sensing techniques and instrumentation used on board of both automatic and manned aerospacecraft. Consideration is given to visual studies from an earth orbit, optimal continuous monitoring space complexes, and complex synchronous aerospace experiments.

The author, who is Senior Researcher in the Department of Remote Sensing of the Earth at the Bulgarian Academy of Sciences, is a well-known expert in the field of techniques and instrumentation used in studying the Earth's ecological problems. The book presents the results from his long career as researcher and lecturer. The book is based on the lectures delivered by the author at various educational stages in the Department of Earth and Environmental Sciences at the New Bulgarian University, where he was a co-founder of the programs "Aerospace Techniques in Ecology and Environment". The book presented here is the logical continuation and further development of the three previously published books by the author: "Combating Ecological Catastrophes from Space", 1993, "Ecocatastrophes", 1995, and "Natural Ecocatastrophes and Their Remote Aerospace Study", 1999.

The book is easy to read and provides a valuable information source. It is intended for a broad readers' audience: researchers, specialists, and

students working in the field of ecology, preservation of environment, the overall complex of Earth sciences (geography, geophysics, geology, hydrology, meteorology etc.), aviation and aeronautics, military staff, civil protection experts etc.

Prof. Dipl. Eng. Nikolay Georgiev, DSc

Mardirossian, G. Aerospace Techniques in Ecology and Environmental Studies. *Prof. Marin Drinov* Publishing House, Sofia, 2003, 208 p.

INSTRUCTIONS TO AUTHORS

The ***Aerospace Research in Bulgaria*** series publishes original articles in the theoretical and applied field of space and aviation science and practice.

Conditions:

- Articles shall be submitted in duplicate in English. Bulgarian authors shall also supply Bulgarian version for verification of translation.
- Each article shall be accompanied by a diskette or a CD containing text and figures.
- Manuscripts (including tables and references) shall not exceed 15 standard pages (1800 symbols per page, spaces included) written on font "Times New Roman", font size 12, standard office format A4 with margins: top 8.2 cm, bottom 2 cm, left and right 4 cm.
- Each article shall have an abstract (up to 15 lines) in English and Bulgarian.
- The submitted articles shall not be published, nor submitted for publication elsewhere.
- Measurement units shall comply with the SI.
- Authors shall be asked to proof-read their articles once within a term to be specified by the publisher.
-
- **Layout:**
- ***Title page***. The first page of the article shall indicate the title of the article (in bold, capital letters), the author(s) full name(s), and affiliation (in Italics, small letters).
- ***Abstract***. The English abstract shall precede the article. It shall be written on font "Times New Roman", font size 10, Italics. The Bulgarian abstract shall come in the end of the article. It shall be written on font "Times New Roman", font size 12.
- ***References***. They shall be indicated in the text by placing the appropriate number in parentheses, e.g. [1]. The list references shall be printed in the end of the article, before the Bulgarian abstract, arranged chronologically by their order of reference throughout the text. The name(s) of the author(s) shall be double-spaced, the first author's name being inverted. The title of the article shall be followed by the title of the journal (collection), volume, year of publication, issue number, and pages cited. The titles of the monographs shall be followed by the name of the city, year of publication, and number of pages.
-
- **Example:**
- Krustanov L., K. Serafimov. Proc. BAS, XX, 1974. Vol.2, p.29.
- Nestorov G. Physics of the Low Ionosphere. S., BAS, 1969, p.63.

Address: Authors may submit their articles in person or send them to the following address:

Editorial Board
Aerospace Research in Bulgaria
Space Research Institute
Bulgarian Academy of Sciences
6, Moskovska St., 1000 Sofia, Bulgaria

ISSN 0861-1432

УКАЗАНИЯ ЗА АВТОРИТЕ

В поредицата **"Аерокосмически изследвания в България"** се публикуват оригинални статии в областта на теорията и приложението на космическата и авиационната наука и практика.

Условия:

- Статиите се представят в два екземпляра на английски език. Българските автори представят и вариант на български език за проверка на превода.
- Всяка статия трябва да се придружава от дискета или CD, съдържаща/о текста и фигурите.
- Материалите (включително таблиците и литературата) трябва да бъдат в размер до 15 стандартни страници (1800 знака на страница, като се отчитат и празните полета) в шрифт "Times New Roman", 12 пункта, стандартен офис формат А4 с полета: горе 8.2 см, долу 2 см, ляво и дясно 4 см.
- Всяка статия трябва да има резюме (до 15 реда) на английски и на български език.
- Представените статии не трябва да са публикувани или да са представени за публикуване на друго място.
- Мерните единици трябва да бъдат в системата СИ.
- Авторите трябва да направят един контролен прочит на текста в срок, определен от издателя.

Оформление:

- ***Заглавна страница***. На първата страница се изписва заглавието на статията (в черно, с главни букви), пълното име/на на автора/ите, и местоработата му/им (в курсив, с малки букви).
- ***Резюме***. Резюмето на английски език се поставя в началото на статията. То трябва да бъде написано на шрифт "Times New Roman", 10 пункта, в курсив. Резюмето на български език се поставя в края на статията. То трябва да бъде написано на шрифт "Times New Roman", 12 пункта.
- ***Литература***. Цитираната литература се указва в текста с номера, съответстващ на реда на изброяването ѝ, поставен в средни скоби, напр. [1]. Списъкът на използваната литература се поставя в края на статията, преди резюмето на български език, написан в хронологическия ред на използването му в статията. Името/ната на автора/ите се изписват с двойна разредка, като името на първия автор е в обратен ред. След заглавието на статията се изписва заглавието на списанието (сборника), номера на тома, годината на публикуване, номера на книжката и номерата на цитираните страници. За монографии след заглавието се посочва името на града, годината на публикуване и броя на страниците.

Пример:

- Кръстанов Л., К. Серафимов. Докл. БАН, XX, 1974. том.2, с.29.
- Несторов Г. Физика на ниската атмосфера. С., БАН, 1969, с.63.

Адрес: Авторите могат да представят статиите си лично или да ги изпратят на следния адрес:

Редакционна колегия
"Аерокосмически изследвания в България"
Институт за космически изследвания
Българска академия на науките
ул."Московска" № 6, 1000 София, България